Impact of bending related faulting on the seismic properties of the incoming oceanic lithosphere offshore of Nicaragua

Dissertation

zur Erlangung des Doktorgrades
der Mathematisch-Naturwissenschaftlichen Fakultät
der Christian-Albrechts-Universität zu Kiel

vorgelegt von
Monika Ivandić

Kiel, 2008

Referent:	PD. Dr. Ingo Grevemeyer
Koreferent:	Prof. Dr. Wolfgang Rabbel
Tag der mündlichen Prüfung:	28. April 2008
Zum Druck genehmigt:	13. May 2008
Der Dekan:	Prof. Jürgen Grotemeyer

Abstract

The subduction of H_2O is inherently related to the hydrogeology of the oceanic lithosphere entering the trench. Water transported within the subducting oceanic plate affects a number of processes, such as intraslab earthquakes and arc magmatism. Bending related faulting in the subducting lithospheres may intensify hydrothermal flow through aged crust and provide pathways for seawater to reach lower crustal and upper mantle depths. A number of seismic wide-angle reflection and refraction experiments were conducted offshore of Nicaragua to investigate the impact of bending related normal faulting on the seismic properties of the oceanic lithosphere prior to subduction. Based on the reflectivity pattern of multi-channel seismic reflection (MCS) data collected offshore of Nicaragua it has been suggested that bending-related faulting facilitates hydration and serpentinization of the incoming oceanic plate. First seismic wide-angle and refraction data were collected along the profile p50 which extends from the region well seaward of the outer rise, not yet affected by subduction, into the trench northwest of the Nicoya Peninsula, where multibeam bathymetric data show prominent normal faults on the seaward trench slope. A tomographic joint inversion of the seismic refraction and wide-angle reflection data yields a decrease in P-wave velocities in the crust and uppermost mantle as the plate approaches the trench. Seaward of the outer rise velocities are typical for ∼24 Myr old oceanic lithosphere. In the near-trench region, however, crustal velocities are reduced by 0.2-0.5 km/s compared to normal mature oceanic crust. Seismic velocities of the uppermost mantle are 7.6-7.8 km/s and hence 5-7% lower than the typical velocity of mantle peridotite. These systematic changes in P-wave velocity indicate an evolutionary process in the subducting slab consistent with percolation of seawater through the faulted and fractured lithosphere and serpentinization of mantle peridotites. Two other profiles, located northwest of the profile p50, are parallel to the trench axis. This geometry was chosen to reveal if serpentinization is a common process in the subducting Cocos plate offshore of Nicaragua and not just a local feature. Tomographic inversion of both data sets indeed has shown that seismic velocities are profoundly reduced along the entire lenght of the profiles, both in the crust and uppermost mantle. Upper crustal velocities are not higher than 3.8-4.0 km/s, and the upper mantle is characterized by strong alteration that has

caused a reduction of the seismic velocities by 8-10%. The anomalous behaviour is more profound here than in the profile p50, but this observation is most likely due to the geometry of the lines, i.e. fault density is higher along a line parallel to the trench than along one which lies perpendicular. The modeling of the impact of water-filled microcracks on the elastic properties of rocks shows that they could significantly influence the seismic behavior of fractured media. The modeling of the S-wave velocities of the profile p50 has revealed that velocities in the crust are more profoundly reduced than in the P-wave structure. This is an indication that fracture porosity is extensively developed and, thus, has a significant impact on the seismic properties of the crust. One can assume a similar scenario for the upper mantle within a few kilometers just below the Moho. As both processes, hydration and fracturing, are related to each other, it is difficult to separate their effects on seismic properties. Thus, an estimate of 12-17% serpentinization in the uppermost 3-4 km of the mantle is just an upper limit of hydration, i.e. if the reduced velocities we observe in our velocity models were due solely to hydration.

Zussammenfassung

Die Subduktion von Wasser bestimmt wesentlich das hydrogeologische Verhalten ozeanischer Lithosphäre im Bereich des Tiefseegrabens. Wasser, welches als Teil der subduzierten ozeanischen Platte transportiert wird, beeinflusst dabei maßgeblich Prozesse wie die Seismizität innerhalb dieser Platte sowie im weiteren Verlauf der Subduktion Schmelzvorgänge im darüber liegenden Mantel. Durch die Biegung der subduzierten ozeanischen Lithosphäre hervorgerufene Störungssysteme können dabei den hydrothermalen Fluss verstärken und dadurch für Meerwasser den Weg bereiten bis in Tiefenbereiche der unteren Kruste und des oberen Mantels. Mehrere refraktionsseismische Messungen vor Nicaragua wurden durchgefürt um den Einfluss dieser Störungssysteme auf die seismischen Eigenschaften ozeanischer Lithosphäre unmittelbar vor ihrer Subduktion zu untersuchen. Das Reflektionsverhalten seismischer Mehrkanal-Streamerdaten vor Nicaragua hat bereits gezeigt, dass Biegungsbrüche die Hydration und Serpentinisierung der subduzierten ozeanischen Platte ermöglichen. Zum ersten mal wurden jetzt seismische Refraktionsdaten entlang eines Profils aufgenommen, welches seewärts vom Outer Rise weit vor dem Bereiche beginnt, der durch Biegungsbrüche geprägt ist, und bis zum Tiefseegraben nordwestlich der Nicoya Halbinsel verläuft, wo Fächerecholotdaten deutliche Dehnungsbrüche seewärts des Tiefseegrabens zeigen. Eine gemeinsame tomographische Inversion von Weitwinkelreflexions- und Refraktionsdaten zeigt eine Reduzierung der P-Wellengeschwindigkeit innerhalb der Kruste und des oberen Mantels im Bereich in Richtung des Tiefseegrabens. Im Gegensatz dazu zeigen entsprechende P-Wellengeschwindigkeiten seewärts des Outer Rise typische Werte für 24 Ma alte ozeanische Lithosphäre. Die beobachtete Geschwindigkeitsreduzierung innerhalb der Kruste im Bereich des Tiefseegrabens beträgt 0.2-0.5 km/s. Geschwindigkeiten von 7.6-7.8 km/s im oberen Mantel sind hier 5-7% niedriger als typische Geschwindigkeiten für Mantelperidotit. Diese systematischen Änderungen der P-Wellengeschwindigkeit deuten auf Prozesse innerhalb der subduzierten Platte hin, die mit der Durchsickerung von Meerwasser durch tektonisch beanspruchte Bereiche der Lithosphäre und der damit zusammenhängenden Serpentinisierung von Mantelperidotit erklärt werden können. Zwei weitere refraktionsseismische Profile wurden weiter nördlich parallel zum Tiefseegraben aufgenommen. Mit Hilfe dieser Profile sollte geklärt werden, ob es sich bei der

Serpentinisierung um ein örtlich begrenztes Phänomen handelt oder ob größere Bereiche der Cocos Platte vor Nicaragua davon geprägt sind. Die tomographische Inversion beider Datensätze zeigt deutlich erniedrigte seismische Geschwindigkeiten sowohl innerhalb der Kruste als auch im oberen Mantel jeweils entlang der gesamten Länge der Profile. Die Geschwindigkeiten in der oberen Kruste betragen maximal 3.8-4.0 km/s, und der obere Mantel ist gekennzeichnet durch starke Alterationsprozesse, die sich in einer Geschwindigkeitsreduktion von 8-10% manifestieren. Die Geschwindigkeitsanomalien sind hier stärker ausgeprägt als auf Profil P50, was sehr wahrscheinlich mit dem grabenparallelen Profilverlauf und der damit einhergehenden größeren Störungsdichte zusammenhängt. Die Modellierung des Einflusses von wassergefüllten Mikrobrüchen im Gestein auf die elastischen Eigenschaften zeigt, dass dieses die seismischen Geschwindigkeiten sehr stark beeinflusst. Die Modellierung der S-Wellengeschwindigkeiten auf Profil P50 zeigt, dass die beobachtete Geschwindigkeitsreduzierung in der Kruste stärker ausgeprägt ist als im entsprechenden P-Wellenmodell. Das ist ein Hinweis auf eine stark entwickelte Zerklüftungsporosität im Gestein und hätte somit einen deutlichen Einfluss auf die seismischen Eigenschaften der Kruste. Ein ähnliches Szenario wäre für die obersten Kilometer des Mantels vorstellbar. Weil Hydration und Zerklüftung unmittelbar mit einander zusammenhängen, ist es mit dem zur Verfügung stehenden Datensatz unmöglich, den jeweiligen Einfluss auf die seismischen Geschwindigkeiten zu trennen. Eine ermittelte Serpentinisierung von 12-17% in den obersten 3-4 km des Mantels ist demzufolge nur als Maximalwert in einem Szenario anzusehen, in dem die beobachteten Geschwindigkeitsanomalien ausschließlich auf die Hydration des Gesteins zurückzuführen sind.

Contents

List of Figures

Chapter 1

Introduction

The understanding of the Earth's water cycle is inherently linked to the subduction of water at subducting plate boundaries. The transfer of water into the deep Earth's interior is related to the alteration and hydration of the incoming lithosphere. The release of water from subducting lithospheres affects the composition of the mantle wedge, enhances partial melting and triggers intermediate-depth earthquakes. Water is transferred with the incoming plate into the subduction zone as water trapped in sediments and void spaces in the igneous crust and as chemically bound water in hydrous minerals in sediments and oceanic crust [e.g., *Staudigel et al.*, 1996; *Jarrad*, 2003]. However, if water reaches upper mantle rocks prior to subduction, significant amounts can be transferred into the deep subduction zone as water-bearing mineral serpentine [*Morgan*, 2001; *Peacock*, 2001; 2004]. Serpentinites have nearly the same chemical composition as mantle peridotite except that they contain approximately 13 wt% water in mineral structures and are less dense.

The mechanism by which dehydration reactions trigger intermediate-depth earthquakes is based upon a pore pressure increase that reduces effective normal stress and hence can promote seismic rupture [*Raleigh and Paterson*, 1965; *Meade and Jeanloz*, 1991]. Serpentinized mantle generally dehydrates at higher temperature and pressure than sediment and hydrothermally altered crust. The most stable serpentine mineral antigorite dewaters progressively down to appoximately 200 km depth, suggesting that serpentines may be the primary agent to deliver water into the mantle.

This work has been done as a part of the project SFB 574 "Volatiles and Fluids in

subduction zones", whose scientific aim is to investigate the role of fluid and volatile recycling in subduction zones.

1.1 Normal Faulting and Outer Rise Earthquakes

The bending of the plate is associated with tension in the upper ∼20 km [*Christensen and Ruff*, 1983]. Outer rise earthquakes have been attributed to plate bending tensional stresses [*Chapple and Forsyth*, 1979]. Fault plane solutions of events seaward of the trench axis indicate normal faulting mechanisms [*Ranero et al.*, 2005; *Chapple and Forsyth*, 1979] and are therefore consistent with the idea that plate bending is governing the fault pattern in the incoming oceanic lithosphere. In addition, bathymetric observations of abundant faults on the seaward side of the trench axis [e.g. *Masson*, 1991; *Dmowska et al.*, 1996; *Kobayashi et al.*, 1998] suggest that plate bending and normal faulting are inherently related. Multi-channel seismic reflection (MCS) data indicate that a number of these faults cut through the crust into the uppermost mantle [*Ranero et al.*, 2003*; Grevemeyer et al.*, 2005]. Large amounts of seawater may percolate through these faults into the oceanic lithosphere and change its chemical composition and mechanical and seismic properties. It has been suggested that most of the hydration by this mechanism occurs at the outer rise [e.g., *Ranero et al.,* 2003; *Pecock*, 2004], where seismological studies suggest that faults cut >20 km into the lithosphere [*Kanamori*, 1971; *Christensen and Ruff*, 1988; *Hasegawa et al.*, 1994], providing potential pathways for seawater to infiltrate and react with the underlying mantle. However, so far evidence for an impact of serpentinization on the seismic properties has only been found within tectonically dominated ultraslow spreading crust by [*Osler and Louden*, 1995; *Grevemeyer et al.*, 1997].

However, seismic wide-angle and refraction data recently collected offshore of Nicaragua along the line p302 [*Grevemeyer et al.*, 2007] (Fig. 2.2) where *Ranero et al.* [2003] imaged faults that cut up to 20 km into the mantle suggest that seismic velocity in the uppermost mantle are anomalously low (<7.7 km/s). Existing datasets, however, cover only the area trenchward of the outer rise bulge and hence fail to show that crust cutting faults and low mantle velocities are related to an evolutionary process caused

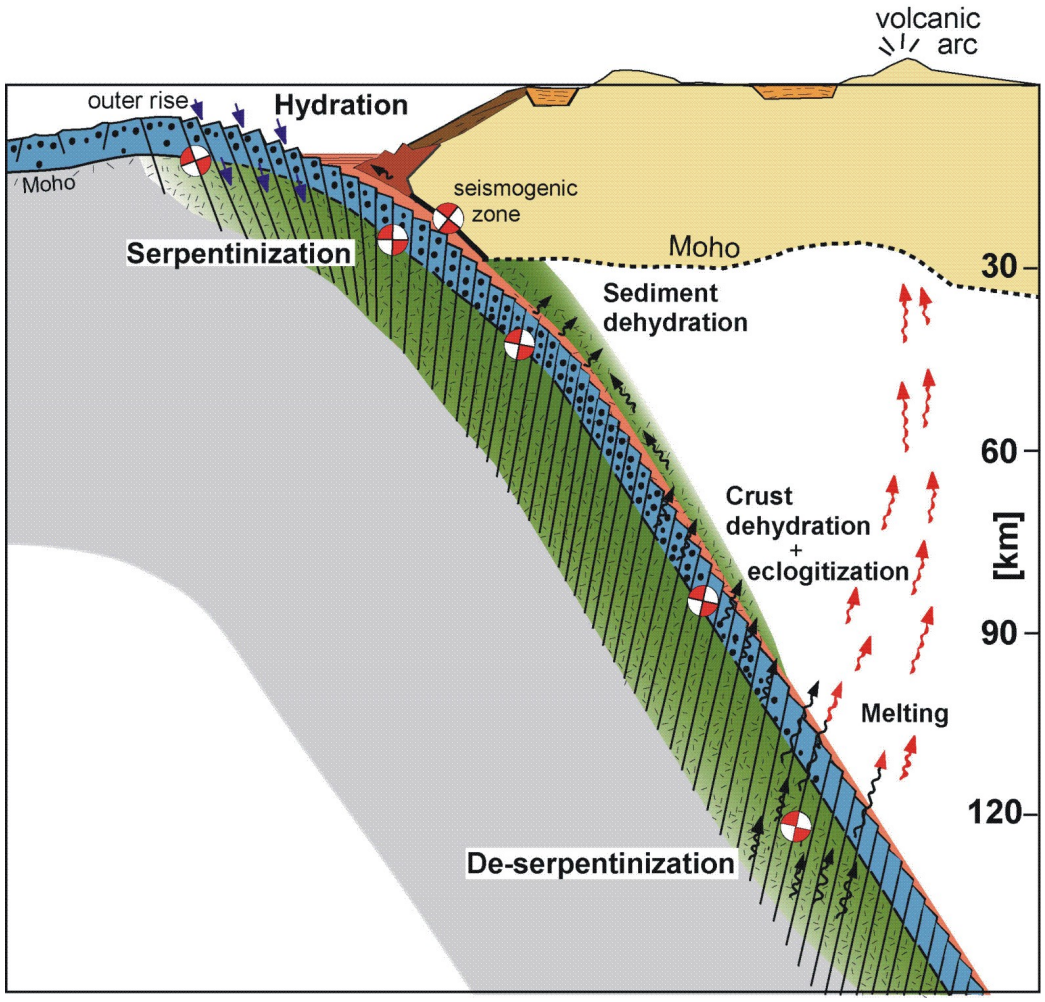

Figure 1.1: Schematic description of hydration and dehydration processes occurring from the trench-outer rise down to ∼120 km where the generation of arc magmas occurs (modified from *Ranero et al.*, 2005).

by bending-related faulting as the plate approaches the deep sea trench. Thus, the observed features may have been inherited at the spreading center.

In order to determine whether low velocities in the mantle are indeed caused by processes related to the plate bending and faulting prior to subduction, additional data were collected offshore of Nicaragua aboard of the German research vessel *Sonne*. Our profile p50 crosses the trench-outer rise, extending from far seaward of the outer-rise, where the lithosphere is still not affected by bending stresses and hence faulting, to the trench axis. Additionally, two profiles located northwest of the profile p50 and laying parallel to the trench axis, were conducted to reveal lateral changes of the subducting Cocos lithosphere, i.e. to show if serpentinization is a common process in the subducting Cocos plate offshore of Nicaragua and not just a local feature. In the end, all the seismic experiments carried out offshore of Nicaragua should help to determine the amount of water carried by the incoming oceanic lithosphere into the deep subduction zone, what is a crucial element in understanding the subduction zone dynamics.

1.2 Serpentinization

Serpentinization is a process whereby rock, usually ultramafic, is changed, by the addition of water into the crystal structure of the minerals found within the rock. Serpentinite forms when uppermost-mantle rocks peridotite (or dunite) come into contact with seawater or groundwater at low pressures and temperatures ($< 500\,^{\circ}$C). Peridotite hydration occurs along mid-oceanic ridges, transform fracture zones, subduction zones and non-volcanic (or magma poor) continental margins (where mantle rocks are exhumed at the ocean-continent transition, [e.g. *Whitmarsh et al.*, 2001], because seawater can access the uppermost mantle in each of these tectonic settings. An important characteristic of serpentinization is that the hydration reactions in the mantle rocks are exothermic - that is, they consume water and produce a significant amount of heat during the transformation of olivine to serpentine and magnetite. The amount of heat produced is directly proportional to the amount of water that is taken up to form the mineral serpentine. The heat released by a complete serpentinization reaction of 1

kilo of peridotite is 250 joules, enough to bring the temperature of 1 liter of water up by 50 degrees under normal temperature and pressure conditions. Because peridotite hydration reactions are generally exothermic they can be self-propagating, powering their own hydrothermal cell, sustaining seawater access and continued hydration. Serpentinization is also accompanied by a change of the physical properties of the rock. The volume increases by up to 30 %, with concomitant decrease of density. Serpentine is indeed a much less dense mineral than olivine and pyroxenes. A non-serpentinized peridotite has a density of 3300 kg/m^3 whereas a serpentinite has a density of approximately 2600 kg/m^3. Hydration of peridotite not only causes volume expansion but also mechanical weakening. Localised deformation in the brittle regime and distributed deformation in the ductile regime are accommodated in serpentinite by intragranular and grain boundary shear micro-cracks. Because of this micro-structural behaviour, a serpentinised body can behave as a weak inclusion [*Koyi and Skelton*, 2001; *Skelton et al.*, 2005], capable of vertical and/or lateral viscous flow in response to deformation and/or volume expansion. *Escartin et al.* [2001] showed that this change in rheological properties occurs at a serpentine content of 10-15% or less. Thus slightly serpentinised peridotites are as weak as completely serpentinised peridotite. Serpentinization also affects other geophysical properties of the oceanic crust by lowering the seismic velocities of the rocks, changing their gravity signatures and mechanical properties, and by increasing their degree of magnetism. In parallel, the speed of propagation of seismic waves decreases during serpentinization: from nearly 8 km/s in non serpentinized peridotites, to 5.5 km/s in serpentinites. In the recent years, several investigators have measured the seismic properties of serpentinized peridotites [*Christensen*, 1966; *Kern and Tubia*, 1993; *Horen et al.*, 1996; *Iturrino et al.*, 1996; *Carlson and Miller*, 2003]. Peridotites are low-silica rocks that contain olivine and pyroxenes, a mineral group high in magnesium as well as iron. At relatively cool temperatures, these minerals oxidize to serpentinite plus brucite (Mg(OH)2), magnetite (Fe3O4), and leftover hydrogen ions. The resulting fluid is alkaline rather than acidic, and rich in calcium.

$MgSiO_3 + Mg_2SiO_4 + 2H_2O \longrightarrow Mg_3Si_2O_5(OH)_4$

pyroxene + olivine + water $\longrightarrow$ serpentine

31.47 cm^3 43.79 cm^3 108.5 cm^3

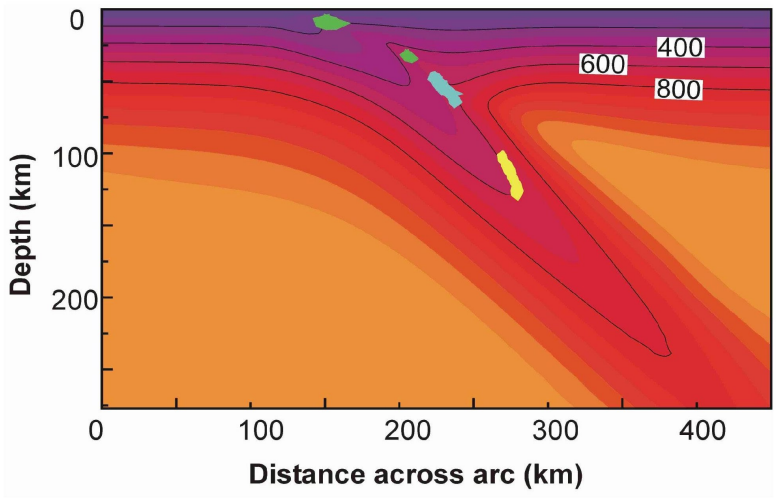

Figure 1.2: Fluid release with subduction depth from sediments (green), crust (blue) and serpentinized mantle (yellow) (from *Rüpke et al.*, 2002).

Δ V_{solids} = +33.2 cm^3 (approx. 40% bulk expansion)
Δ H0 = -16 $kcalmol^{-1}$

or,

$2Mg_2SiO_4 + 3H_2O \longrightarrow Mg_3Si_2O_5(OH)_4 + Mg(OH)_2$
olivine + water $\longrightarrow$ serpentine + brucite
87.58 cm^3 108.5 cm^3 24.63 cm^3
Δ V_{solids} = +45.5 cm^3 (approx. 50% bulk expansion)
Δ H0 = -19.5 $kcalmol^{-1}$

If tectonic forces move it nearer to the surface, the reduction in T&P cause that minerals pyroxene and olivine change to mineral serpentine. When oceanic plates undergo subduction, the heat and pressure reverse the serpentinization reaction and release the water into the deep lithosphere, where it gives rise to volcanoes. In this way dehydration of the subducting slab controls forearc fluid venting and arc magmatism.

However, the mechanism by which oceanic lithospheric mantle is serpentinized is still unclear. It has been proposed by a number of authors [*Peackok*, 2001; *Ranero et al.*, 2003] that plate bending outboard of the trench causes extension and normal faulting on the incoming plate, allowing water to infilitrate and serpentinize the uppermost mantle. Yet, it has been little known about the real amounts of water stored within the upper mantle of the subducting lithospheres, even though it could be the main slab fluid, as one of the most stable serpentine minerals, antigorite, dewaters progressively after ∼200 km depth, whereas the sediment and crust release water at much shallower depths (Fig. 1.2). Therefore, serpentine is a good candidate for the initial transport of hydrogen to the deep mantle, and its subsequent high-pressure descendants may also serve as water reservoirs.

1.3 Outline and objectives of the thesis

The main objective of this thesis is to study the impact of the incoming plate on the subduction process and possible serpentinization (mantle hydration) in subducting plates prior to subduction. To achieve this goal, we use active source seismic tomography to study the seismic structure of the crust and upper mantle of the subducting Cocos Plate offshore of Nicaragua, i.e. to image potential systematic changes of the seismic properties as plate approaches the trench. Changes in the seismic velocity are then used to estimate the amount of water trapped within the crust and mantle. In Chapter 2 are presented results of the first seismic experiment acquired northwest of Nicoya Peninsula, where multichannel seismic reflection data have revealed that subducting Cocos lithosphere is pervasively fractured and faulted due to the bending.

In Chapter 3 I investigate if plate hydration is a general feature of the incoming plate offshore of Nicaragua. For that purpose two trench parallel profiles were conducted offshore of northwestern Nicaragua during the research vessel METEOR cruise M66/4. As one of the two profiles crosses two seamounts, it was possible to explore the impact of seamounts on hydrogeological properties of the oceanic crust.

Chapter 4 deals with the impact that aligned water-filled microcracks could have on the elastic properties of the subducting crustal and upper mantle rocks. Here I

attempt to evaluate the contribution of fractures to the P-wave and S-wave velocity anomalies observed in the seismic models.

In chapter 5 I use synthetic seismograms to obtain a more solid evaluation of how well the proposed model is able to explain the observed seismic data. This method also provides more detailed constraints on velocity anomalies in the crust and upper mantle.

Chapter 6 gives a summary and conclusion of this study and provides an outlook for future investigations of physical and hydrological properties of oceanic lithospheres at subducting plate boundaries.

Chapter 2

Hydration of the subducting lithosphere offshore of Nicaragua

Multichannel seismic reflection data from the incoming plate offshore of Nicaragua shows that the subducting Cocos lithosphere is pervasively fractured and faulted (*Ranero et al.*, 2003). Some faults can be tracked in the multibeam bathymetry for at least 50 km along the trench. Trenchward dipping reflections have been interpreted as faults cutting the crust and entering several kilometers into the upper mantle, allowing penetration of seawater and widespread hydration. A case study was conducted offshore of Nicaragua in 2003 aboard of the German research vessel *Sonne* to reveal changes in the seismic structure of the subducting Cocos lithosphere. The profile was located northwest of the Nicoya Peninsula, close to the MCS profiles [*Ranero et al.*, 2003]. It extends from much seaward of the outer rise, where the plate is still not affected by subduction, into the trench. This location and orientation of the profile was chosen to reveal changes in the velocity structure due to the impact of bending related normal faulting and possible hydration process they could facilitate. The results of this experiment presented here document that the crust and upper mantle rocks of the subducting Cocos plate, formed ∼24 Myr ago at the fast-spreading East Pacific Rise, indeed undergo an extensive alteration (perhaps hydration) proir to subduction due to the bending related faulting. These results have been published [*Ivandic et al.*, 2008].

2.1 Tectonic Settings

The study area is located offshore of Nicaragua seaward of the Middle American Trench, where the Cocos plate, formed at the fast spreading East Pacific Rise to the West and the Cocos Nazca Spreading Center to the South, subducts beneath the Caribbean plate, dragging down crustal material and sediments (Fig. 2.1). Off Nicaragua, the Cocos slab subducts with a rate of about 91 mm/yr [*DeMets et al.*, 1990] in a northeasterly direction. The dip of the Benioff zone, obtained from teleseismic [*Burbach et al.*, 1984] and local network [*Protti et al.*, 1994] seismic data, ranges from 25 $^\circ$ in the seismogenic zone to 84 $^\circ$ between 100-220 km depth. Before entering the trench, the incoming plate, which was formed roughly 24 Myr ago at the East Pacific Rise, is pervasively normal faulted with offsets of up to 100-500 m and length of 10-50 km [*von Hune et al.*, 2000; *Ranero et al.*, 2003]. Offshore of Nicaragua, faulting and fault growth between the outer rise and the trench generate a prominent stairway-like seafloor relief prior to subduction (Fig. 2.1). Normal faults are poorly developed or absent seaward of the outer bulge apparantly forming as the plate approaches the trench. Deep-tow video observations show that normal faults often expose basement; heat flow data suggest that these exposed faults govern a hydrothermal circulation system in the incoming plate [*Grevemeyer et al.*, 2005]. In addition, seamounts off Nicoya Peninsula seem to control the thermal state of the incoming plate and mine heat from the Cocos plate [*Fisher et al.*, 2003]. Multi-channel seismic reflection (MCS) data acquired offshore of Nicaragua [*Ranero et al.*, 2003] suggest that some normal faults may cut through the entire crust of the incoming plate, reaching several kilometers into the upper mantle and hence may facilitate migration of seawater down to the upper mantle.

2.2 Data and Modeling

The data used in this study consist of ocean bottom hydrophone data from a wide-angle profile acquired in summer 2003 during the research vessel *Sonne* cruise SO173-1 (Figure 2.1). The working area of the cruise was located at the Pacific continental margin off Costa Rica and Nicaragua. The profile P50 was shot with three 32-liters BOLT Inc. airguns, providing a total volume of 96 liters and the airguns were

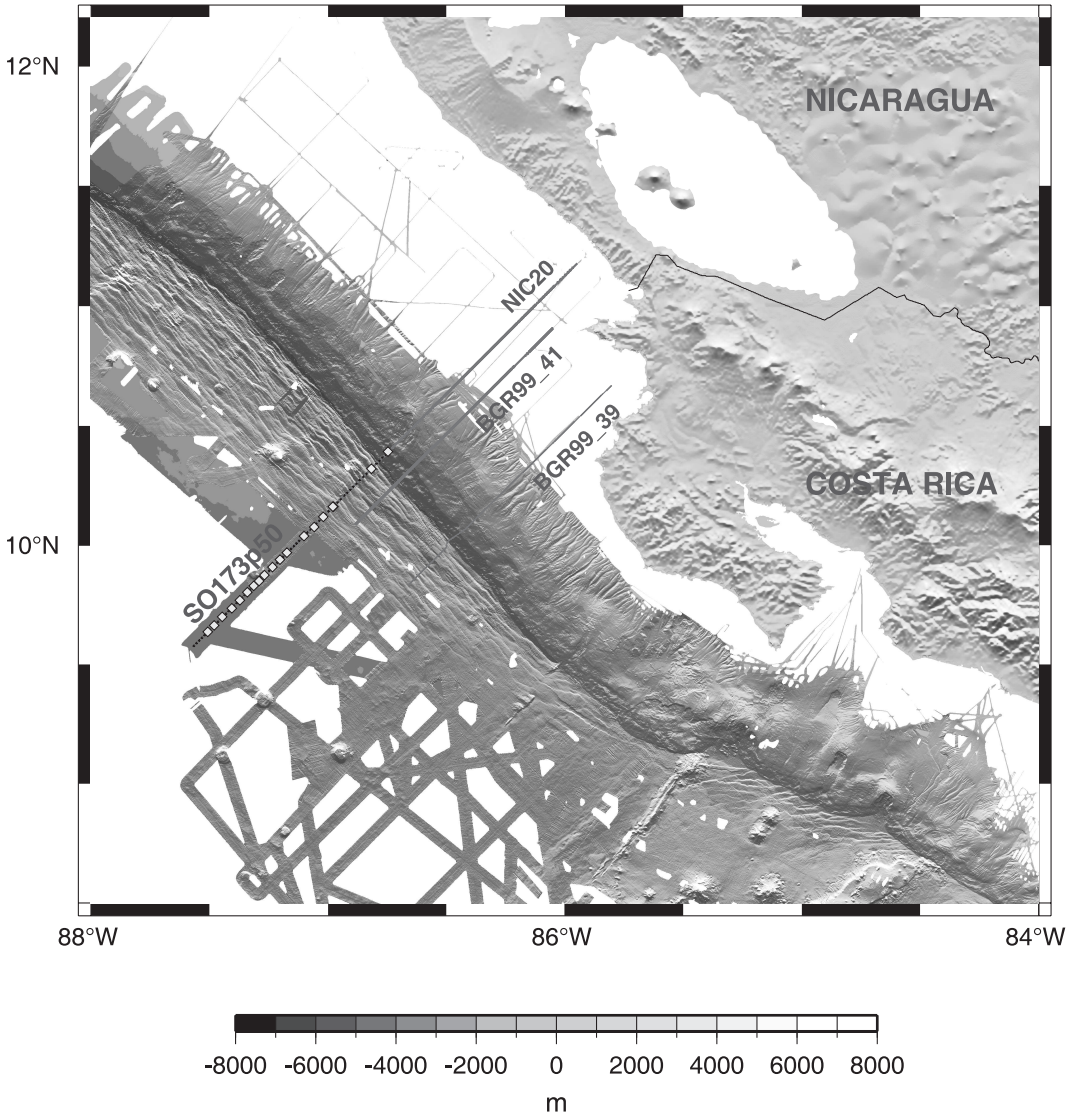

Figure 2.1: Bathymetric-topographic map of the Central American subduction zone offshore of Costa Rica and Nicaragua. The working area of the cruise SO173-1 with the wide-angle and refraction profile p50 is located northwest of the Nicoya Penninsula. Circles indicate ocean bottom stations used in the seismic modeling. Three stations from the line NIC20 in the trench and on the lower continental slope were included into the data inversion procedure. Along MCS profiles BGR99_41 and 39 *Ranero et al.* [2003] imaged trenchward-dipping reflectors, interpreted as faults cutting through the crust into the mantle.

operated at a pressure of 150 bar. A shot interval of 60 s and a speed of 3.5 knots yields an average shot spacing of 100 m. The seismic data were recorded by 12 ocean bottom hydrophones (OBH) [*Flueh and Bialas*, 1996] and 5 ocean bottom seismometers (OBS) [*Bialas and Flueh*, 1999]. P50 is 140 km long and extends from the outer rise into the trench northwest of the Nicoya Peninsula. This location was chosen because it covers the area of significant bending and as a consequence normal faults are abundant in swath mapping bathymetric data [e.g., *Ranero et al.*, 2003]. In addition, a major portion of the profile is coincident with the seismic MCS line NIC20 shot in the year 2000 with the multi-channel seismic equipment of Lamont Doherty Earth Observatory's seismic vessel Maurice Ewing (Fig. 2.2). The seismic MCS data imaged the sedimentary blanket and oceanic crust, including a prominent Moho reflection at ∼1.8 s below basement (Fig. 2.3). Unfortunately, the rough seafloor and basement topography scatters away seismic energy where plate bending and normal faulting is most prominent [*Berhorst*, 2006]. Therefore, Moho and faults cutting through the crust into the mantle could not be imaged within 20 km off the trench axis. In addition, NIC20 provides additional seismic refraction data from the trench and the continental slope. Three stations from NIC20 (OBH01, OBH02 and OBH03) in the trench and on the lower continental slope were included into the data inversion procedure. The recorded sections obtained at selected OBH's are shown in Fig.2.4 - Fig.2.7.

The main aim of this study is to reveal changes in the structure of the oceanic crust that might be associated with bending related fracturing and hydration occurring in the outer rise and near the trench axis. Therefore we have studied deviations from 'normal' oceanic crust. Most refraction surveys with this objective are interpreted relative to the average structure of oceanic crust as defined by *White et al.* [1992]. However, it is known that the oceanic crust in the East Pacific ocean is generally much thinner than the 6.48 ± 0.75 km thickness given by *White et al.* [1992] for crust younger than 30 Myr [e.g., *Collins et al.*, 1989; *Grevemeyer et al.*, 1998; *Walter et al.*, 2000]. Therefore, we based our one-dimensional reference velocity model on the structure of crust studied during the presite survey work of Ocean Drilling Program (ODP) Leg 206 in the Guatemala Basin westward of Nicaragua [*Wilson et al.*, 2003]. In this one-dimensional model, upper crustal velocities are 4.5-5 kms^{-1}. The transition to lower crust is at ∼1.5 km below the basement. Lower crustal velocities are between 6.8 and 7.1 kms^{-1}. Total crustal thickness is ∼5-5.5 km. Upper mantle peridotite velocity of

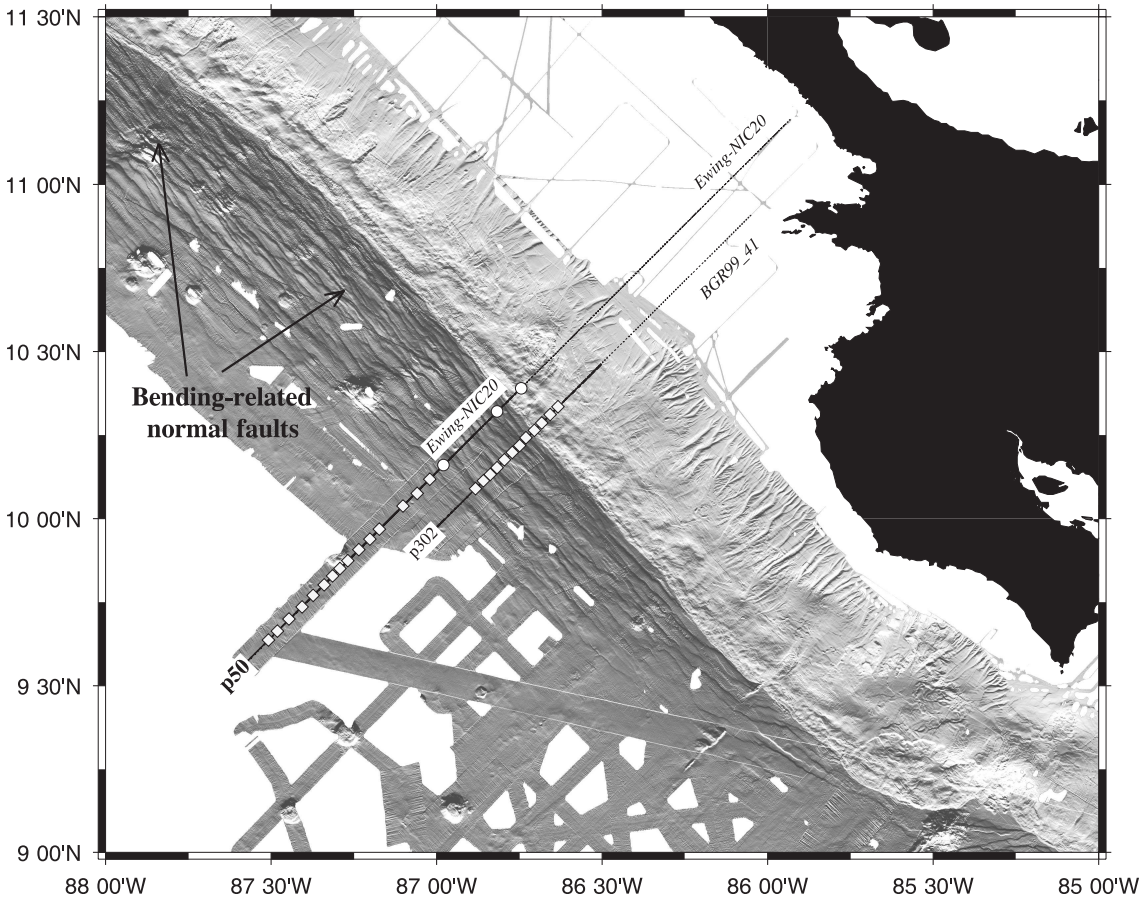

Figure 2.2: Multibeam bathymetric map of the Cocos Plate and continental slope offshore Nicoya Penninsula, Costa Rica, and Nicaragua. A major portion of the profile p50 is coincident with the MCS line NIC20. A wide-angle and refraction profile p302 from *Grevemeyer et al.* [2007] acquired during research vessel Sonne cruise SO173-1 covers only the area trenchward of the outer rise bulge.

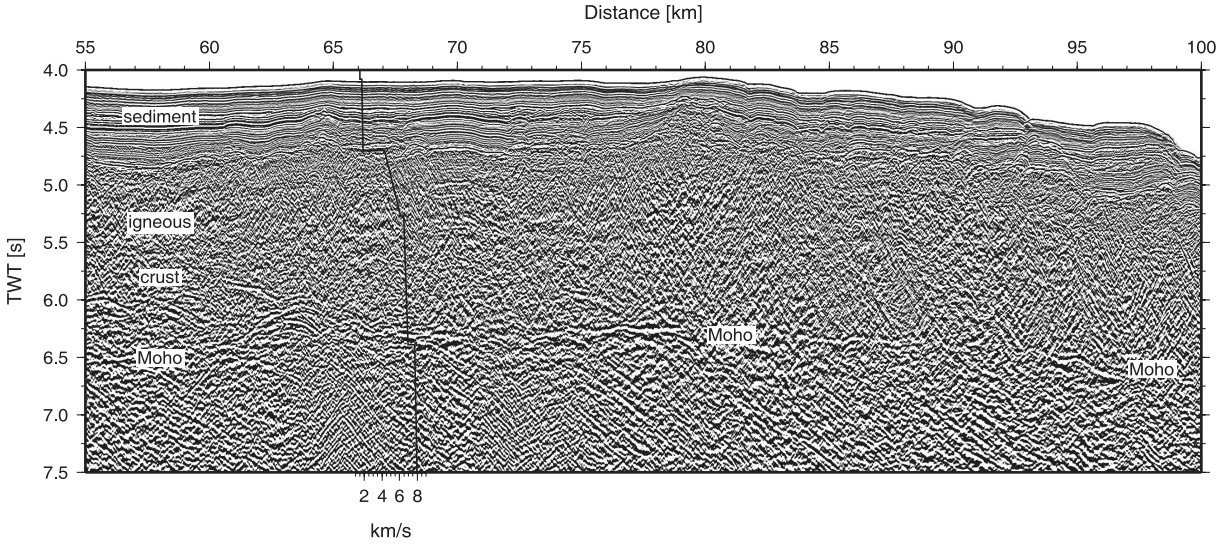

Figure 2.3: Seismic data from the MCS line NIC20 imaged the sedimentary blanket and oceanic crust, including a prominent Moho reflection at 1.8 s below the basement. The 1-dimensional velocity profile is a time converted velocity-depth profile from the modelling approach, showing an excellent fit between MCS and seismic refraction and wide-angle data. The distance scale coincides with the one in the seismic refraction line.

8.2 kms^{-1} is included in the model.

A two-dimensional velocity model along the profile was calculated using the joint refraction and reflection inversion method of *Korenaga et al.* [2000], which solves for the seismic velocity field and the depth of a reflecting interface. The forward problem is solved by a hybrid method based on the shortest path [e.g. *Moser*, 1991] and the ray-bending [e.g. *Moser et al.*, 1992] methods, and the inverse problem uses a sparse least-squares method [*Paige and Saunders*, 1982] to solve a regularized linear system. Tomographic inversion approach is given in the Appendix. We applied this method in a layer-stripping approach, where the appropriate phases are used to constrain the shallow structure first and then to progressively constrain the deeper layers. A total of 3596 Pg, 1894 PmP and 1747 Pn phases were hand-picked from 19 instruments (16 P50, 3 NIC20). A low ambient noise level and a good quality of the waveforms made picking of the first breaks relatively straightforward. Upper crustal arrivals could be picked to ±12 ms, or better. However, for larger offsets signal-to-noise ratio decreases. The largest uncertainties, of ± 90 ms, have been assigned to some Pn and PmP arrivals.

The two-dimensional velocity field is parameterized by a grid of nodes hanging from the seafloor topography with 0.5 km lateral nodal spacing and variable vertical nodal spacing (0.05 km within the upper 2 km and increasing to 0.4 km at the bottom). The Moho is parametrized as a floating reflector with nodes every 1 km with one degree of freedom in the vertical direction. We applied smoothing constraints on both velocity and depth perturbations using predefined correlation lengths in order to stabilize the inversion. In addition, damping constraints for velocity and depth are added to the regularized linear system. A detailed description of the method and parameters is given elsewhere [*Korenaga et al.*, 2000]. The model is 135 km long and 20 km deep. The horizontal correlation length values increase from 4 at the top to 10 at the bottom, and vertical correlation lengths vary from 0.1 km at the top to 3 km at the bottom. Also, the depth sensitivity is weighted by a depth kernel weighting parameter w. For the inversion of Pg and PmP phases we used w=1, which allows the same perturbations for both velocity and depth, and for the final inversion step, where all the phases were included, this parameter had a value of 0.1, allowing more perturbations for the velocity than for the depth. The two-dimensional P-wave velocity model and reflector geometry obtained after 5 iterations of the inversion process are shown in Figure 2.8. The *rms* travel time misfit obtained for the final model is 50 ms [$\chi 2$= 0.99], significantly reducing

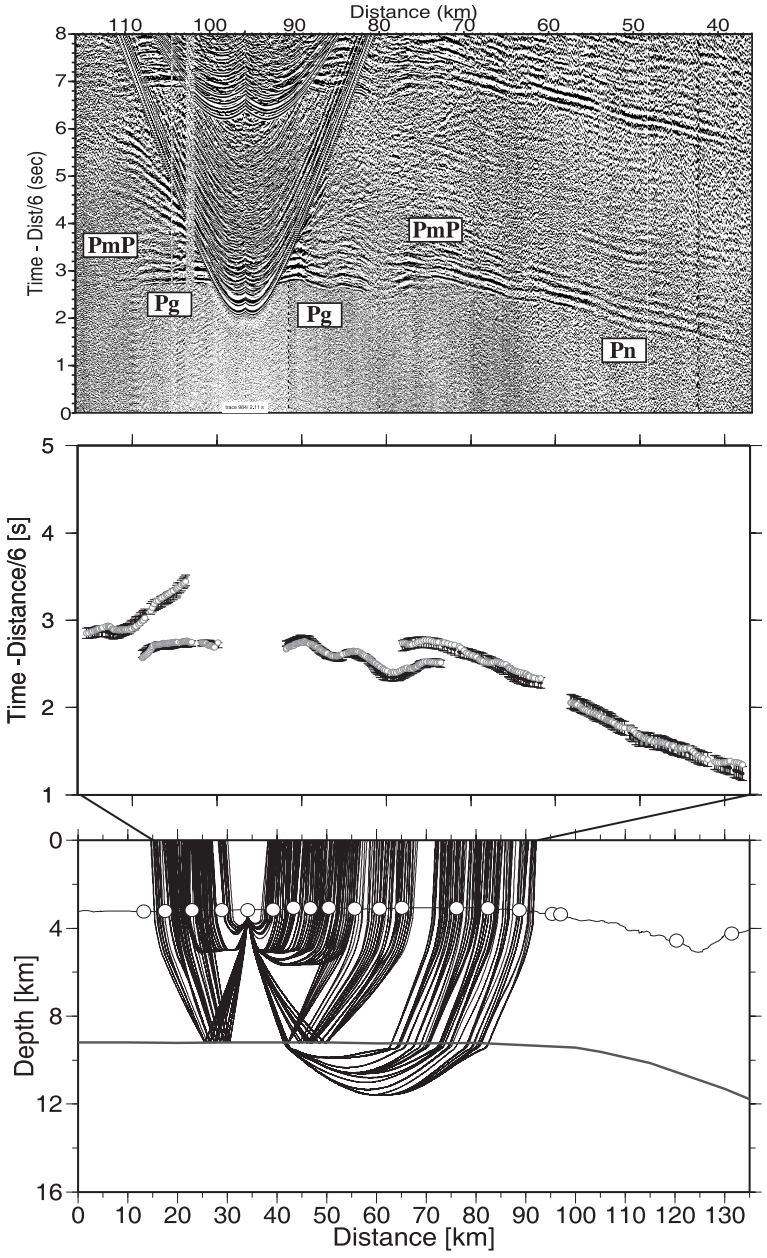

Figure 2.4: Wide-angle data examples from selected instruments. Data have been reduced by 6 km/s. Picked travel times (solid circles with error bars) and predicted travel times (white circles) for Pg, PmP and Pn phases are shown in the middle plots. Corresponding ray paths are plotted at the bottom. OBH38

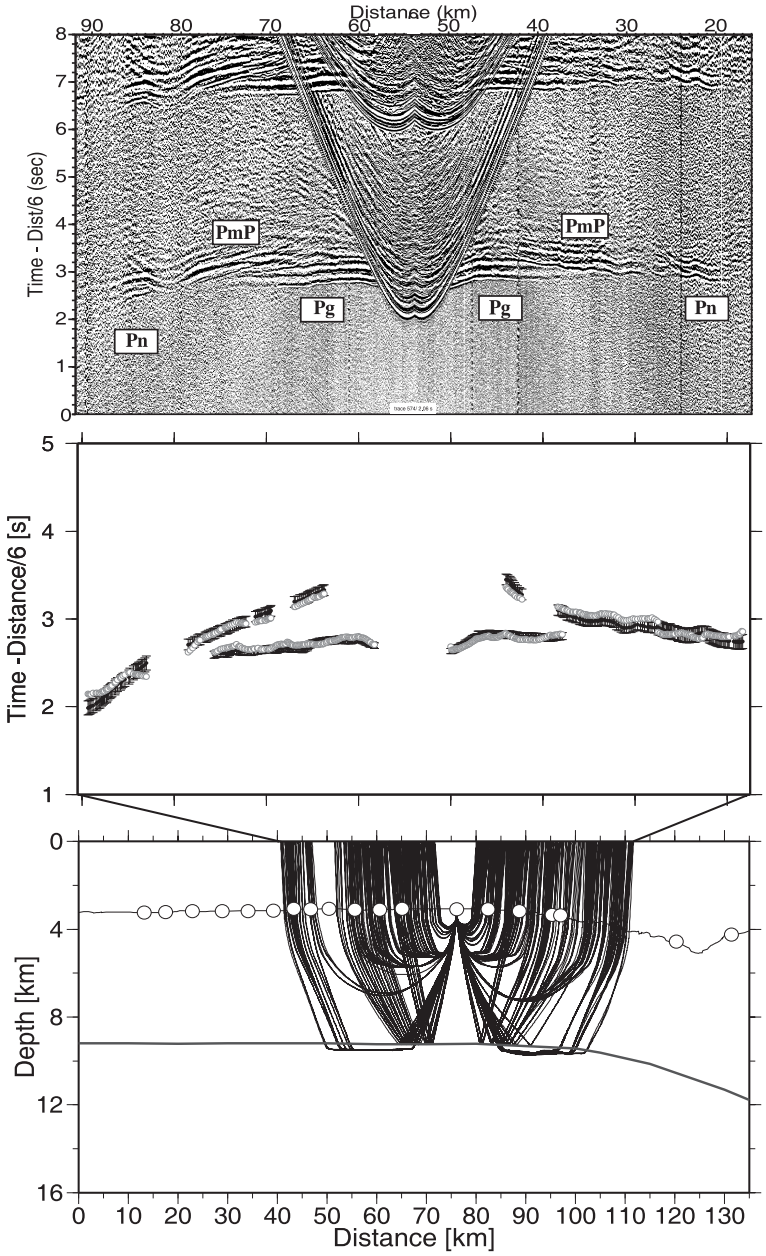

Figure 2.5: Same as Fig. 2.4 for OBH47.

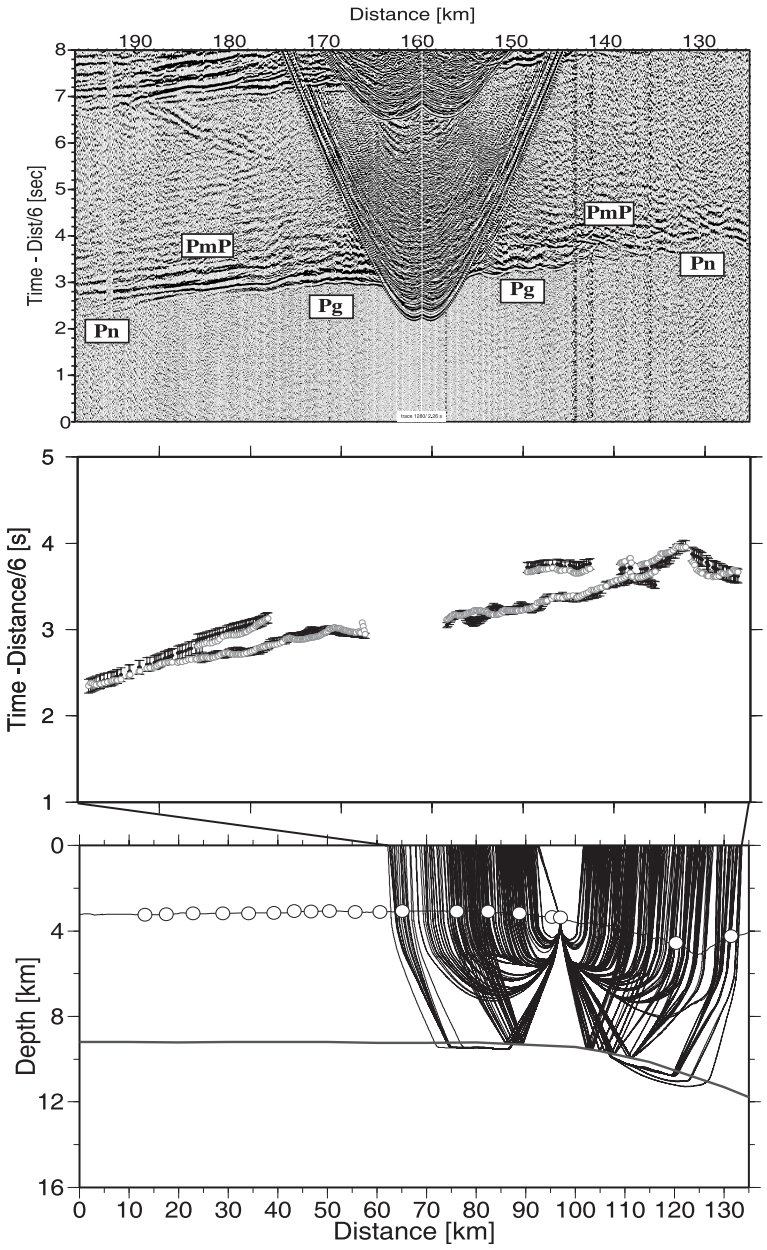

Figure 2.6: Continued; OBH 01.

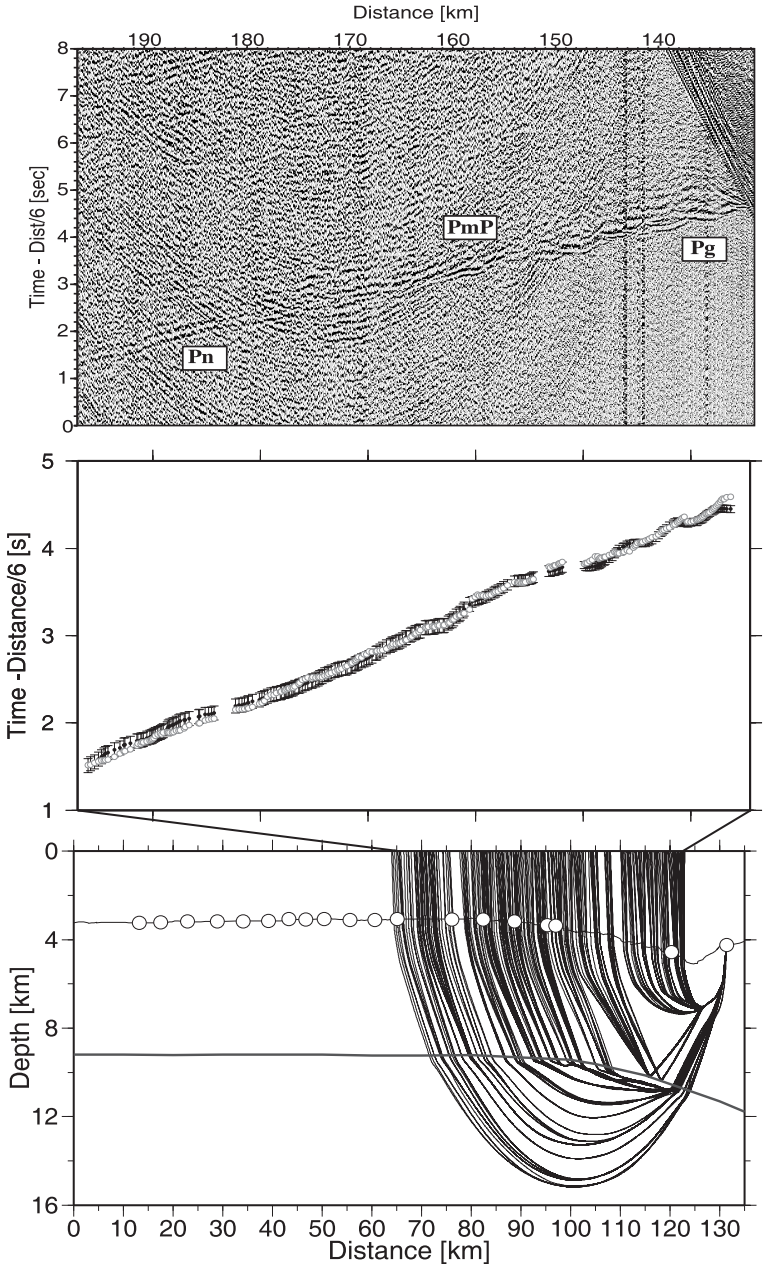

Figure 2.7: Continued; OBH 03.

the initial misfit of 143 ms. Picked and calculated travel times, and raytracing from four ocean bottom instruments are shown in Fig.2.4 - Fig.2.7.

2.3 Seismic structure

The structure of the subducting oceanic lithosphere is resolved by intracrustal refractions (Pg), Moho reflections (PmP), and upper-mantle refractions (Pn). The resultant two-dimensional velocity model reveals systematic changes in seismic properties of the lithosphere affected by plate flexure and faulting. No refracted phase from the sediment is observed, but seismic reflection data from NIC20 provide information on sediment thickness. The thin sediment cover has an average thickness of ∼500 m with velocities ranging from 1.7 up to 1.8-1.85 kms^{-1}. The oceanic crust is typically divided into two primary layers: an upper crust (layer 2) characterized by a rapid increase in seismic velocity with depth (∼1 $kms^{-1}km^{-1}$), and a thicker lower crust (layer 3) which is distinguished from layer 2 by both a higher P-wave velocity and a much smaller vertical velocity gradient (0.1-0.2 $kms^{-1}km^{-1}$). In the outer rise region no significant lateral changes are found within the crust and uppermost mantle. Upper crustal velocities increase from 4.4-4.5 kms^{-1} at the top of the basement to 6.0-6.2 kms^{-1} at the bottom of layer 2, which is found at a depth of ∼1.5 km below the basement uniformly along the profile.

These velocities have been commonly attributed to normal mature oceanic upper crust [*Grevemeyer et al.*, 1998; 1999; *Carlson*, 1998] and would correspond to a layer mainly composed of extrusive basalts and underlying sheeted dikes. Lower crustal velocities increase steadily from 6.5-6.7 kms^{-1} at the top to 7.0-7.1 kms^{-1} at the crust-mantle boundary, suggesting a crust of gabbroic composition [e.g., *White et al.*, 1992]. Strong wide-angle reflections from the Moho indicate a uniform crustal thickness of ∼5.5 km along the profile, confirming the results from the MCS survey. Below the Moho, in the uppermost mantle, we find a typical velocity of unaltered olivine-rich peridotites of 8.1-8.2 kms^{-1}.

Towards the trench, however, crustal and upper mantle velocities are reduced compared to velocities expected for ∼24 Myr old mature oceanic lithosphere [e.g., *White et*

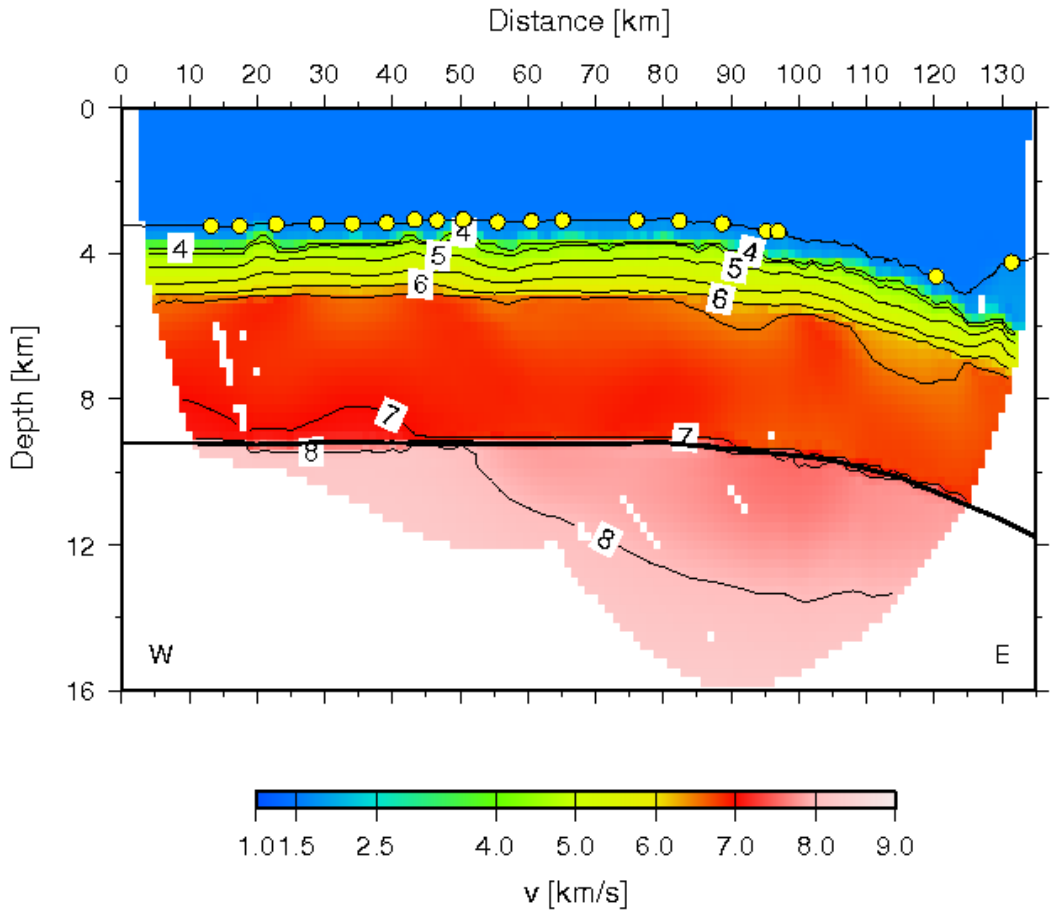

Figure 2.8: Final velocity model with isovelocity contours. Thick black line represents Moho boundary derived from inversion of PmP phases. Yellow circles indicate OBH and OBS stations.

a)

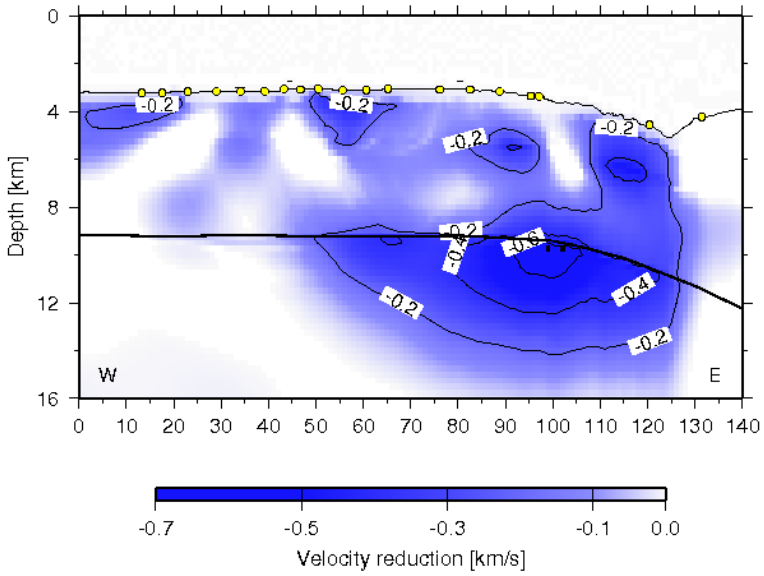

b)

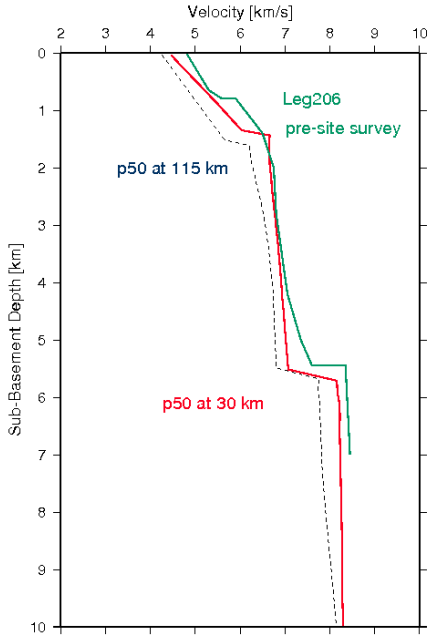

Figure 2.9: a) Velocity reduction within the model; b) Velocity-depth profiles at two selected locations in the outer-rise and near-trench region and 1D reference velocity model from the presite survey work of ODP Leg 206 in the Guatemala Basin.

al., 1992; *Carlson*, 1998; *Grevemeyer and Bartetzko*, 2003], indicating a change in physical or/and chemical properties of rocks. Upper crustal velocities in layer 2 decrease to 4.1-4.3 kms^{-1} at the top and to 5.7-6 kms^{-1} at the base.

Velocity reduction in the lower crust can perhaps best be shown by using the 6.8 kms^{-1} isovelocity contour as a 'marker'. The 6.8 kms^{-1} isovelocity contour in the lower crust starts to dip at ∼65 km distance from the trench axis and at ∼35 km distance it reaches the crust-mantle boundary. In the near-trench region velocities of the lower crustal rocks are reduced to 6.2-6.4 kms^{-1} at the top to ∼6.6-6.9 kms^{-1} and the bottom of layer 3. Two possible mechanisms may explain the observations: (i) fracture porosity has been increased, and/or (ii) crustal rocks have been hydrated. However, the most prominent feature of the seismic velocity model is an extensive zone of reduced velocity in the uppermost 3-4 km of the mantle in the near-trench region. Changes in seismic strucuture start at ∼60 km distance from the trench; the anomaly reaches its largest amplitude and extent near the trench axis. The velocity just below the Moho boundary is reduced to 7.6-7.8 kms^{-1}, what is 5-7% lower than the ∼8.1-8.2 kms^{-1} found in the outer rise region, perhaps indicating partially hydrated mantle associated with bending-related faulting [*Grevemeyer et al.*, 2007]. Figure 2.9b shows velocity-depth profiles extracted at selected locations in the outer-rise and near-trench region, indicating a change in the seismic structure as the plate approaches the trench.

2.4 Resolution and Uncertainty Test

The derivative weight sum [DWS] is a measure of ray density near a grid node [*Toomey and Foulger*, 1989]. This value depends on both the number of rays affecting the velocity of a particular node and the distance between the rays and the node. The DWS for crustal phases is shown in the Figure 2.11a. The DWS for all the phases used to construct the final velocity model is shown in Figure 2.11b.

In order to estimate the uncertainties of the final model we applied Monte Carlo analysis [e.g., *Korenaga et al.*, 2000]. The uncertainty of a nonlinear inversion can be expressed in terms of the posterior model covariance matrix [e.g., *Tarantola*, 1987],

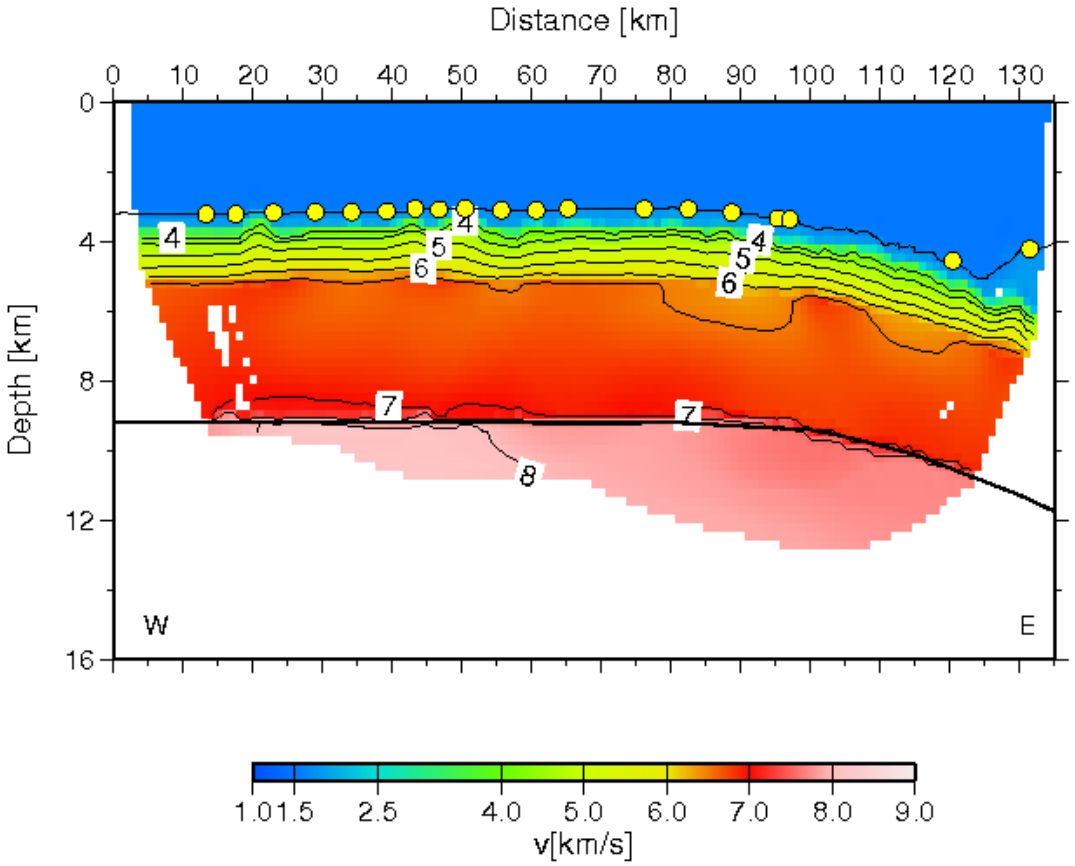

Figure 2.10: Result of tomographic inversion along profile p50 using a starting model with velocities well reduced compared to the first starting model.

which can be approximated by the standard deviation of a large number of Monte Carlo realizations assuming that all the realizations have the same probability [e.g., *Tarantola*, 1987]. A set of 10 initial models is constructed by randomly perturbing the velocity of the crustal and upper mantle velocities into several nodes (0.3 km/s) of our reference model. We also generated 10 different data sets by adding random phase gradient errors (0.50 ms) and common receiver noise (0.30 ms) to the initial data set [*Zhang and Toksöz*, 1998]. We obtained 100 Monte Carlo realizations by inverting all the combinations of the 10 initial velocity models with the 10 observation vectors, using the same model parameterization as in the final solution. All of the Monte Carlo inversions converged in less than 6 iterations to $\chi^2 \sim 1$, where χ^2 is the normalized sum of the *rms* misfits divided by the corresponding picking uncertainties. The standard deviation of the velocity is found to be lower than 0.1 km/s in the upper and lower crust and lower than 0.05 km/s in the major part of the upper mantle. The uncertainties of the model are plotted in Figure 2.12.

The results of a tomographic inversion may depend on the structure of the reference model. In our case the reference model turned out to be representative of the western-most section of the seismic profile. To examine the robustness of the results, we chose a reference or starting model that was characterized by velocities reduced relative to the first starting model. With respect to the first approach, this model contained reduced velocities of -4% in the crustal layer and -7% just below the Moho in the upper mantle.

The *rms* travel time misfit using this starting model is 160 ms ($\chi 2 = 7.66$), and for the final model (after five iterations) it is 50 ms ($\chi 2 = 1.01$). The velocities in the outer rise region were considerably increased already after the first iteration and yielded after five iterations average crustal and upper-mantle values. Near the trench, reduced velocities given in the starting model retained their values in the vicinity of the trench, where the slab is highly affected by tensional stresses (Fig. 2.10). The similarity between this result and our final model confirms the robustness of the resolved features.

Additionally, a series of resolution tests were conducted in order to assess the resolving power of our data set. Synthetic models are constructed using the final velocity model with and without ±5-7% Gaussian anomalies of different sizes placed at various depths along the profile. Synthetic noise with *rms* amplitude of 0.05 s is added to the synthetic travel times obtained from the perturbed velocity model to simulate the addition of actual travel time variation. Both data sets, with and without perturbations,

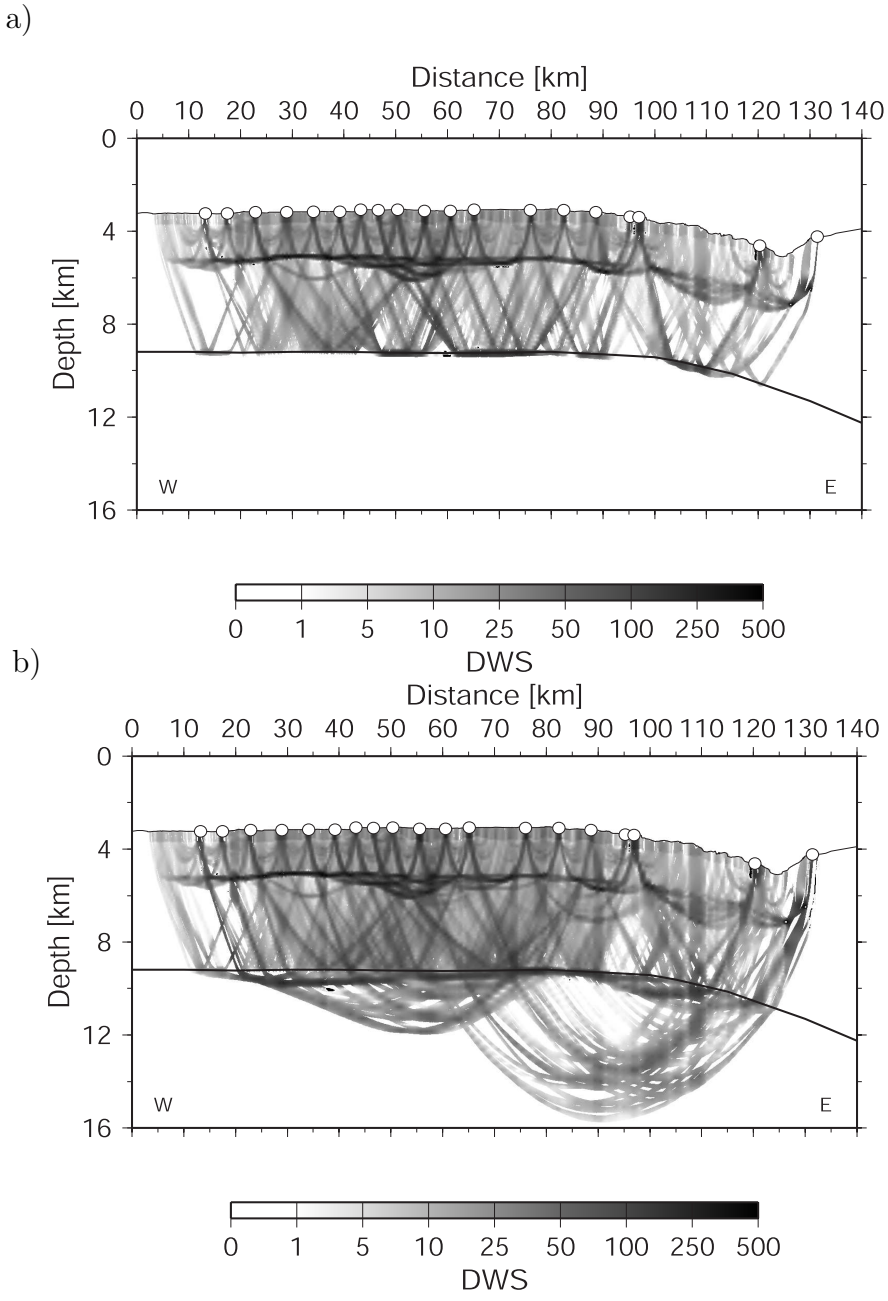

Figure 2.11: a) Derivative weight sum (DWS) for crustal and PmP phases shows that the MCS data (Fig.2.2) provide good constraints on the Moho depth.; b) Distribution of DWS values for the final velocity model shown in the Figure 2.8.

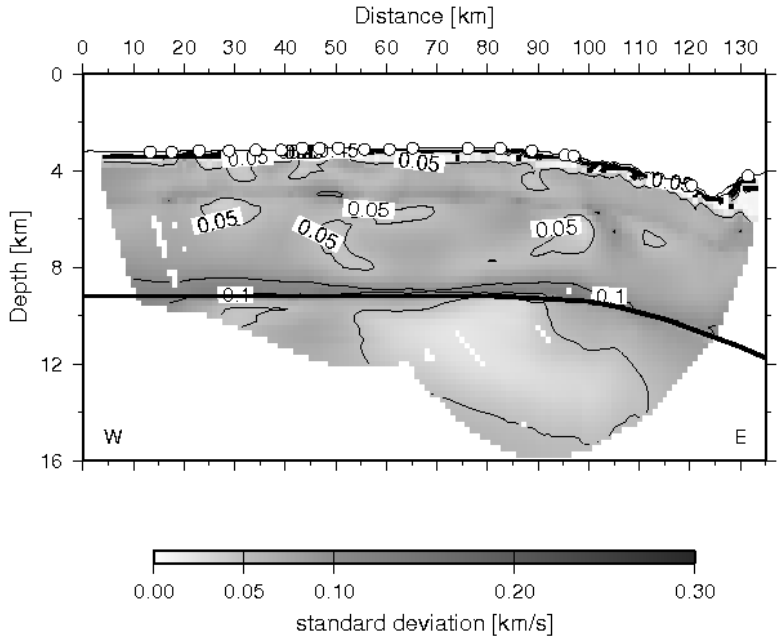

Figure 2.12: Velocity uncertainties derived from the Monte Carlo analysis.

were inverted using the same inversion parameters as the actual model inversions. In the end, the inverted model without perturbations was subtracted from the inverted model with perturbations to yield the final output.

After 3 iterations a good resolution was obtained. In Figure 2.13 are shown the input velocity anomalies and the final outputs. The velocity anomalies are reasonably well recovered, both in size and amplitude. The ray coverage of our data set is sufficient to resolve features in the uppermost mantle up to ∼4 km below Moho, indicating that a region of reduced velocities within the upper mantle can be resolved and that the crustal and upper mantle velocity reduction in the vicinity of the trench is not an artifact of the seismic tomographic inversion procedure but a real feature. The total depth extent of that anomaly, however, could not be sampled. Owing to the high density of Pg rays, the reconstructed anomalies within the crust are remarkably well resolved with the same lateral extent as the original ones. The weaker amplitude and vertical and lateral smearings of some of the anomalies near the Moho and in the upper mantle are related to the lower ray coverage at these depths. The degree of recovery

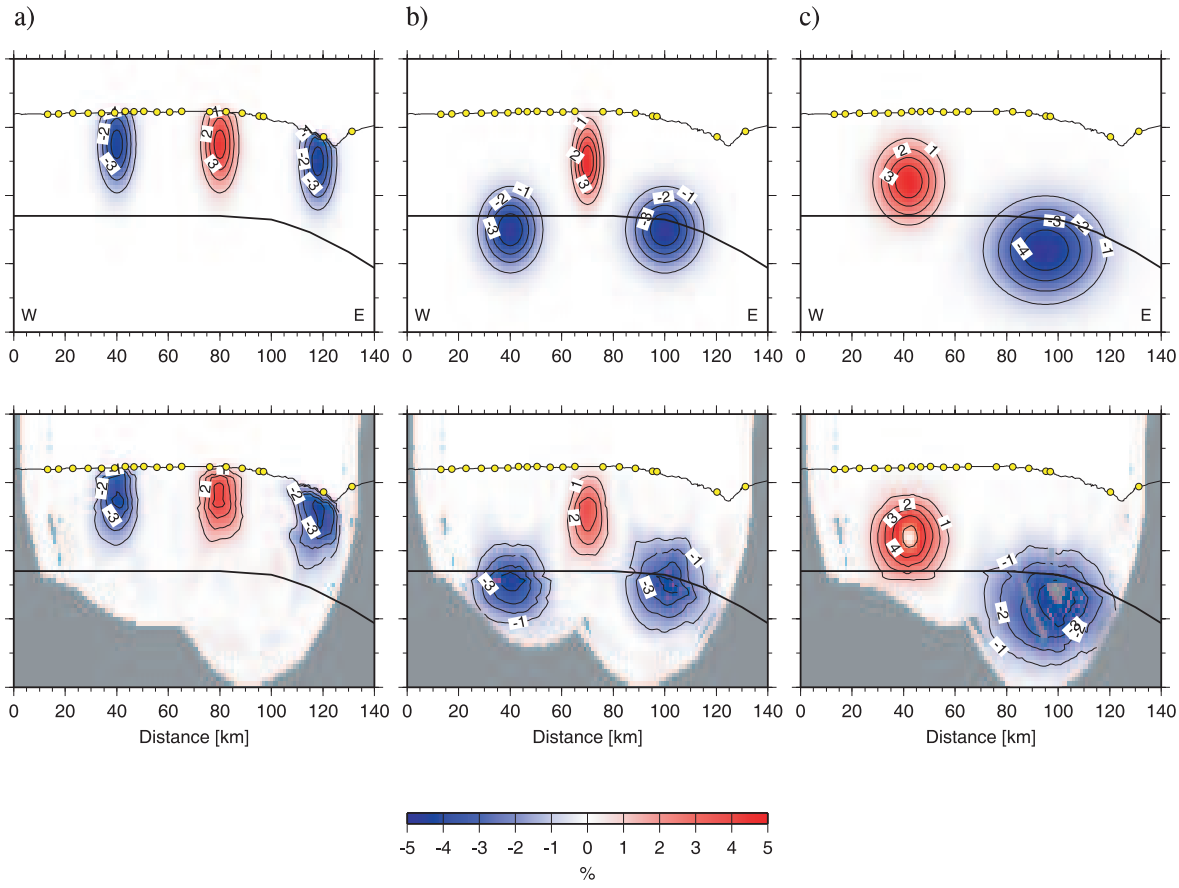

Figure 2.13: Results of the resolution tests for (a) crustal and (b-c) near Moho depths. Velocity anomalies of -5% to 5% in the synthetic models are given with respect to the final model displayed in Figure 2.8.

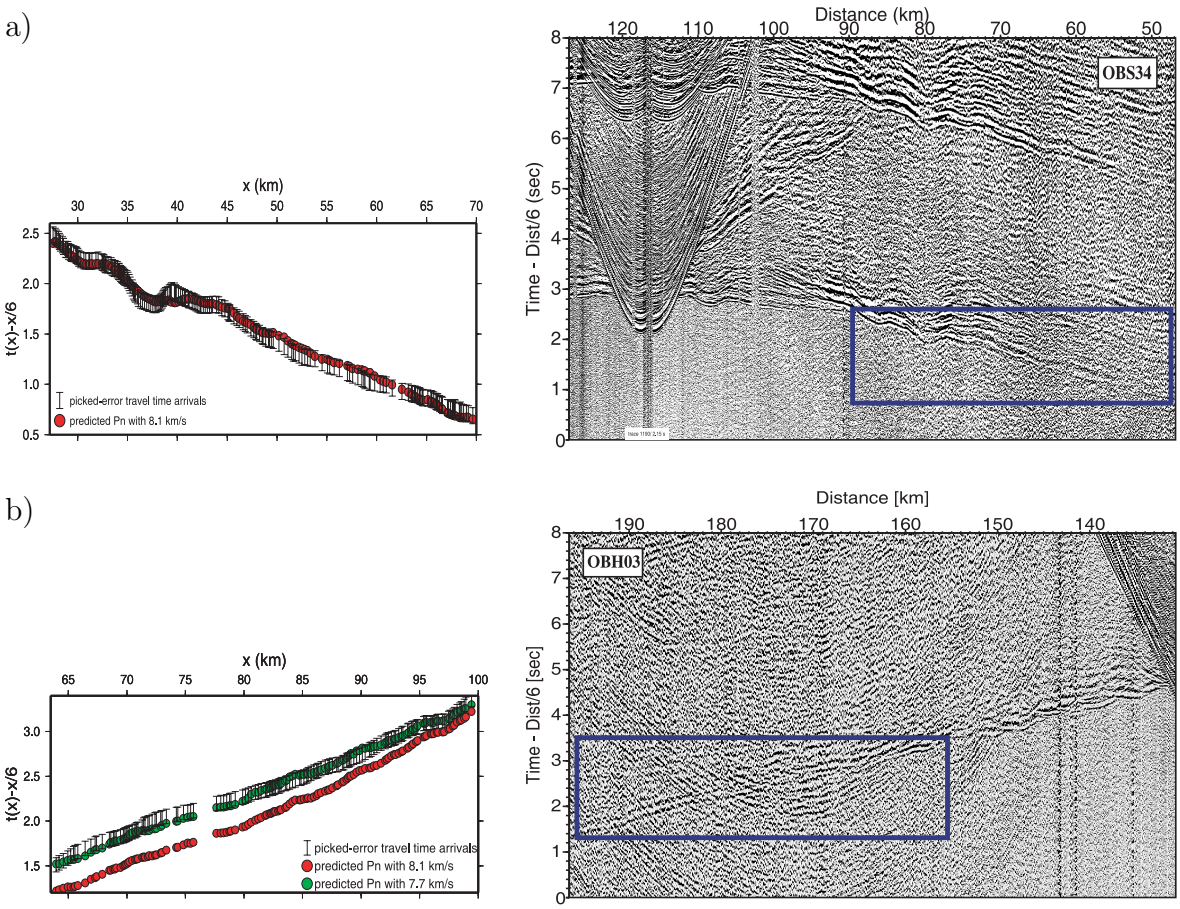

Figure 2.14: Detailed forward analysis of Pn travel times. (a) Trench-ward branch of seismic record section of OBS34; (b) Ocean-ward branch of seismic record section of OBH03.

is also sensitive to the model parameters used to conduct the inversion.

2.5 Discussion

Application of the seismic tomography method to the Middle America subduction zone, offshore of Nicaragua, reveals new structural details within the subducting oceanic slab. The most significant feature of the tomographic image is an extensive zone of reduced velocities in the crust and upper mantle in the near-trench region,

which is an indication for changes of the physical properties consistent with hydration of the subducting oceanic slab, produced after fracturing caused by bending of the subducting slab and perhaps percolation of seawater along the outer rise faults. The systematic change from normal oceanic crust seaward of the outer rise towards reduced velocities in crust and upper mantle indicates that we are observing an evolutionary process. Previous datasets failed to show this characteristic [*Grevemeyer et al.*, 2007].

Multibeam bathymetric coverage of the outer rise region supports the idea that the oceanic plate may become pervasively fractured prior to subduction [*Masson*, 1991; *Kobayashi et al.*, 1998; *von Huene et al.*, 2000]. A detailed study on the relationship between bending related faulting at trenches and intermediate-depth seismicity along segments of Middle America and Chile trenches shows that the distribution of nodal planes of the intermediate-depth events are remarkably similar to the orientation and dip of the bending-related faults, for each segment of the study area, and therefore supports the model where the outer rise faults are reactivated at depth [*Ranero et al.*, 2005]. The depth down to which the faults cut into the crust or mantle is poorly known, because the centroid depth of earthquakes is difficult to determine for shallow events occurring below the oceans [e.g., *Yoshida et al.*, 1992], though detailed waveform inspection of Central American trench-outer rise earthquakes suggest that events of M>6 cut ∼15 km into the mantle [*Lefeldt and Grevemeyer*, 2008]. However, multichannel seismic reflection images acquired offshore of Nicaragua show a pervasive set of trenchward dipping features that cross the crust and extend into the mantle to depths of ∼20 km below the seafloor [*Ranero et al.*, 2003]. Additionally, the same images show that the number of faults and their offsets increase towards the trench axis, which is in agreement with our model, where we find an increase in amplitude and extent of the velocity anomalies as one approaches from the outer rise to the trench. Heat flow data from the Nicaragua trench suggest that faulting of the trench-ocean slope reactivates a vigorous hydrothermal circulation system in the incoming plate. Heat flow decreases towards the trench and hence indicates that seawater mines heat [*Grevemeyer et al.*, 2005]. Interfingering between an upper crustal hydrothermal circulation system and faults cutting down to mantle depth may facilitate migration of seawater along the fault to reach and hydrate the uppermost mantle.

Reduced crustal velocities at the trench can be explained by both hydrothermal alteration and the effect of crustal cracks and fissures on seismic velocity. An increase

in fracture porosity just by a few percent may have a significant impact on the seismic velocity structure of the crust. The *Kuster and Toksöz* [1974] model for cracks with varying pore geometry was used by *Wilkens et al.* [1991] to study the evolutionary effect of hydrothermal circulation through the flanks of mid-ocean ridge on the seismic properties of the crust. They have investigated basalt velocity-porosity relationships for a wide range of pore sizes. Their efforts concentrated on how seismic velocities can change by the presence of cracks. Their model suggested a pore space modification with crustal age, where low aspect ratio pore spaces (small and thin cracks) are bridged first and then large aspect ratio voids (wider cracks). In this way seismic velocities can easily be increased with a small reduction of effective porosity, because of the control that thin cracks have on velocity. It is likely that plate bending increases the fracture porosity. Due to the geometry of normal faults, it might be reasonable to hypothesize that bending causes low aspect ratio cracks in crust and mantle. Small changes in fracture porosity may therefore explain reduced velocities. However, open cracks and faults in the crust will certainly facilitate fluid migration. Both mechanisms, fracturing and hydration, are therefore related to each other and it might be difficult to separate their effects on seismic properties.

The water content of the lower oceanic crust is, therefore, difficult to constrain. Some estimates have been made for chemically bound water based on the modal mineralogy and seismic properties of oceanic diabase and gabbro samples [*Carlson*, 2003; *Carlson and Miller*, 2004]. Their analysis shows that the H_2O content of diabase dike rocks ranges from 1-3 %, with an average of 1.5 %; gabbros that have velocities typical of the lower oceanic crust (6.7-7.0 km/s) contain 0.2 to 0.7 % H_2O, with a mean near 0.5 %.

Anomalously low velocities of the uppermost mantle rocks of 7.6-7.8 km/s (Fig. 2.14) reveal extensive alteration due to percolation of seawater and serpentinization of mantle peridotite. Based on the model developed by *Carlson and Miller* [2003] that relates the degree of serpentinization and water content of partially serpentinized peridotites to their seismic P-wave velocities, we estimate that the water stored in this region may range from 1.55 to 2.17 wt%, which corresponds to a 12-17 % increase in serpentine content. Considering the effects of fracture porosity, this is, of course, an upper bound on the water content of a hydrated mantle.

Offshore of south-central Chile P-wave velocity of the subducting uppermost mantle

is found to be reduced to ∼7.8 km/s (∼9% serpentinization) [*Contreras-Reyes et al.*, 2007]. The lower anomaly here, compared to the estimates for our study area, or for the Nazca plate at the north Chile trench (∼17% serpentinization) [*Ranero and Sallares*, 2004], is most likely due to the much thicker sediment cover (∼2 km). *Contreras-Reyes et al.* [2007] speculate that hydration in a sedimented trench is caused by fluid inflow through basement outcrops, like seamounts, in the outer rise area that penetrate the thick sediment blanket. However, the water/rock ratio will be much lower and hence we would expect a lower degree of hydration.

A high water content in the subducting lithosphere off Nicaragua is consistent with the measurements of water concentration in olivine-hosted melt inclusions along the Central American arc. *Roggensack et al.* [1997] have found very high water concentrations in mafic melt inclusions at Cerro Negro Volcano in Nicaragua (>6 wt%), the highest in any basaltic liquid on the planet. Central American arc volcanism shows strong regional trends in lava chemistry, which reflects different slab contributions to arc melting. The Nicaraguan volcanic arc shows globally among the highest concentrations of geochemical tracers for oceanic crustal fluid (e.g. boron). Ratios such as B/La, Ba/La and ^{10}Be/Be indicate that subducted slab signal is the greatest in Nicaragua arc, where the dip is the steepest, and decreases towards Costa Rica to its minimum [*Carr et al.*, 1990; *Morris et al.*, 1990; *Leeman et al.*, 1994]. It has been proposed that the stronger slab signal in Nicaraguan, compared to Costa Rican arc lavas, reflects greater amounts of fluid released from the dehydration of more extensively serpentinized slab mantle [*Rupke et al.*, 2002.]. It should be noted that the Nicaraguan slab, relative to the other Pacific slabs, enters the trench at a very steep angle, what might induce deeper fracture penetration in the slab to account for the high fluid fluxes from the oceanic crust [*Kirby*, 1995; *Patino et al.*, 2000].

2.6 Conclusions

A tomographic joint inversion of seismic refraction and wide-angle reflection data collected offshore of Nicaragua yields anomalously low seismic P-wave velocities in the crust and uppermost mantle of the subducting Cocos Plate. Seismic velocities of the

subducting lithosphere change systematically from seaward of the outer rise towards the trench, indicating an evolutionary process.

Seaward of the outer rise bulge, where the plate is still not affected by the bending stresses, velocities in the crust and upper mantle are typical for mature unaltered oceanic lithosphere. However, as the plate approaches the trench, velocities decrease and the low-anomaly zone increases both in extent and amplitude. This velocity trend coincides with the multi-channel seismic reflection (MCS) data acquired offshore of Nicaragua, which shows an increase in the number of bending related faults and their offsets towards the trench axis.

Reduced crustal and upper mantle velocities at the trench are most likely caused by both hydrothermal alteration and an increase in fracture porosity. This cracks have a strong impact on seismic properties.

In the close vicinity of the trench axis upper mantle velocities are in the range 7.6-7.8 kms^{-1}, which is 5-7% lower than the ∼8.1-8.2 kms^{-1} found seaward of the outer rise. As the degree and impact of fracture porosity is unknown, an estimate of 12 to 17% for an increase in serpentine content in the uppermost 3-4 km of the mantle is only an upper bound on the degree of hydration.

The anomalously low velocity zone within the Cocos oceanic lithosphere at the trench offshore of Nicaragua supports the idea that pervasive bending related faulting of a subducting slab creates pathways for seawater to reach and react with cold mantle rocks producing serpentine, what implies that deep and widespread hydration (serpentinization) of the incoming lithosphere can occur when the lithosphere is strongly faulted; thus, the subduction zone water cycle is closely related to the crustal structure and hydration of the incoming plate.

Chapter 3

Trench-parallel changes of the seismic velocities of the incoming plate

Previous active seismic experiment offshore of Nicaragua conducted during the research vessel *Sonne* cruise SO173-1 [*Ivandic et al.*, 2008] has revealed evolutionary changes in the seismic structure of the subducting Cocos lithosphere at the trench, what has been explained as being due to the bending related faulting and hydration (serpentinization) [*Ranero et al.*, 2003]. So far there is a little direct evidence that serpentinization is a common process in subducting lithospheres at subducting plate boundaries. One of the objectives of the Meteor cruise M66 Leg 4a was to conduct seismic profiles parallel to the trench offshore of Nicaragua, in order to reveal lateral changes of the seismic properties of the slab approaching the trench and to confirm the speculation that serpentinization is a common process offshore of Nicaragua. The two seismic profiles, p01 and p02, were acquired in the area northwest of the previous profile p50. The profile p01 runs along the trench axis and the profile p02 runs approximately 60 km seaward of the profile p01. The bathymetry map offshore of Nicaragua shows that the outer rise faults here extend even further seaward of the trench than in the southern region, what could be an indication for steeper subduction, and thus more pervasive faulting and hence hydration.

3.1 Tectonic settings

The study area of the cruise M66-4a is located offshore of northern Nicaragua seaward of the Middle American Trench, where the Cocos plate subducts beneath the Carribbean plate with a rate of about 91 mm/yr [*DeMets et al.*, 1990] in a northeasterly direction. The topography of the incoming plate reveals that seafloor spreading and magnetic anomalies off Nicaragua strike almost parallel to the trench axis [*Barkhausen et al.*, 2001]. A subducting ∼24 Myr old Cocos lithosphere formed at the East Pacific Rise (EPR), is pervasively faulted with offsets of up to 500-700 m on back-tilted normal faults [*Kelly and Driscoll*, 1998]. This is possibly associated with extensional tectonics caused by the flexure of the subducting crust. Multi-channel seismic reflection data suggest that the faults cut the lithosphere down to 18-20 km depth. Beneath Nicaragua, Cocos plate dips steeply (up to 84 $^\circ$ between 100-220 km depth), as indicated from regional seismological observation [*Protti et al.*, 1995]. The offsets decrease to <200 m as the plate approaches Nicoya Peninsula and the maximum depth of the seismicity gradually becomes shallower from Nicaragua (∼200 km) to southern Costa Rica (∼45 km). Local swath bathymetry data [*Ranero et al.*, 2003] show that offshore of northern Nicaragua the system of half-grabens bordered by faults parallel to the trench is more prominent and wider than anywhere else in the region (Fig. 3.1). The outer rise network, which was deployed over a time period of 33 days in July and August 2003, detected high seismicity rate with ∼3 local microearthquakes per day, what is consistent with the topography and indicates strong faulting in the incoming oceanic lithosphere [*Grevemeyer et al.*, 2007].

3.2 Seismic experiment and data

The two wide-angle and refraction profiles, p01 and p02, were conducted in November 2005 during the research vessel Meteor 66-4a cruise (Fig. 3.1). They were conducted seaward of the trench in the outer rise area offshore of Nicaragua and northwest of the previous profile p50. The instruments were deployed at intervals between

4.5 and 9 nm. Four GI-Guns for high-resolution surveys with a generator volume of 250 cinch and an injector volume of 105 cinch were used for shooting along the lines. They were fired at intervals of 60 s, which at speed of 4.5 kn results in an average spacing of 130 m. Figures 3.2-3.5 show examples of the data quality available for interpretation. Twelve ocean bottom seismographs (OBS) and ocean bottom hydrophones (OBH) were deployed along both profiles p01 and p02.

The profile p01 is 120 km long and runs parallel to the trench axis. As the profile p01 intersects the trench at 11 $^{\circ}$N, ending in the margin wedge at its northwestern part, one station deployed on the top of the margin wedge was excluded from the modeling. The 120 km long profile p02, with the same orientation as the profile p01, is located $\sim$60 km seaward of the trench axis. Data passed an anti-aliasing filter of 50 Hz and were continuously recorded with a sampling rate of 200 Hz on all OBH and OBS stations. The data were played back and split into single shot records stored as a receiver gather in SEG-Y format. The instruments were deployed by free fall, using Global Positioning System (GPS) for drop-point positioning; instrument locations were further constrained using water-path travel times from the shots collected while the ship was navigated with GPS. Spectral analysis and filter tests show that the seismic energy is in a band ranging from 5 to 30 Hz. We ran this test for both near-offset and far-offset traces and chose a time- and range-dependant bandpass filtering approach. In addition, amplitudes were multiplied by distance to partly compensate the spherical divergence, simultaneously showing the level of both seismic signal and ambient noise.

The one-dimensional reference velocity models were, like in the previous modeling of the profile p50, based on the crustal structure gained from the results of the presite survey work of Ocean Drilling Program (ODP) Leg 206 in the Guatemala Basin westward of Nicaragua [*Wilson et al.*, 2003], which should represent a 'normal' unaltered oceanic lithosphere. The thickness of the upper crust is $\sim$1.5 km and its velocities range from 4.5 to 5 kms^{-1}. Lower crustal velocities increase from 6.8 kms^{-1} at the top of the layer to 7.1 kms^{-1} at the Moho boundary. Total crustal thickness is $\sim$5-5.5 km. For the upper mantle rocks we assumed unaltered peridotites with typical velocities of 8.1-8.2 kms^{-1}.

The main aim of this study is to reveal lateral changes in the structure of the oceanic crust and upper mantle that might be associated with bending related faulting and hydration occurring in the outer rise-trench region. In the end, the results would

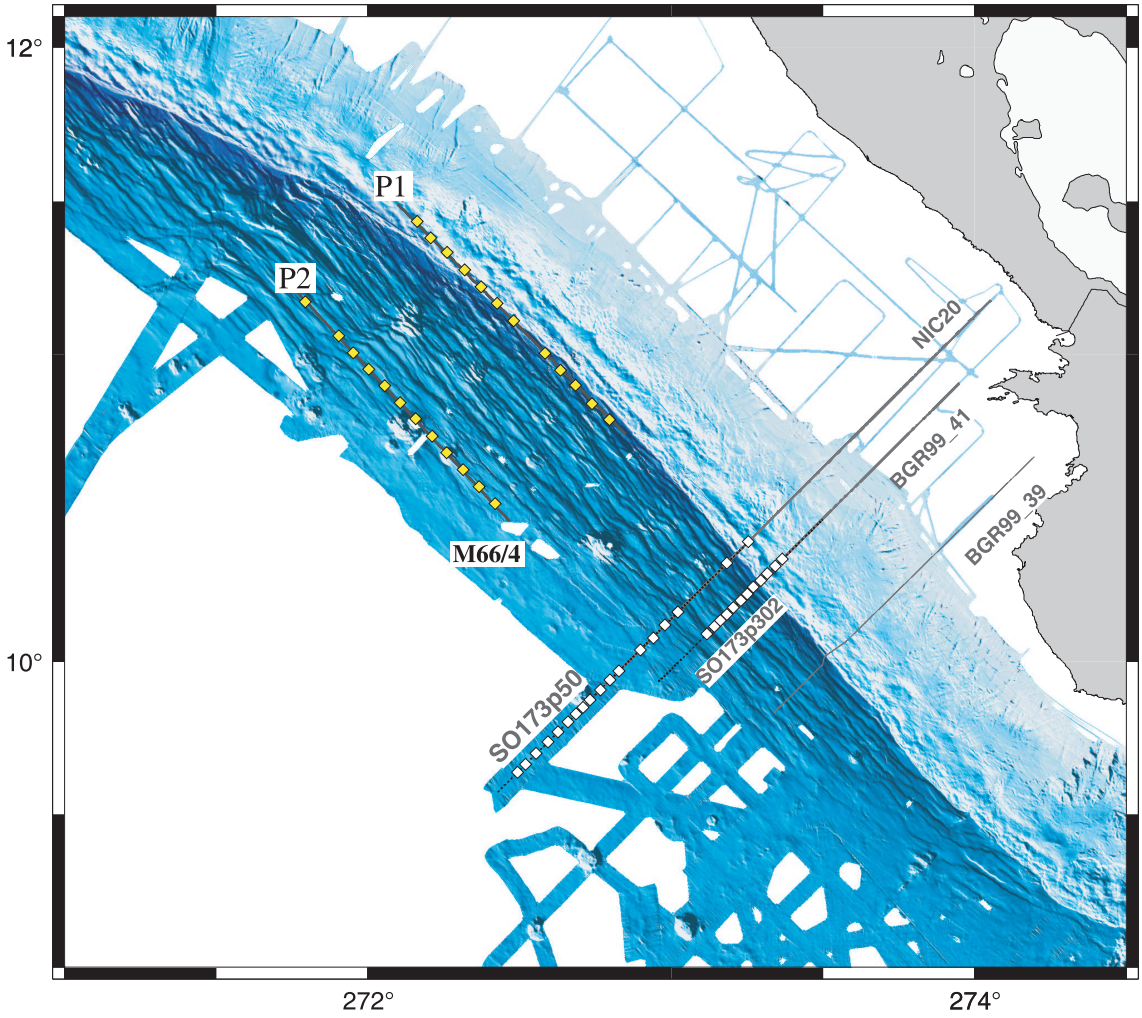

Figure 3.1: Bathymetry map of the offshore region of northwestern part of Nicaragua. Thick solid lines designated P1 and P2 are the seismic profiles conducted during the M66-4a cruise, with instrument locations denoted by squares. The profiles run parallel to the Middle America Trench.

reveal if serpentinization is a common process offshore of Nicaragua.

3.3 Tomographic travel time inversion

The two-dimensional velocity models were obtained using the joint refraction and reflection traveltime inversion code from *Korenaga et al.* [2000], that simultaneously solves for the seismic velocity field and the depth of a reflecting interface. The models are parametrized as sheared meshes hanging from the seafloor topography with 0.5 km lateral nodal spacing and vertical node spacing ranging from 0.05 km at the top to 0.5 km at the bottom of the model. The Moho depth nodes, spaced every 1 km with one degree of freedom in the vertical direction, define the floating reflector.

The data set of the profile p01 consisted of 2658 Pg, 1126 PmP and 834 Pn phases, that were hand-picked from 11 instruments. The model is 110 km long and 20 km deep. The horizontal correlation length values vary from 3 at the top of the model to 8 at the bottom, and vertical correlation lengths increase from 0.1 km at the top to 3 km at the bottom. The depth sensitivity is weighted by a depth kernel weighting parameter (w). For the inversion of Pg and PmP phases we used w =1, which means that velocity and depth nodes are equally weighted. For the final inversion step, where all the phases were included, this parameter had a value of 0.1, allowing more perturbations for the velocity than for the depth. The *rms* travel time misfit obtained for the final model is 56 ms [$\chi 2$= 1.26], significantly reducing the initial misfit of 147 ms. Picked and calculated travel times, and raytracing from two ocean bottom instruments are shown in Fig. 3.2 and Fig. 3.3.

In the inversion of the data set of the profile p02 we used similar parametrization. The horizontal grid spacing is 0.5 km, and vertical grid nodes are 0.05 km distant at the top of the model and about 0.6 km at the bottom. The horizontal correlation lengths range from 3 at the top to 7 at the bottom, and the vertical correlation lengths are the same like in the profile p01. In total 2855 Pg, 1124 PmP and 1189 Pn were handpicked from 12 stations and inverted. In total 5 iterations were enough to obtain a good fitting between the observed and calculated travel times with the final *rms* of 57 ms [$\chi 2$= 1.08]. Picked and calculated travel times, and raytracings from two ocean

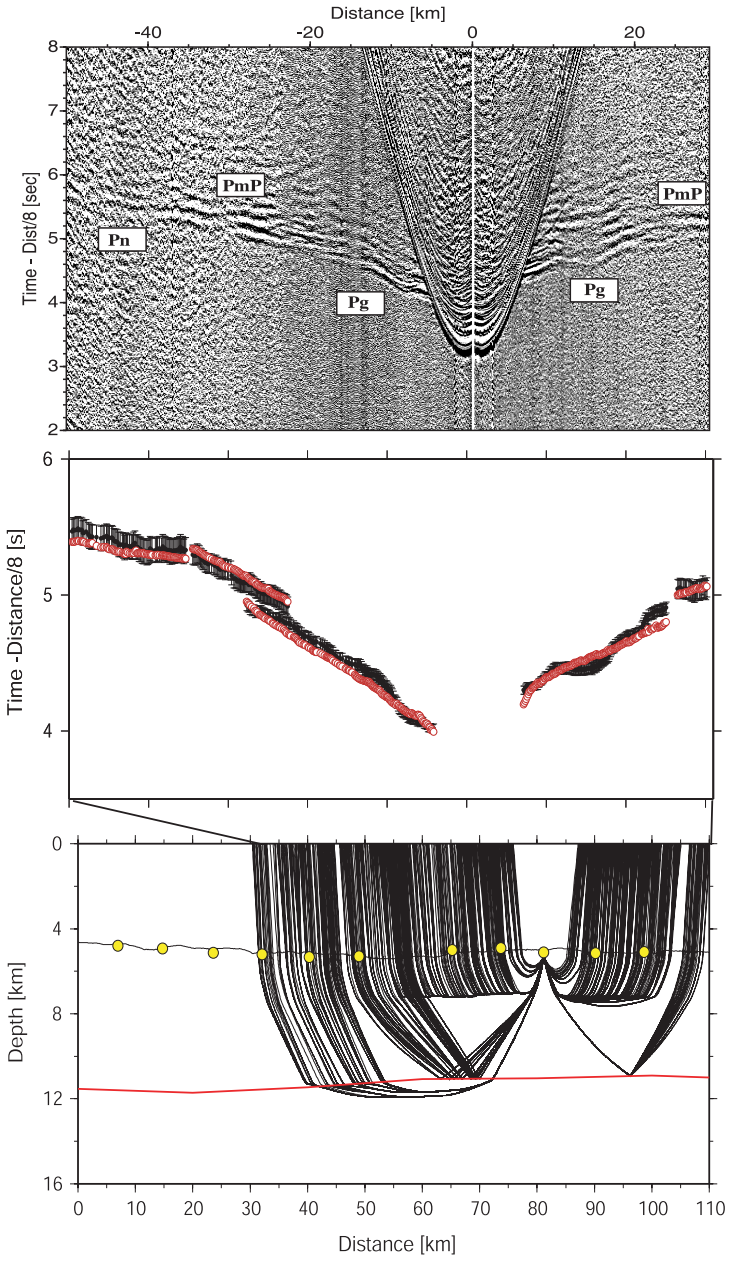

Figure 3.2: Observed seismic record sections from selected instruments from the profile p01.Data have been reduced to 8 km/s and band-pass filtered between 5 and 30 Hz. Wide-angle data examples from the profile p01 are shown for OBS 35 and OBS37 . Picked travel times (solid circles with error bars) and predicted travel times (red circles) for Pg, PmP and Pn phases are shown in the middle plots. Corresponding ray paths are plotted at the bottom. OBS 35.

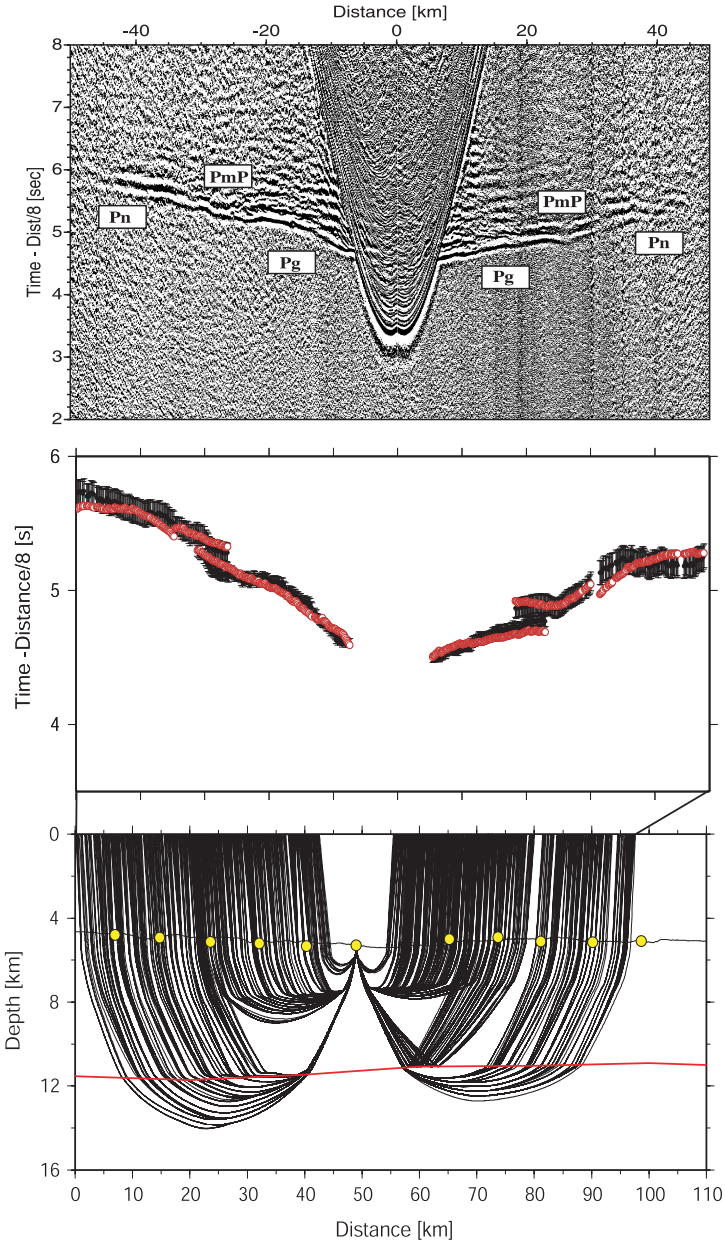

Figure 3.3: Continued. OBS 37.

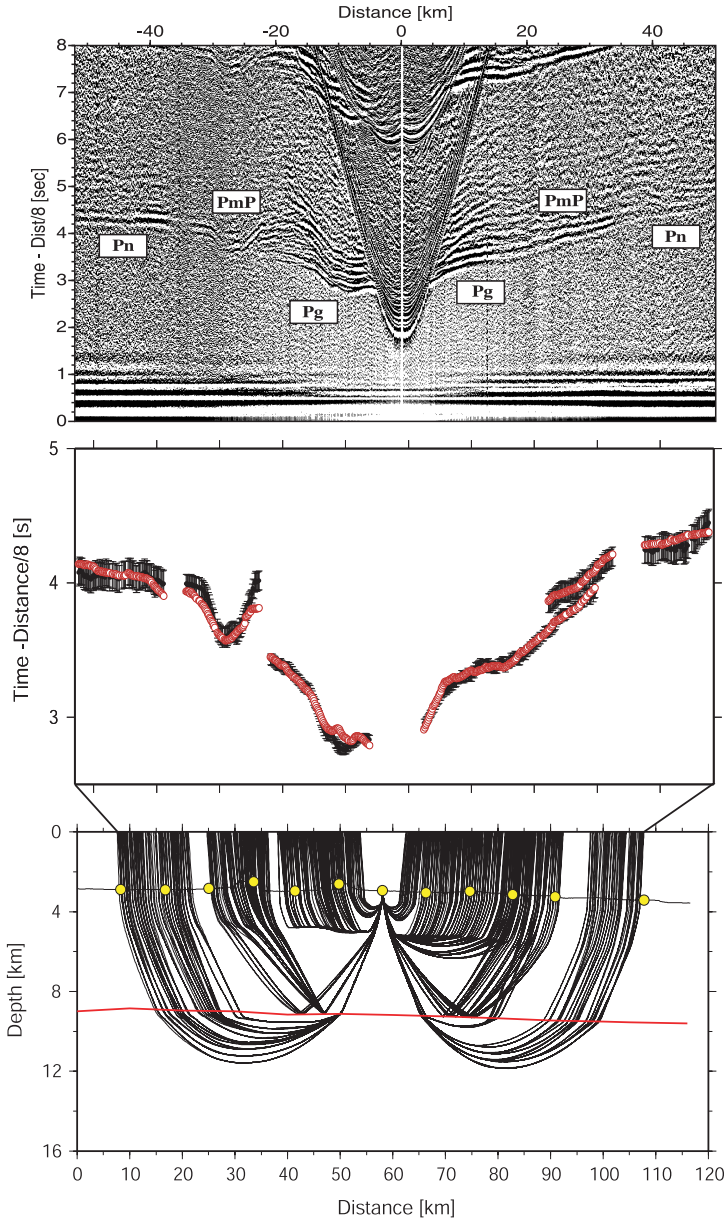

Figure 3.4: Same as in the Figures 3.2 and 3.3 for profile p02. OBH 27.

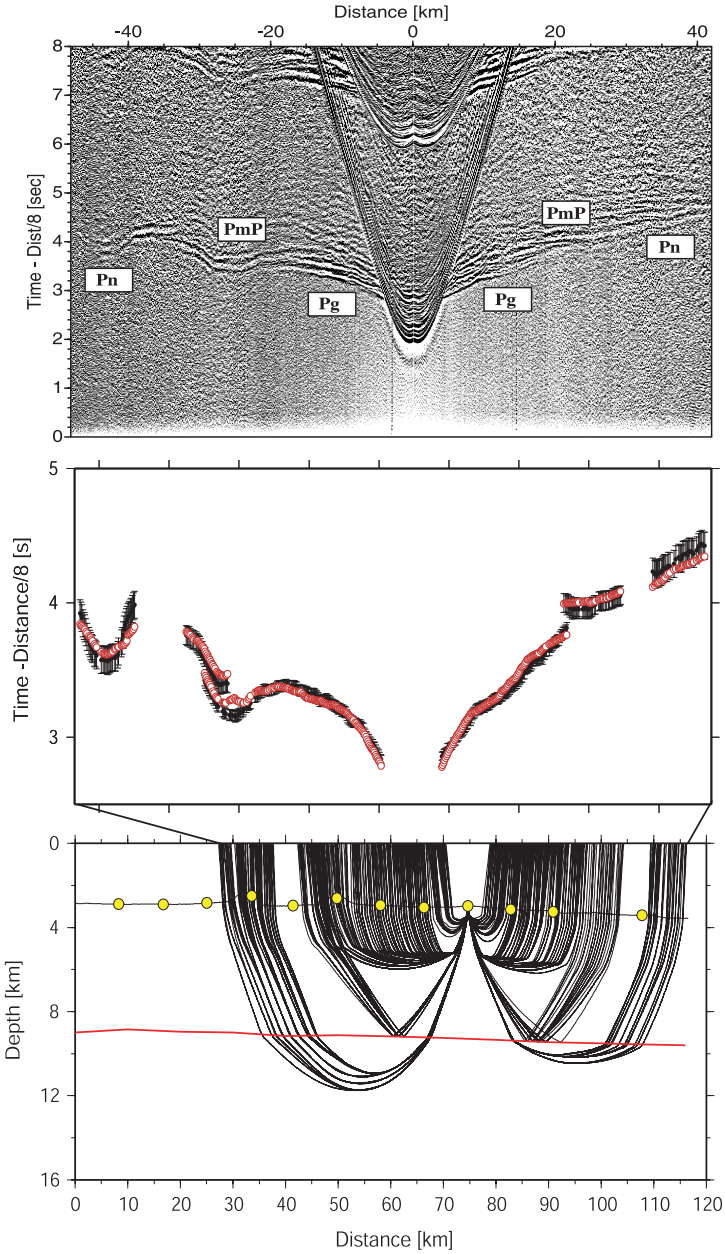

Figure 3.5: Continued. OBH 43.

bottom instruments from that profile are shown in Fig. 3.4 and Fig. 3.5.

3.4 Seismic structures

The crustal and upper mantle structures along the two profiles were obtained by modeling intracrustal refractions (Pg), Moho reflections (PmP), and upper-mantle refractions (Pn). The seismic structures along the two profiles are quite similar. The oceanic crust is typically constituted of two primary layers: the upper layer with large velocity gradients ($\sim$1 kms^{-1}km^{-1}), and a thicker lower layer, considered to be the lower oceanic crust, is characterized by both a higher P-wave velocity and a much smaller vertical velocity gradient (0.1-0.2 kms^{-1}km^{-1}). The crust in this region is about 5.6-5.8 km thick. The sediment thickness of $\sim$400-500 m is quite uniform along the lines, except in the $\sim$ 30 km of the northwestern part of the profile p01, which extends into the lower continental slope, and where it is up to $\sim$ 500 m larger. The velocity of the sediment cover ranges from 1.65-1.9 kms^{-1}. The two-dimensional P-wave velocity model of the profile p01 with the reflector geometry obtained after 5 iterations is shown in the Figure 3.6a. The crustal and upper mantle velocities are strongly reduced compared to velocities expected for $\sim$24 Myr old mature oceanic lithosphere [e.g., *White et al.*, 1992; *Carlson*, 1998; *Grevemeyer and Bartetzko*, 2003], indicating alteration in seismic and chemical properties of the rocks. Velocities in the layer 2 increase from 3.5-3.8 kms^{-1} at the top to 5.6-5.7 kms^{-1} at the boundary with the layer 3. Reduced velocities are also typical for the lower oceanic crust and range from 6.4 kms^{-1} at the top to 6.6-6.7 kms^{-1} at the bottom just above the Moho. Below the Moho the upper mantle rocks with velocities of 7.3-7.5 kms^{-1} are found along the entire profile.

The final velocity model of the profile p02 is shown in the Figure 3.7a. Upper crustal velocities range from 3.8-4.0 kms^{-1} at the top to 5.6-5.8 kms^{-1} at the bottom. The velocities at the top of the lower crust are 6.4-6.5 kms^{-1} and they increase to 6.7 kms^{-1} at the Moho boundary. Bellow the Moho upper mantle velocities are strongly reduced and have values of 7.3-7.5 kms^{-1}. The p02 line runs across the two seamounts in its southeastern part. Bellow them we observe crustal seismic velocities by 0.2 kms^{-1}

a)

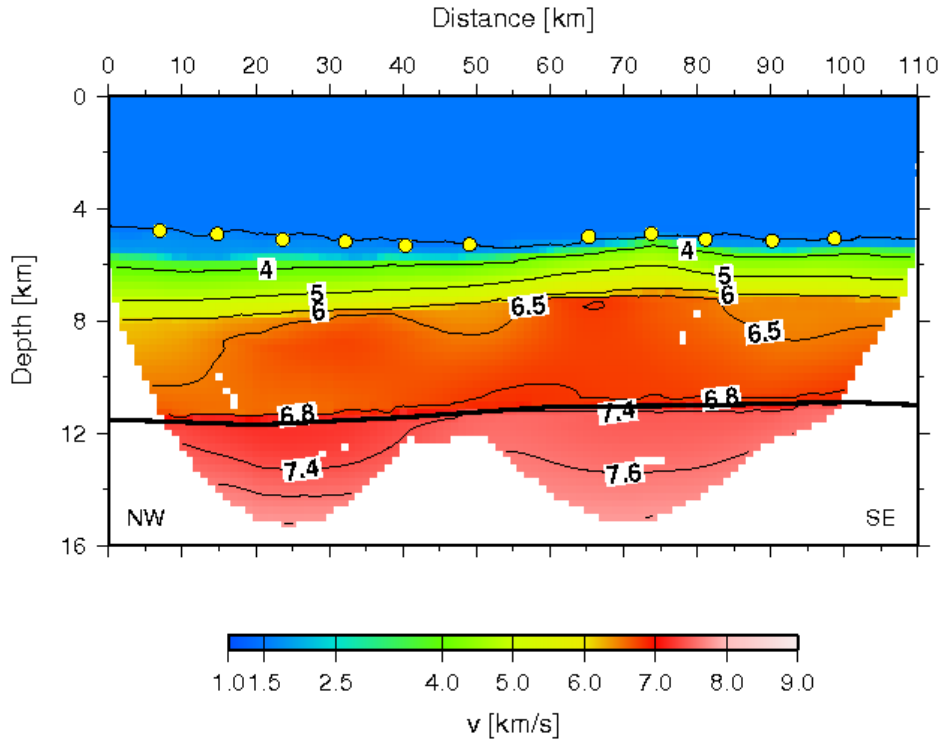

b)

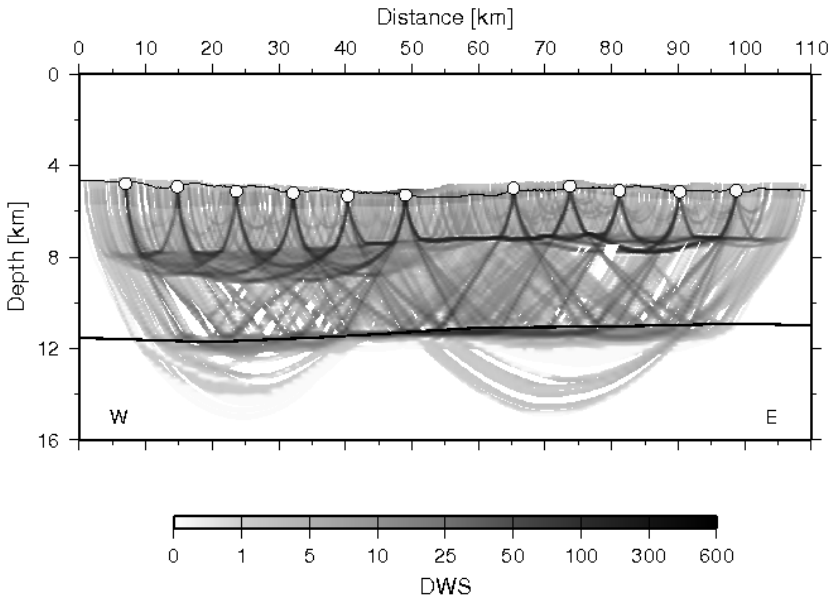

Figure 3.6: a) P-wave velocity model for the profile p01; b) Derivative weight sum.

a)

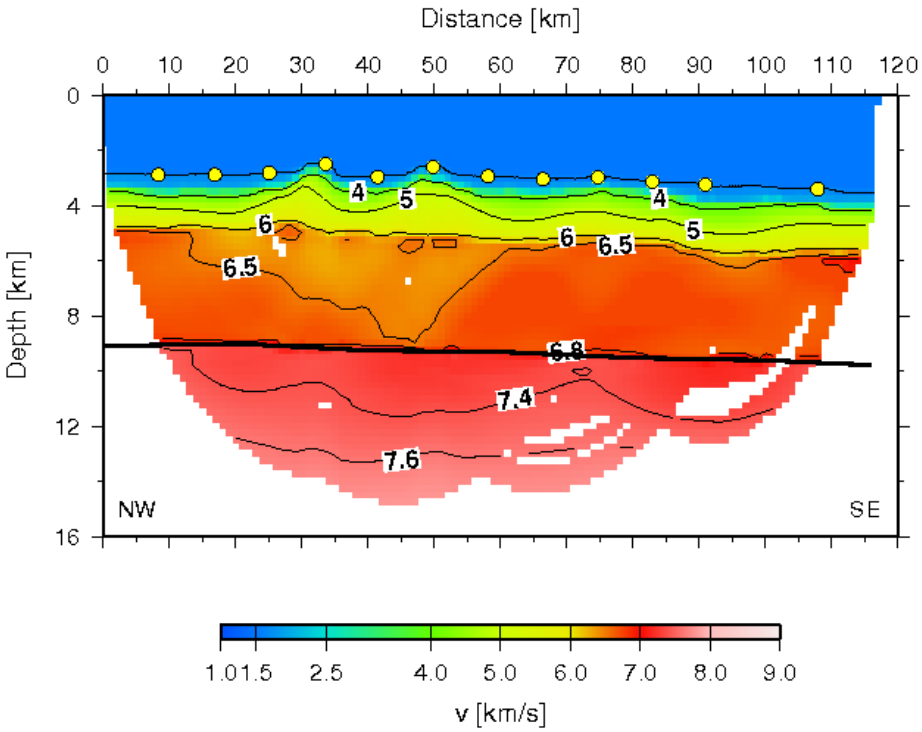

b)

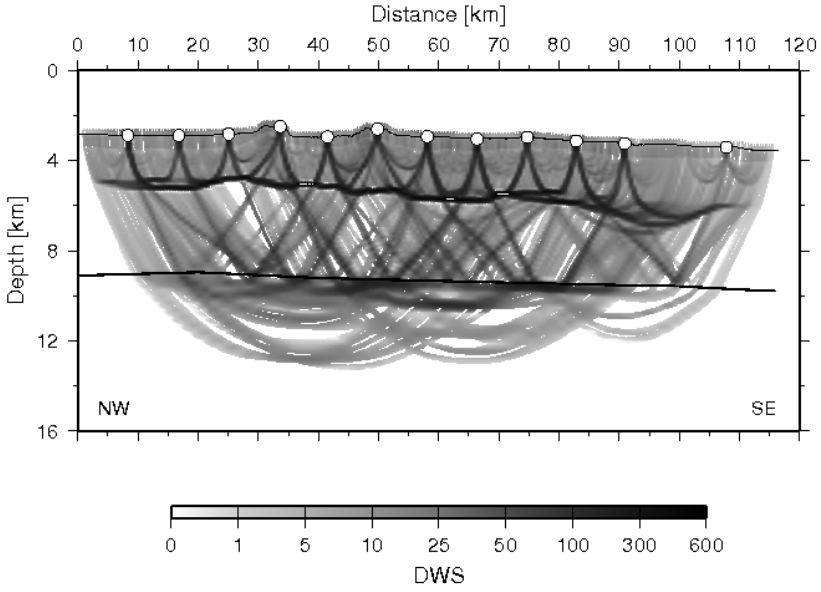

Figure 3.7: a) P-wave velocity model for the profile p02; b) Derivative weight sum.

lower than anywhere else along the profile. This considerable velocity decrease can be nicely recognized by following the isolines. The isovelocity line of 6.3 kms^{-1}, which runs at the top of the layer 3 along the line, starts to dip in the vicinity of the two seamounts and bellow them even reaches the Moho depth. This feature indicates rocks with higher porosity developed in this area.

Alterations in the seismic structures are uniformly present along both profiles. This has been interpreted to be due to the pervasive faulting and hydration of the subducting Cocos lithosphere offshore of Nicaragua caused by high bending stresses the plate experiences in the trench-outer rise area.

3.5 Resolution and Uncertainty Tests

The sensitivity of our final model to different input models we estimated by averaging the solutions of 100 Monte Carlo realizations [e.g. *Korenaga et. al.*, 2000]. The degree of dependence of the final solution on the starting model can be assessed by conducting a number of inversions with a variety of randomly generated initial models and noisy data sets. If all models have the same probability and the starting models cover the full region of non-null probability within the parameter space, the a posteriori covariance of the solutions obtained can be interpreted as a statistical measure of the solution uncertainty [*Tarantola*, 1987]. To estimate the velocity and Moho depth uncertainty a set of 10 1-D reference models were constrained for both profiles by randomly varying the Moho depth (σ = 0.5 km) and the velocity (σ = 0.3 km/s) and inverting them with 10 noisy data sets constructed by adding random common phase errors (±50 ms) and common receiver errors (±50 ms) to the initial data set [*Korenaga et al.*, 2000]. In the end the mean deviation of all realizations describes the uncertainty of the velocity model [*Tarantola et al.*, 1987].

Velocity uncertainty is lower than 0.1 kms^{-1} within most parts of the models, both in the crust and upper mantle, indicating that velocity anomalies are well recovered (Fig. 3.8). Moho depth uncertainty along the major part of the profile p01 is not higher than 0.15 km. Maximum values of 0.2-0.25 km are found in the part which extends into the lower continental slope area. Uncertainty of the Moho depth along the entire profile

a)

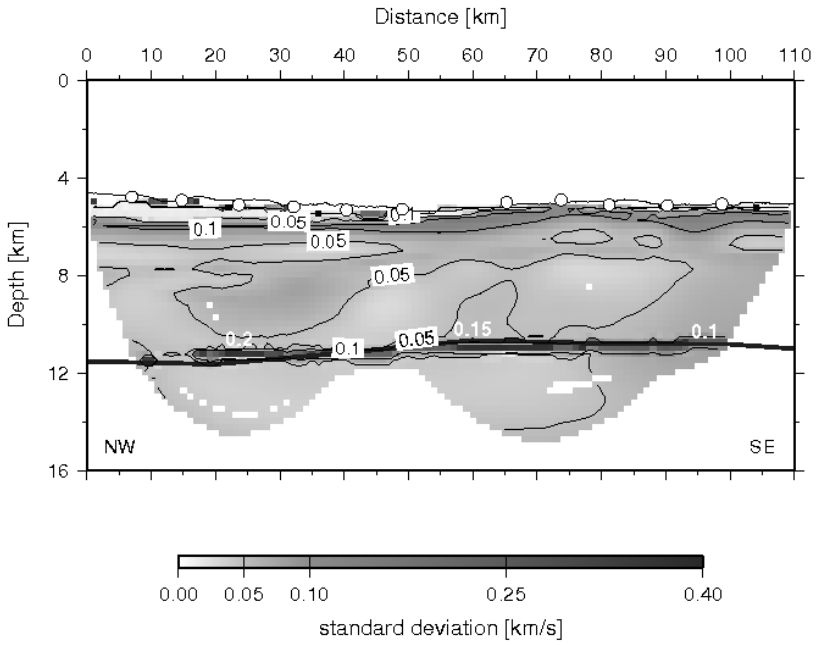

b)

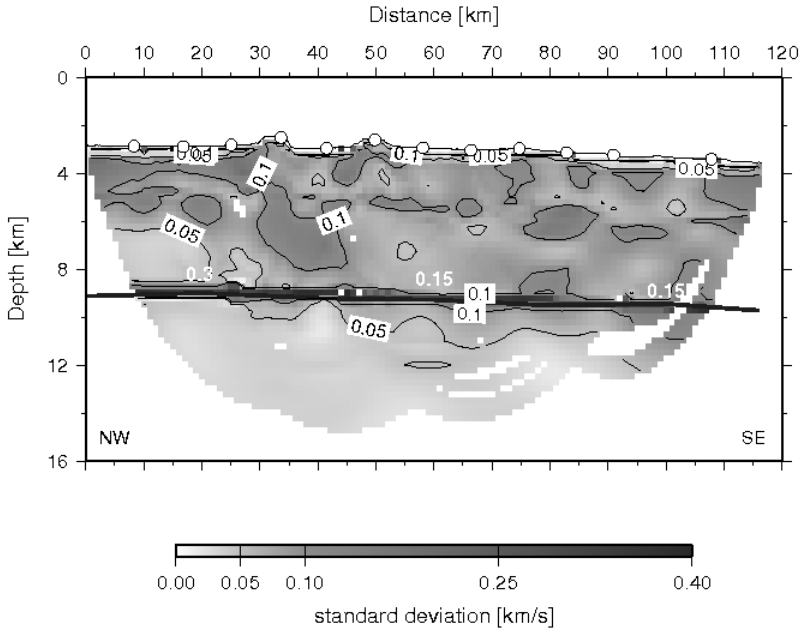

Figure 3.8: Velocity and Moho depth uncertainties estimated from the Monte Carlo analysis for a) profile p01 and b) profile p02

p02 is as low as 0.15 km, except for its northwestern edge, where it reaches 0.3 km. The derivative weight sum [DWS] values, which describe the relative ray density near a given velocity node, providing crude information on the model resolution [*Toomey and Foulger*, 1989], are, for both velocity models, shown in Figures 3.6b and 3.7b.

In order to assess whether our data sets can resolve different velocity anomalies we performed a series of resolution tests. Like in the resolution tests of the p50 model (Chapter 2), synthetic models were constructed using the final velocity model with and without ±5% Gaussian anomalies of different sizes placed at various depths. Synthetic noise with *rms* amplitude of 0.05 s is added to the synthetic travel times obtained from the perturbed velocity model to simulate the addition of actual travel time variation. The results reveal good resolution in both models. All the velocity anomalies are well recovered, what proves that the ray coverage of our data is sufficient to resolve features in the uppermost ∼4 km of the mantle, confirming that the reduced velocities within the upper mantle can be resolved.

Owing to the high density of Pg rays, the reconstructed anomalies within the crustal layer in both p01 and p02 models are remarkably well resolved with the same lateral extent as the original ones [Figures 3.9 and 3.10]. The weaker amplitude and vertical and lateral smearings of some of the anomalies in the upper mantle and near the Moho boundary are related to the lower ray coverage at these depths. Thus, the total depth extent of that anomaly could not be fully resolved.

3.6 Discussion

The reduced seismic velocities in the crust and upper mantle we are observing along the two profiles running parallel to the trench axis indicate alteration in chemical and physical properties of the subducting lithospheric rocks offshore of northern Nicaragua. Multibeam bathymetry data of this area reveal prominent faults which extend further seaward than in the previous study area, where the profile p50 was acquired. This indicates that the plate is subjected to large bending stresses, what could induce deep normal faulting and widespread hydration (serpentinization) of the crustal and upper mantle rocks. P-wave velocity models of the crust and upper mantle along

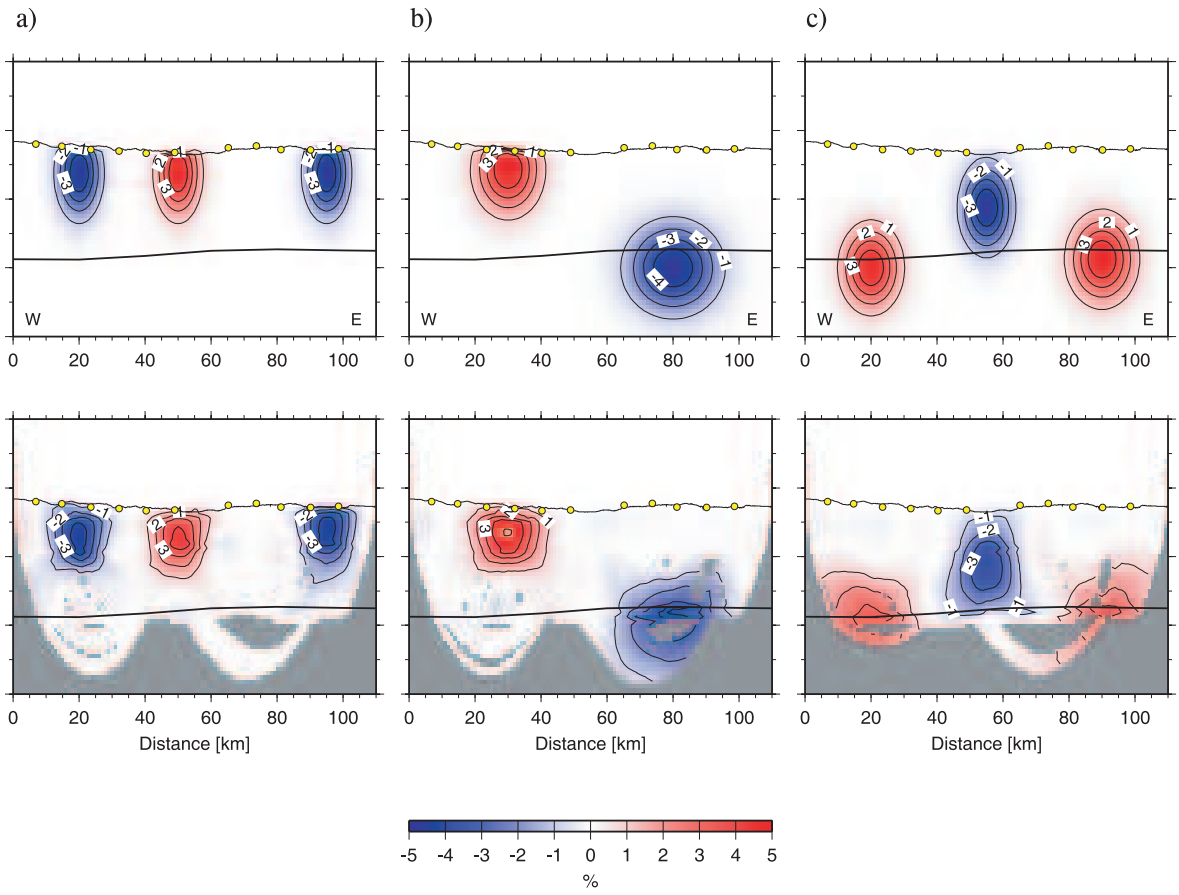

Figure 3.9: Results of the resolution tests for profile p01.(a) shows crustal anomalies and (b) anomalies at Moho depths and in the upper mantle. Velocity anomalies of -5% to 5% in the synthetic models are given with respect to the final model displayed in Fig. 3.6 a)

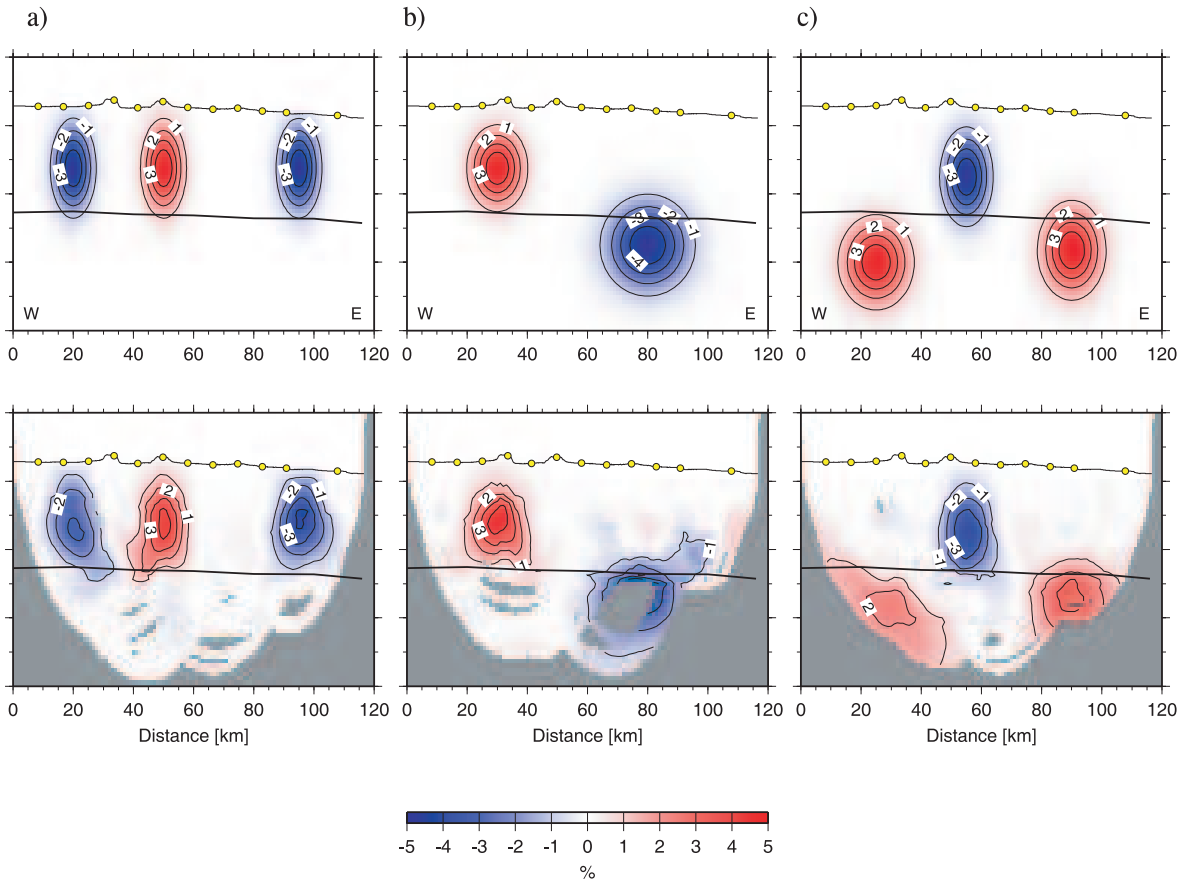

Figure 3.10: Results of the resolution tests for profile p02. (a) shows crustal anomalies and (b) anomalies near Moho and in the upper mantle. Velocity anomalies of -5% to 5% in the synthetic models are given with respect to the final model displayed in Fig. 3.7 a)

the two profiles indeed support this hypothesis. Crustal velocities are reduced by up to 15-20 % at the top of the basaltic layer and by up to 8% at the bottom. The lower gabbroic layer is characterized by a velocity reduction of ∼5%. Upper mantle velocities of 7.3-7.5 kms^{-1} are by 8-10 % lower than those found seaward of the outer rise (Chapter 2). These velocity anomalies are uniform along the profiles (Fig. 3.11) and stronger than those found in the p50 velocity model, what coincides with the rougher seafloor topography in this area. Furthermore, the profiles are oriented parallel to the trench, and thus seismic waves are affected by much denser network of faults and fractures.

A certain degree of azimuthal seismic anisotropy could also arise from lattice preferred orientation of minerals (LPO). Tectonic plate motion is thought to cause solid-state plastic flow within the underlying upper mantle and accordingly lead to the development of a lattice preferred orientation of the constituent olivine crystals, which stabilizes during spreading and attenuates during subduction. The mechanical anisotropy that results from such a preferred orientation typically produces a direction of maximum seismic wave velocity parallel to the plate motion direction. Azimuthally varying Pn wave velocities were first recorded in the shallow upper mantle beneath Hawaii [*Hess*, 1964], showing that surface waves travel ∼10% faster in the E W direction than in the N S. The degree of compressional wave anisotropy depends also on spreading rates, so while 3% to 4% have been found in the slow-spreading North Atlantic [*Keen and Tramonti*, 1970; *Gaherty et al.*, 2004], higher 7% has been observed near the fast spreading East Pacific Rise [*Dunn et al.*, 2000]. Much lower degree of Pn anisotropy has been found offshore of Southern Central Chile, in the trench-outer rise area of the oceanic Nazca plate created at the fast spreading Chile Rise. Comparison of the uppermost mantle velocities at the crossing points of perpendicular profiles revealed ¡2% degree of Pn anisotropy [*Contreras-Reyes et al.*, 2008]. A lower degree of anisotropy that has been found in the outer-rise environment or in ophiolites [e.g. *Schmitt et al.*, 2007] has been proposed to reflect an increased degree of serpentinization, because of the random orientation of serpentine minerals which replace preferentially aligned olivines.

At lower crustal depths lithostatic pressures would minimize the effects of cracks on the velocities by closing the intergranular pore spaces and fracture openings, thus providing information about the preferred mineral orientation. Water percolation would, however, prevent crack closure, what makes evaluation of their separate effects on the

seismic properties more difficult.

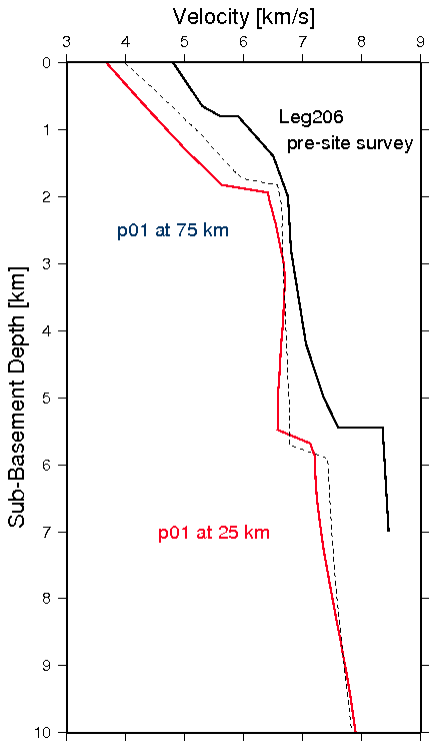

Figure 3.11: Velocity-depth profiles at two selected locations along the profile p01 and 1D reference velocity model from the presite survey work of ODP Leg 206 in the Guatemala Basin.

An another distinctive feature in the model of the p02 profile is a significant velocity reduction in the crustal layer beneath the two seamounts. Velocities here are reduced by ~ 0.2 kms^{-1} compared to the surrounding crust, what could be an indication for increased porosity here, and hence an enhanced water inflow. The anomalous behaviour in the upper and lower crust is confined to the seamount area and extends down to the Moho boundary. This result is in agreement with the hypothesis that seamounts facilitate inflow of seawater into the oceanic crust and might guide hydrothermal circulation between sites separated by large distances [*Fisher et al.*, 2003b]. *Fisher et al.* have found that seawater can flow up to ∼50 km through the crustal rocks before it comes out through an another seamount. Additionally, recent numerical models of coupled heat and fluid transfer showed that seamounts play a significant role in controlling hy-

drothermal circulation throughout the oceanic crust [*Harris et al.*, 2004]. Conductive lithospheric cooling models predict a heat flux of ∼100 mW/m^2 for ∼18-24 Ma oceanic crust underlying the sites [*Stein and Stein*, 1994]. Heat flux data, however, show that heat flux through the seafloor created at the East Pacific Rise is anomalously low, with values in between 20-40 mW/m^2 [*Langseth and Silver*, 1996; *Fisher et al.*, 2003a], which is only ∼30% of the values predicted by these models. This anomalously low heat flux is attributed to effective hydrothermal cooling of the upper oceanic crust, which is facilitated by seamounts and basaltic outcrops [*Silver et al.*, 2000]. In South Central Chile, the trench basin is heavily filled with up to 2 km of sediments, and hydration of the oceanic lithosphere in the outer rise area is, therefore, less vigorous. Thus, low compressional velocities and anomalous low heat flow values observed in the outer rise here, suggest that infiltration of seawater in this area is happening through basement outcrops, which penetrate the thick sedimentary blanket (and then further through extensional normal faults) [*Contreras-Reyes et al.*, 2007]. Highly serpentinized mantle within the subducting Cocos slab offshore of Nicaragua would be also consistent with the fact that the Nicaraguan volcanic arc shows globally among the highest concentrations of geochemical tracers for oceanic crustal fluid (e.g. boron). Ratios such as B/La, Ba/La and ^{10}Be/Be indicate that subducted slab signal is the greatest in the Nicaragua arc, where the dip is the steepest, and decreases towards Costa Rica to its minimum [*Carr et al.*, 1990; *Morris et al.*, 1990; *Leeman et al.*, 1994]. One interpretation is that Be and B are efficiently removed from the slab by the slab-derived fluids [*Turner et al.*, 1998]. However, the location of the water reservoir is still under debate, as it could reside either in the subducted oceanic lithosphere or in the mantle wedge. [*Tonarini et al.*, 2007] suggest a model in which tectonic erosion, i.e. dragging down of slivers of serpentinized upper plate mantle, is responsible for the occurrence of serpentinite reservoir, 11B-enriched in the forearc by shallow fluids. Previously *Rupke et al.* [2002] have been proposed that the stronger slab signal in Nicaraguan, compared to Costa Rican arc lavas, reflects greater amounts of fluid released from the dehydration of more extensively serpentinized slab mantle [*Rupke et al.*, 2002.].

3.7 Conclusions

After the profile p50 (Chapter 2) has revealed an evolutionary process in the subducting Cocos lithosphere, we have conducted two profiles in the northwestern region offshore of Nicaragua, which were laying parallel to the trench axis. Profile p01 is placed along the trench axis, and profile p02 runs ∼60 km seaward of the profile p01. This geometry system has revealed lateral changes of the seismic properties of the Cocos slab approaching the trench. The seismic velocities of the crust and upper mantle are significantly reduced along the entire profiles. The velocities of the crust are reduced by 0.4-0.7 $kms^{-1}$and upper mantle is characterized by velocities of 7.3-7.5 kms^{-1}. The results presented here confirm the assumption that serpentinization of the upper mantle is a common feature in the subducting lithosphere offshore of Nicaragua. An another interesting feature is a very prominent velocity anomaly in the crust bellow the two seamounts, which are laying on the line p02. Crustal velocity here is reduced by 0.2 kms^{-1} compared to the other parts of the profile, suggesting increased porosity which may enhance water inflow into the upper and lower crust, and perhaps facilitate water migration to mantle depth. Further analysis of the influence of water-filled fractures and microcracks on the seismic properties of the subducting lithosphere, presented in the next chapter, have been done in order to achieve a better overview on the processes that reduce seismic velocities.

Chapter 4

Crustal and Upper Mantle Fracture-Induced Anisotropy

Crack porosity, chemical composition, density and mineral orientation are the most important factors that affect seismic velocity. Our understanding of the anisotropic properties of many rocks is still limited. If stresses are sufficiently large to generate cracks, or to close pre-existing cracks, usually very strong stress- (or crack-) induced anisotropy is induced. The preferential orientation of crack or fracture networks makes the medium azimuthally anisotropic with respect to seismic wave propagation. Compressional waves propagate with different velocities in different directions. As a shear wave travels through an anisotropic medium, the wave is split into two quasi-shear waves: one polarized parallel and one polarized perpendicular to the cracks. The quasi-shear wave polarized parallel to the cracks travels at a higher velocity.

In the Earth's lithosphere, anisotropy may be caused by combined effects of aligned microcracks, shear fabric, layered bedding in sedimentary formations, or highly foliated rocks. In ideal cases, there are two simple styles of alignment in earth materials (horizontal and vertical), and laboratory studies suggest that they give rise to two types of anisotropy. In the horizontal style, or layered case, elastic properties may vary vertically, such as from layer to layer, but not horizontally. Such a material is called transversely isotropic with a vertical axis of symmetry. Waves generally travel faster horizontally, along layers, than vertically. The simplest case of the second type of anisotropy corresponds to a material with aligned vertical weaknesses such as cracks

or fractures, or with unequal horizontal stresses. The brittle failure that rocks experience after a critical stress has been applied, is caused by the nucleation, growth, and microcracks interaction. The growth of microcracks, that are aligned with respect to the principal stress, will cause a mechanical anisotropy of rock [*Costin*, 1987] and the magnitude of the anisotropy provides a measure of crack density. Crack density is an important parameter in rocks. For low crack densities, cracks are generally isolated. As crack density increases, crack interaction takes place resulting in a production of macroscopic fracture. The microcracks accumulation changes the elastic properties of rocks, and hence their seismic velocities. Several effective models of fractured media developed by a number of authors include those based on parallel infinite fractures with linear slip boundary conditions [*Schoenberg*, 1980; 1983], isolated parallel penny-shaped cracks that have the form of oblate spheroids [*Hudson*, 1980; 1981], and partially saturated penny-shaped cracks or hydraulically connected cracks and pores [*Hudson*, 1988; *Thomsen*, 1995; *Hudson et al.*, 1996].

In case of anisotropy which corresponds to a material with aligned vertical weaknesses such as cracks or fractures, elastic properties vary in the direction crossing the fractures, but not along the plane of the fracture. Waves traveling along the fracture direction generally travel faster than waves crossing the fractures. Crustal anisotropy resulting from aligned cracks can be used to determine the state of stress in the crust. In most cases, cracks are preferentially aligned with the direction of maximum compressive stress. In active tectonic areas, such as near faults and volcanoes, anisotropy can be used to look for changes in preferred orientation of cracks that may indicate a stress-field translation. Microcracks within rocks have a significant influence on elastic anisotropy and transport properties. If the crack shapes are idealized as very thin oblate ellipsoids, the modulus of the rock and hence its seismic velocities are calculable in terms of aspect ratios (thickness/length) of the ellipsoids and the elastic properties of the surrounding matrix and fluids [*Budiansky and O'Connell*, 1980]. A number of authors have developed codes for estimating the static anisotropic elastic moduli for rocks with aligned fractures [*White*, 1983; *Schoenberg and Muir*, 1989]. If the crack density is small, the decrease in the modulus also is small and is well understood in terms of the properties of the matrix, the fluid, and the crack geometry. If the crack density is large, the corresponding modulus decrease is large. Thus, variation in elastic moduli and seismic velocities between fault zone and wall rock is a function of fracture

density (ε). Hydrothermal alteration also effects elastic moduli and.seismic velocities, but the changes are much less than those caused by fracturing.

Bending of the lithosphere at subduction zones generates stresses that produce tensional fracturing and normal faulting. The subducting Cocos lithosphere offshore of Nicaragua is characterized by pervasive normal faults which expose the basement. A detailed study on the relationship between bending related faulting at trenches and intermediate-depth seismicity along segments of Middle America and Chile trenches shows that the distribution of nodal planes of the intermediate-depth events are remarkably similar to the orientation and dip of the bending related faults, for each segment of the study area, and therefore supports the model where the outer rise faults are reactivated at depth [*Ranero et al.*, 2005]. There is a growing evidence that intraplate outer rise earthquakes can create pathways for seawater to infilitrate and reach upper mantle, causing extensive hydration of the incoming plate prior to subduction. In this study, where we are attempting to evaluate an impact of fracturing on the mechanical properties of the subducting lithosphere, we assume that the aligned water filled microcracks and fractures are present in the entire crust and in the upper mantle rocks of the subducting oceanic slab, with alignment direction normal to the direction of the maximum tensional stress.

4.1 Seismic velocities in a medium with parallel fractures and aligned cracks - Schoenberg & Douma's model

Fracture porosity is porosity associated with a fracture system or faulting. Fractures themselves typically do not have much volume, but by joining preexisting pores, they significantly enhance permeability. The porosity of a porous medium (such as a rock or sediment) describes the fraction of void space in the material, where the void may contain, for example, air or water. It is defined by the ratio:

$$\phi = \frac{\mathbf{V}_V}{\mathbf{V}_T} \tag{4.1}$$

where V_V is the volume of void-space (such as fluids) and V_T is the total or bulk volume of material, including the solid and void components. Porosity is a fraction between 0 and 1, typically ranging from less than 0.01 for solid granite to more than 0.5 for peat and clay, although it may also be represented in percent terms by multiplying the fraction by 100.

Since cracks in the crust and upper mantle are assumed to be liquid-filled and aligned perpendicular to the direction of minimum compressional stress, the modeling is confined to parallel water-filled cracks. To evaluate dependance of seismic velocities on fractured and cracked media we used a code provided by W. Rabbel at CAU, Kiel, that is based on a model of *Schoenberg and Douma* [1988] for long thin parallel fractures. The code is based on generalized Postma-Backus-Algorithm [*Muir and Schoenberg*, 1989] which calculates effective elastic tensors and seismic velocities for finely layered anisotropic medium, anisotropic background-medium with oriented cracks, as well as for crack-families with different orientations. Voigt and Reuss mixing algorithms and tensor rotations were also applied. *Schoenberg and Douma* considered the fractures as compliant layers. In their model a distributions of parallel cracks is incorporated into the system by representation of layers in the limit of vanishing thickness and stiffness and this elastic medium can be characterized by the compliance matrix. The elastic properties of a rock mass with penetrating, parallel fractures can be then modelled in a manner quite analogous to the layered media illustrated in Figure 4.1. The total thickness of the rock mass is H (in the z-direction), out of which a height H_{fr} is constituted by the fractures. The relative fracture thickness is defined as:

$$h_{fr} = \frac{H_{fr}}{H} \tag{4.2}$$

The vertical fracture strain is

$$\varepsilon_{zz}^{fr} = \frac{\Delta u_z}{H_{fr}} = \frac{1}{\lambda_{fr} + 2G_{fr}} \sigma_{zz} \tag{4.3}$$

The total strain is

$$\varepsilon_{zz} = \frac{\Delta u_z}{H} = \frac{h_{fr}}{\lambda_{fr} + 2G_{fr}} \sigma_{zz} \equiv Z_N \sigma_{zz} \tag{4.4}$$

where Z_N is the normal fracture compliance, defined in the limit when h_{fr} and $\lambda_{fr}+2G_{fr} \rightarrow 0$. The shear strain ε_{xz}^{fr} for the fracture is similarly given by the shear modulus

$$\varepsilon_{xz}^{fr} = \frac{\Delta u_x}{H} = \frac{1}{G_{fr}} \sigma_{xz} \tag{4.5}$$

and the total strain is

$$\varepsilon_{xz} = \frac{\Delta u_x}{H} = \frac{h_{fr}}{G_{fr}} \sigma_{xz} \equiv Z_T \sigma_{xz} \tag{4.6}$$

This defines the transverse fracture compliance Z_T. If the fractures are assumed to be invariant with respect to rotation about the axis normal to the fracture direction and their background is isotropic, the overall fracture compliance tensor depends on those two fracture compliance tensors. Schoenberg & Douma further introduced the relative compliances E_N and E_T:

$$E_N = Z_N(\lambda_b + 2G_b) E_T = Z_T G_b \tag{4.7}$$

The subscript b refers to the background medium (intact rock).

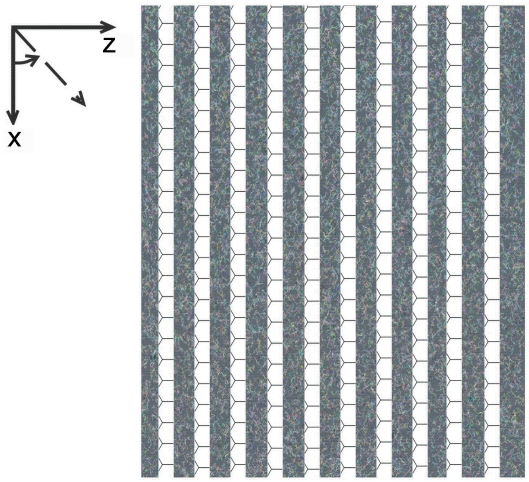

Figure 4.1: A layered solid medium composed of two sets of alternating planes and parallel layers.

4.2 Method and Results

4.2.1 Anisotropy in the lower oceanic crust due to the water-filled microcracks

The mineralogy, crack porosity, density, alteration, and mineral orientation of oceanic rocks are among the important characteristics responsible for significant variations in seismic velocities throughout the oceanic crust. The rock contains vertically aligned water-filled cracks situated in an isotropic background media. A single distribution of aligned cracks is introduced and parameterized using crack density ε defined as:

$$\varepsilon = \frac{Na^3}{V} \tag{4.8}$$

where N is the number of cracks with a radius a in a volume V and crack aspect ratio:

$$\alpha = \frac{d}{a} \tag{4.9}$$

where d is the half width of a crack. The relation which connects crack density and aspect ratio with crack porosity, ϕ, is:

$$\phi = \alpha \cdot \varepsilon \cdot \frac{4\pi}{3} \tag{4.10}$$

It is difficult to determine the values for crack density ε. As the actual fracturing state of the subducting lithosphere offshore of Nicaragua is unknown, we used values which lie in between 0.05, that has been reported for many different tectonic and geological regions [*Crampin and Booth*, 1985; *Roberts and Crampin*, 1986; *Li et al.*, 1988], and 0.2 found in the Kobe fault zone [*Zhao and Mizuno*, 1999]. The result reveals that the presence of thin aligned cracks with aspect ratios of 0.001-0.01 which induce porosity of <1% could be sufficient to cause the observed velocity reduction. For instance, for crack porosity of 0.05 % and aspect ratio of 0.001 compressional wave velocity is already reduced by 0.4 km/s. The same amplitude is found in the lower crust of the profile p50 in the vicinity of the trench. Figure 4.2 shows compressional wave velocities for a range of aspect ratios and crack porosities plotted versus angles of ray incidance. A change in the aspect ratio of the cracks affects the resultant anisotropy. The model shows that lower aspect ratio cracks have greater impact on seismic velocities than cracks with high aspect ratios, what is in agreement with the previous studies [e.g. *Wilkens*, 1991]. This is due to the effective elastic moduli of the rock, which, for a given porosity, reduce more when thin cracks, rather than spherical voids are present. In a medium with very thin cracks, shear waves appear to be sensitive only to changes in crack density. In Figure 4.3 is shown shear wave anisotropy in relation to increasing crack density.

Based on this model velocity is expected to be reduced by 5-12 % for crack densities in the range of 0.05-0.15. As a total velocity anisotropy is produced by crack

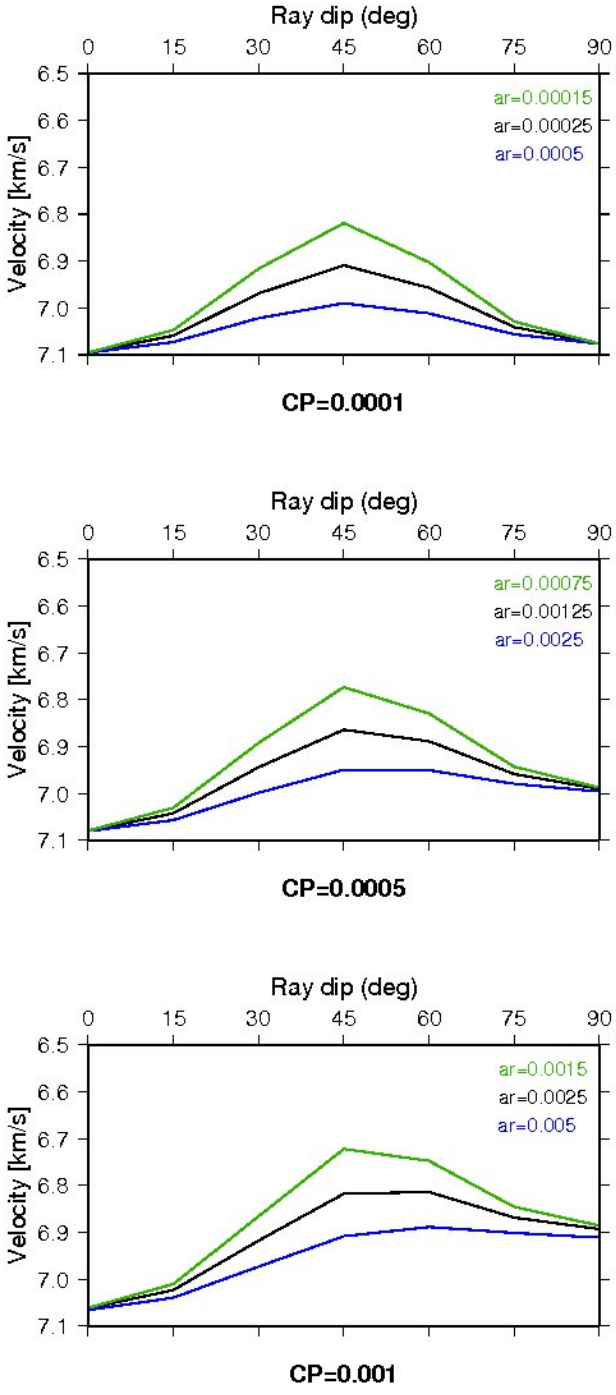

Figure 4.2: P-wave velocities in the lower oceanic crust containing parallel fractures and aligned cracks for different crack densities: 0.05 (blue), 0.1 (black) and 0.15 (green).

.

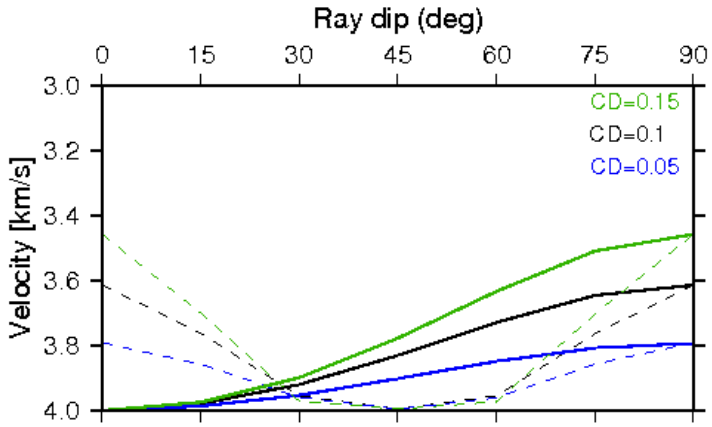

Figure 4.3: Potential impact of aligned water-saturated cracks on the S-wave velocities in the lower oceanic crust; variation in the wave-speed of SH (solid) and SV (dashed) with incidence angle for different crack densities.

populations with a broad range of aspect ratios and crack densities, we can assume that fluid-filled cracks may have a significant impact on the seismic properties of the subducting crust here. It seems reasonable to assume that mineral alteration has minor effect on the seismic velocities of the lower crust. This is supported by the analysis of low-temperature alteration in the gabbroic rocks recovered from Hole 735B, which has shown that the alteration is localized and typically confined to fractured regions where intense alteration of the host rocks can be observed adjacent to veins/veinlets. Besides, typical alteration minerals are secondary plagioclase and amphibole. Amphiboles do not significantly change seismic velocity, because they have properties similar to the pyroxenes they replace [*Iturrino et al.*, 1996].

4.2.2 Seismic anisotropy in the microcracked uppermost mantle

Assuming a similar fracturing state as in the lower crust caused by bending stresses, the same method was applied to the uppermost few kilometers of the mantle

using the same model parametrization. We used the same range of input values for crack density, values which lie in between 0.15, found in the regions where big earthquakes occurred (Kobe), and 0.05, which would be representative of different tectonic and geological environments. The Figure 4.4 shows an influence of very thin cracks of different aspect ratios, in the range from 0.0001 to 0.005, and crack porosities of 0.01 % and 0.05 % on compressional wave velocities in dependance of an angle of ray incidance.

The results indicate that physical properties of the upper mantle rocks could be strongly affected by the presence of aligned water-filled microcracks and fractures. Assuming that the input values are a good approximation to the actual fracturing state of the subducting Cocos lithosphere, the model shows that 3-6% of the reduced velocities in the upper mantle could be caused just by cracked and fractured condition. The P-wave velocity model of the profile p50 (Chapter 2) has revealed that upper mantle velocities in the vicinity of the trench are reduced by 5-7% compared to the unaltered upper mantle rocks, what has been interpreted to be caused by 12-17 % of serpentinization. The model shows that for the same range of crack densities as in the lower crustal layer, velocities can be reduced by up to 5-13 %. In Figure 4.5 is shown a potential effect that parallel water-filled cracks and fractures may have on the shear wave velocities in the uppermost mantle.

Although serpentinization of mantle peridotites is a geologically rapid process at all temperatures above 100 $^{\circ}$ C (*Martin and Fyfe*, 1970), high seismic activity rates caused by strong bending stresses, like in the case of the subducting Cocos lithosphere, would continously develop a new set of microcracks and fractures, through which then seawater could percolate, preventing cracks closure and hence causing anisotropy. Thus, although serpentinization affects geophysical properties of the upper mantle rocks by lowering their seismic velocities, fracturing may play equal or even more important role in this process.

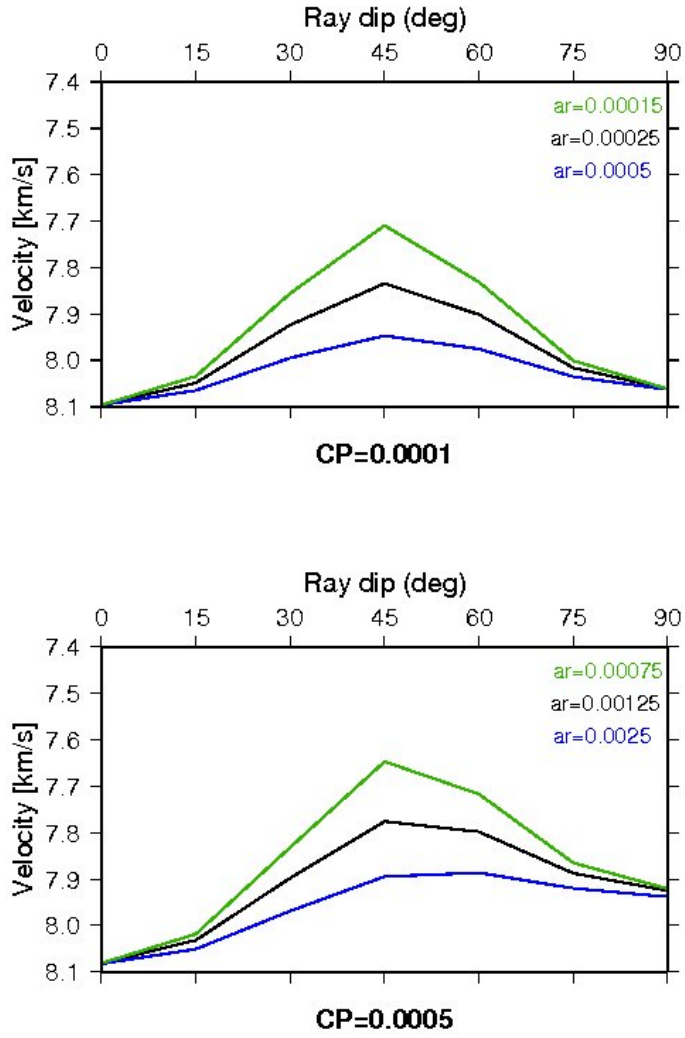

Figure 4.4: P-wave velocities in the upper mantle for the same crack densities used for the lower crust model (Fig.4.2).

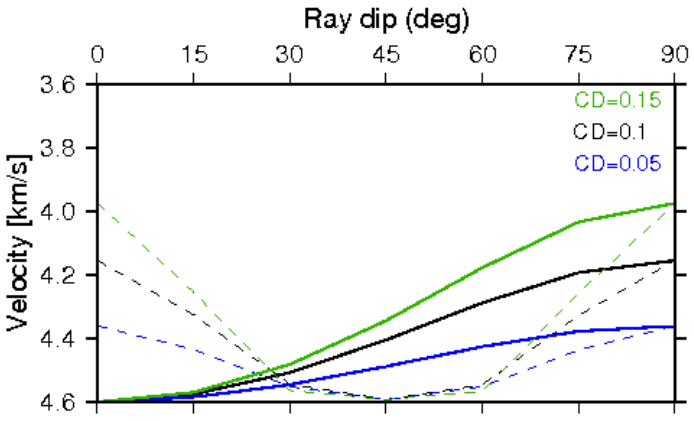

Figure 4.5: Variation in the wave-speed of SH (solid) and SV (dashed) with incidence angle in the upper mantle containing aligned water-saturated cracks.

4.3 S-wave model and V_P/V_S ratio

Fractures are well known to affect wave propagation at the seismic scale. It is known that S-waves are more intensively affected by crack-induced anisotropy than P-waves. Since S-waves are more sensitive to rigidity changes, they are more suited for fracture characterization. Knowledge of the density and aspect ratio of inferred crack populations can be considerably improved with estimates of Poisson's ratio:

$$\sigma = \frac{v_P^2 - 2v_S^2}{2(v_P^2 - v_S^2)} \tag{4.11}$$

Another useful quantity is the V_P/V_S ratio, which is uniquely related to the better-known Poisson's ratio. Seismic wide-angle data from the profile p50, placed in the trench-outer rise area northwest of the Nicoya Peninsula (Chapter 2) were first used to derive a 2D P-wave velocity model. In order to obtain a shear velocity model we used a PS converted phase, which is an S-wave converted from a P-wave at the bottom of the sedimentary layer. In general, conversion from P-to S waves is more likely to occur

where a sediment blanket is present [*Lewis and McClain*, 1977], since cementation and infilling of cracks result in an increase of S-wave velocity and decrease shear attenuation enough for an efficient P- to S-wave conversion. Because of the low quality of the S-wave data from most of the stations close to the trench, not all the phases could have been picked, specially the mantle phases. Examples are shown in Figures 4.6 and 4.7 (see also Chapter 2, Fig. 2.4 to 2.7) for PS-converted wave record along the profile p50. In total 1548 Sg, 569 SmS and 704 Sn phases were used in the inversion procedure.

The velocity model was constrained using the joint refraction and reflection inversion code from *Korenaga et al.* [2000]. Figure 4.8a shows the S-wave structure. It follows the same pattern found in the P-wave velocity model. In the area seaward of the outer rise we find velocities typical for a mature oceanic lithosphere. Within the $\sim$ 1.5 km thick upper crust velocities increase from $\sim$ 2.5 kms^{-1} at the top of the layer to 3.4 kms^{-1} at the bottom. Uppermost lower crustal S-wave velocities are $\sim$ 3.6 kms^{-1} and reach 4.0 kms^{-1} at the Moho. V_P/V_S ratio within the upper and lower crust is $\sim$ 1.8. The Moho interface is constrained in the previous P-wave modeling (Chapter 2) using Moho reflections (PmP). The seismic behaviour in the lower oceanic crust is typical for unaltered gabbroic rocks. However, as the plate approaches the trench the S-wave velocities decrease. In the S-wave crustal structure velocity anomaly close to the trench (Fig. 4.8b) is more prominent than in the P-wave structure (Fig. 2.9).

V_P/V_S ratio here is in the range 1.9-2.0 (σ = 0.31-0.33) (Fig. 4.9a), considerably higher than 1.8 (σ = 0.28) found seaward of the outer rise, which might reflect the presence of high fracture density zone. *Popp and Kern* [1994] found that both P- and S-wave velocities decrease with increasing crack density, and that Poisson's ratio decreases for dry cracks and increases for saturated cracks. Strong bending-related faulting in the trench-outer rise area may reopen old cracks, created at the spreading ridge, and create new ones, through which seawater may infiltrate and react with the surrounding rocks. The modeling of the impact of water-filled cracks and fractures on the seismic properties (Sections 4.2.1 and 4.2.2) has shown that they could play a major role in the observed velocity reduction. The models with crack densities in the range from 0.05 to 0.15 show that S-wave velocities in the lower crust can be reduced by up to 5-12% and in the upper mantle about 5-13% of the anomaly could be caused solely by cracks and fractures.

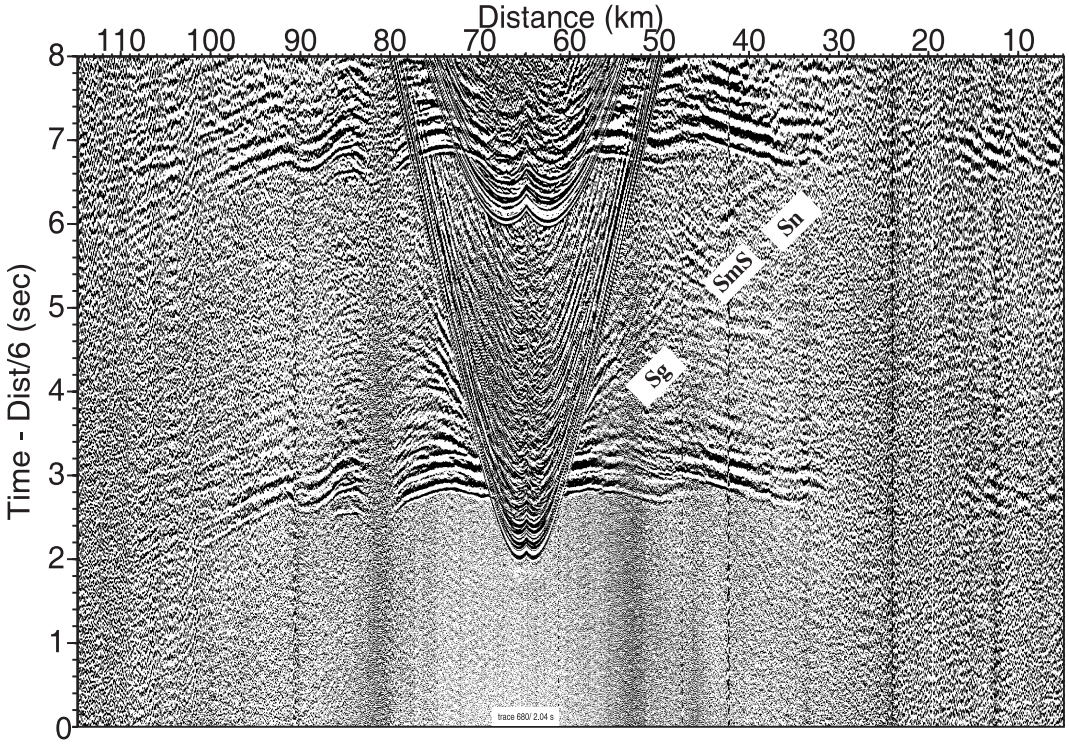

Figure 4.6: Example of wide-angle seismic data. Interpreted seismic arrivals are labeled: Sg (turning rays within the crust), SmS (reflections at the Moho), and Sn (turning rays in the upper mantle). OBS34.

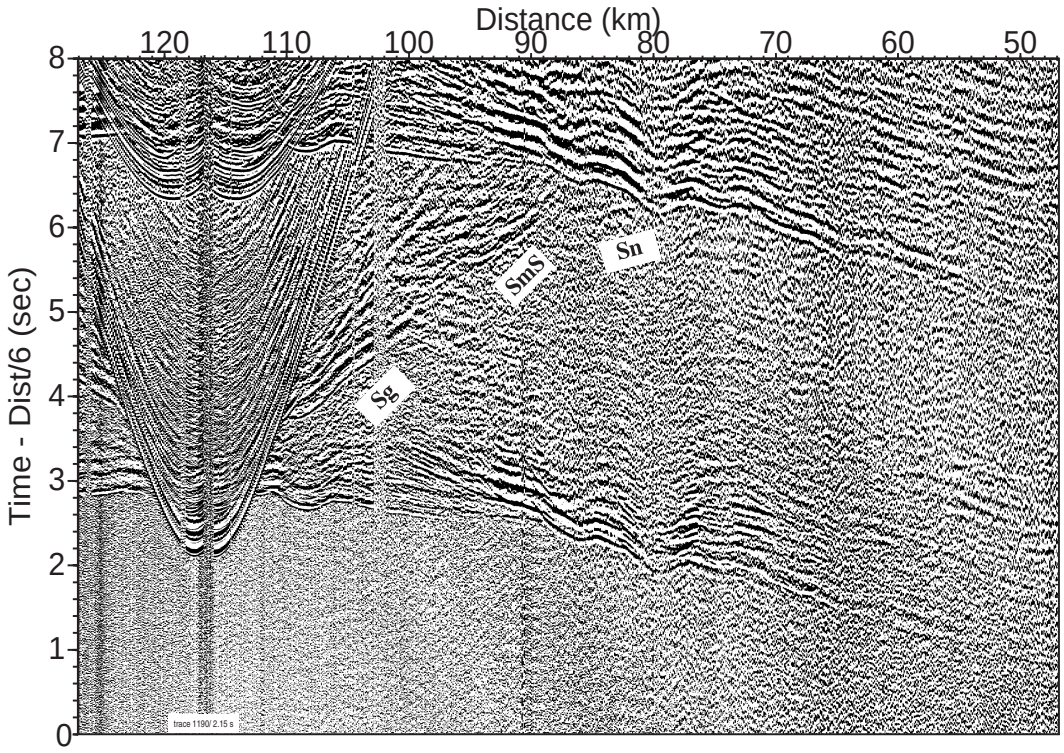

Figure 4.7: Same as Fig.4.6 for OBH45.

a)

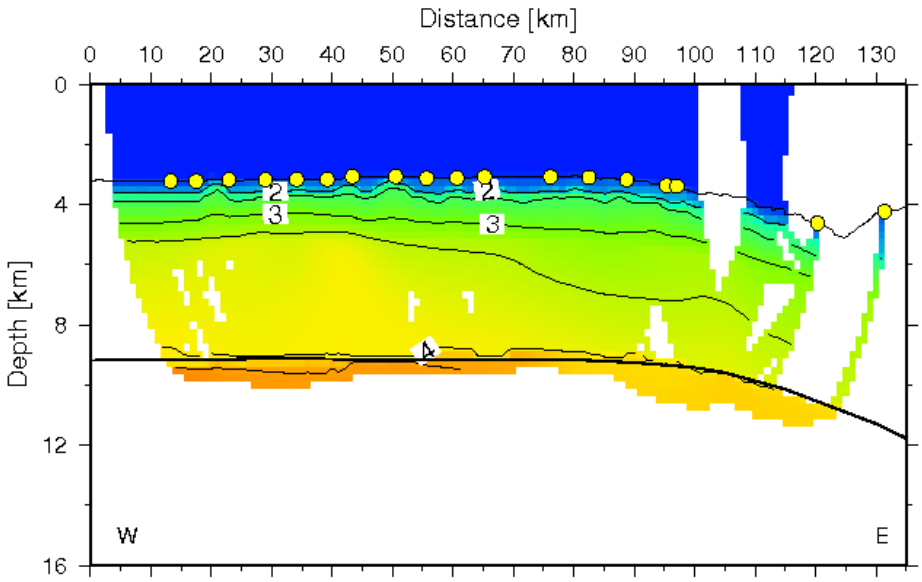

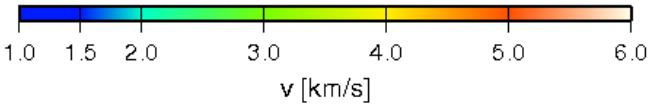

b)

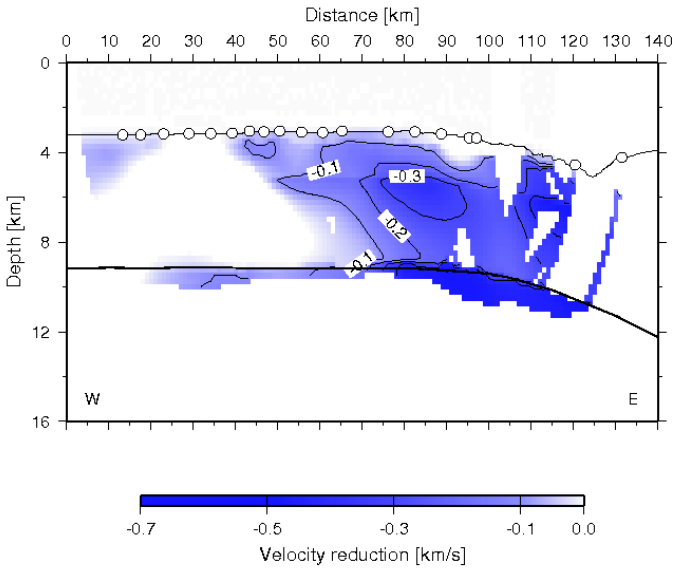

Figure 4.8: a) Final velocity model with isovelocity contours. Thick black line represents Moho boundary derived from inversion of PmP phases. Yellow circles indicate OBH and OBS stations; b) S-wave velocity reduction in the crust and upper mantle.

a)

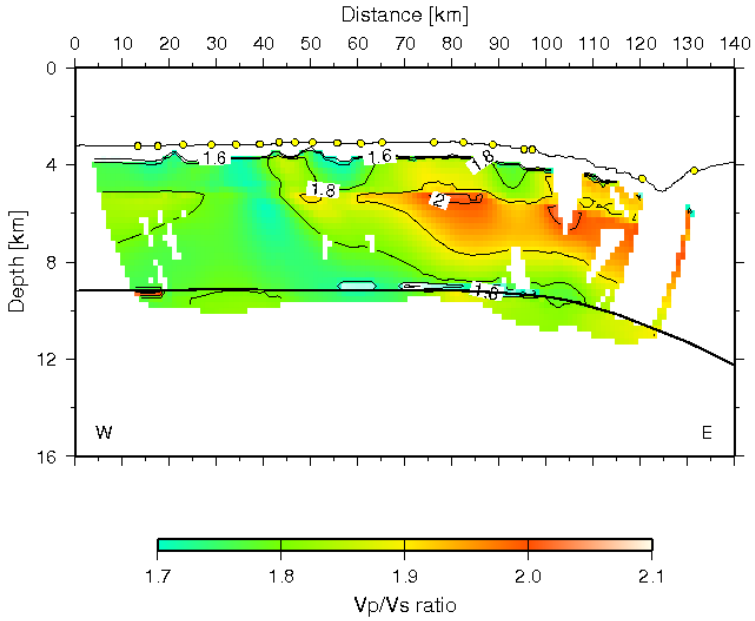

b)

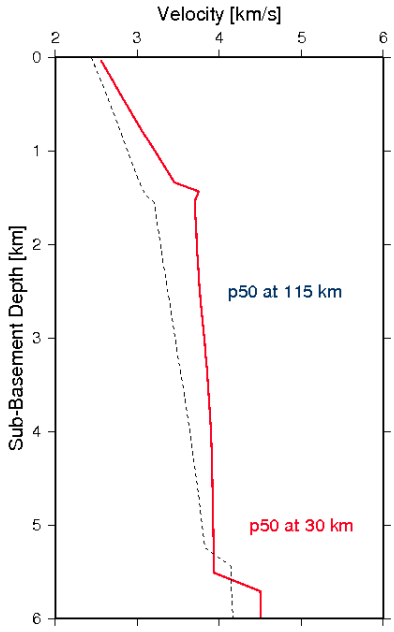

Figure 4.9: a) V_P/V_S ratio; b) V_S-depth profiles at two selected locations in the outer-rise and near-trench region.

4.4 Disscusion

The seismic structure along the seismic profiles offshore of Nicaragua is clearly anomalous. Seismic velocities in the crust and upper mantle are much lower than what is a typical velocity of the mature oceanic lithosphere. This anomaly can be explained by both the presence of the cracks and fractures and hydrothermal alteration of the rocks. The subducting plate is significantly fractured due to the tensional stresses within the uppermost ∼20 km of the lithosphere. In our resulting models for the profile p50 northwest of the Nicoya Peninsula (Chapter 2) and the profiles p01 and p02 which lie offshore of northern Nicaragua (Chapter 3), we find velocities well reduced compared to those expected for ∼25 My old litosphere, both in the crust and upper mantle. Those anomalies are most likely due to a combination of progressive fracturing and hydration. Some estimates for water content in the uppermost mantle have already been done (Chapter 2) based on the velocity anomalies in the uppermost mantle and under the assumption that they were due only to hydration. The impact that the fractures and cracks have on the elastic properties of the crustal and upper mantle rocks here is very difficult to constrain due to the unknown fracture network parameters (crack density and aspect ratio, anisotropy and percolation properties of the fracture network) and the fact that both mechanisms, fracturing and hydration, are related to each other.

The results we have got from all three profiles, which lie perpendicular (p50) and parallel to the trench (p01 and p02), have also shown an azimuthal seismic anisotropy in the crust and upper mantle. Fluid-filled microcracks [*Nur and Simmons*, 1969; *Crampin*, 1984] and mineral alignment [*Christensen*, 1966; *Babuska*, 1981; *Christensen and Szymanski*, 1988] are the most likely causes for seismic anisotropy in the crust and upper mantle. As fracture-induced anisotropy can lead to observable azimuthal variations of seismic properties, they can be used for characterizing a fracture system. Azimuthally varying P-wave attenuation can document the presence of aligned saturated fractures. Both P- and S- wave propagation across the fractures are expected to be significantly delayed, and attenuated, with a lower dominant frequency than the uncracked rock.

It should be noted that a certain amount of azimuthal variation in seismic velocity

could also be caused by the flow-induced mineral alignment in the Earth's mantle. Strong lattice-preferred orientation (LPO) develops during upwelling and the preferred orientation of minerals stabilizes during spreading and attenuates during subduction. Seismic anisotropy associated with LPO of minerals in peridotites contributes to the effective anisotropy. Seismic anisotropy in the shallow upper mantle was first recorded beneath Hawaii [*Hess* 1964; *Morris et al.* 1969], where observed surface waves traveled 10% faster in the E-W direction than in the N-S. Because of the orientation of olivine minerals P-wave velocity should be higher perpendicular than parallel to the trench axis, and, thus, it would reduce the effect of fracture-induced anisotropy. However, it is difficult to separate its contribution from the fracture-induced anisotropy, specially because hydrothermal alteration of the rocks also affect the mineral alignment in the Earth's mantle.

The development and presence of fractures will depend on several parameters interacting each other: fluid supply, enhanced fluid flow in the permeable fracture, and fluid flow through the surrounding porous material. Fluids in the lower crust can maintain open microcracks by reducing the effective confining pressure at those depths [*Walder and Nur*, 1984]. However, fluids may react rapidly with surrounding rocks and be consumed. The dynamics and kinetics of crack closure is still not well understood, and an extensive study should include various parameters, like stress, temperature, fluid chemistry and initial geometry of a crack. *Nur and Walder* [1990] determined that fluid filled cracks can remain open in the deep crust for no more than about 107 years without fluid replenishment. Also, fluid-filled microcracks in the lower crust would reduce the P-wave velocity [*Spencer and Nur*, 1976].

The pathways of fluid flow and the timing of hydrothermal fluid penetration into the intact gabbro rock at low temperatures is still not well defined. ODP Hole 735B penetrates more than 1500 m into the lower oceanic crust which was generated at the very slow spreading Southwest Indian Ridge and later formed the 5-km-high Atlantis Bank on the inside corner high of the Atlantis II Fracture Zone. The gabbroic rocks recovered from Hole 735B preserve a complex record of plastic and brittle deformation and hydrothermal alteration. The lowermost section (500-1500 mbsf) in the Southwest Indian Ocean, which has been affected by a complex and multistage low temperature ($<250\,^{\circ}$C) alteration, has shown that the extent of this low-T alteration is localized and typically confined to fractured regions. Typical alteration minerals are amphibole

and secondary plagioclase [*Iturrino et al.*, 1996]. A Vp-Vs plot at 200 MPa shows that most of the isotropic samples from Hole 735B fall in a region bounded by lines of constant Poisson's ratio which range from 0.25 to 0.30 (average 0.28). This corresponds to Vp/Vs ratios from 1.76 to 1.85, with an average value of 1.81. The S-wave velocity model along p50 (Fig. 4.8a) has revealed that S-wave velocity reduction in the crust is more prominent than in the P-wave velocity model, what is in agreement with the prediction from the crack models (Sections 4.2.1 and 4.2.2). Analysis of Vp/Vs ratio here has shown that in the crustal layer near the trench this value is in the range 1.9-2.0 (σ = 0.31-0.33) (Fig. 4.9a), which is considerably higher than the values observed on the gabbroic rocks recovered from Hole 735B. In fact, Vp/Vs ratio of 1.8 (σ = 0.28) is found seaward of the outer rise. Thus, it is reasonable to assume the presence of high fracture density zone in the part of the lithosphere affected by the bending stresses.

A similar scenario can be assumed in the uppermost mantle layer. If seawater indeed penetrates upper mantle, it can be assumed that, due to the strong tectonic and seismic activity in the subducting Cocos lithosphere, seawater keeps microcraks open, reducing the effective elastic moduli of the rocks. Therefore, reduced seismic velocities we observe in our final model could be, aside serpentinization processes, explained by the presence of water-filled microcracks. As shown by *Martin and Fyfe* [1970] serpentinization is geologically a rapid process at all temperatures above 100 $^{\circ}$C and is controlled by the rate at which water is supplied to the reaction surfaces. However, once serpentine has formed on a fracture surface, further reaction must depend on water diffusion rates through serpentine minerals. Experimental studies on serpentine permeability have shown that, for instance, at 300 $^{\circ}$C a layer of serpentine 1 km thick will be formed in about 1 Ma [*MacDonald and Fyfe*, 1985]. In case of the subducting Cocos plate with high seismic activity, one can assume continuous supply of seawater, what would keep the microcraks open and develope a new set of microcracks, which would significantly reduce seismic velocities. Crack-modeling, with the same parametrization as in the case of the lower crust, showed that cracks could reduce the seismic velocity of the uppermost mantle by 3-6%. Thus, the existance of water-filled aligned cracks and fractures could significantly contribute to the velocity reduction we are observing along the seismic profiles offshore of Nicaragua, both in the crust and upper mantle.

4.5 Conclusions

The analysis shows that the major part of the observed velocity reduction in the seismic velocity models offshore of Nicaragua could be explained by the presence of water-filled microcracks, both in the lower crust and upper mantle, because of the strong impact of the microcracks on the elastic properties of the rocks. The crack-model shows that lower aspect ratio cracks have greater impact on seismic velocities than cracks with high aspect ratios. Due to the geometry of normal faults in subducting lithospheres, it might be reasonable to hypothesize that bending causes low aspect ratio cracks in crustal and upper mantle rocks. The difficulty in determing the actual impact of fractures on the seismic properties of the subducting plate is due to the unknown fracture system of the lithospheric rocks. Thus, for fracture density we used endmember values that range from 0.05, which had been reported for different geological and tectonic regions, to 0.2, found in the Kobe fault zone. The presence of thin aligned cracks with aspect ratios of 0.001-0.01 which induce porosity of $<0.05\%$ could be sufficient to cause the observed velocity reduction in the crust and 3-6% of the reduced velocity in the upper mantle could reflect the cracked and fractured condition. This is supported by the analysis of the crustal Vp/Vs ratio structure along the profile p50, which has shown that Vp/Vs ratio is much higher here than those observed in hydrothermally altered gabbros. Thus, based on this model, we can assume that about 50% of the velocity anomaly found in the subducting Cocos lithosphere (Chapter 2) might be caused by water-filled cracks, what reduces the estimate of the potential serpentine content in the uppermost mantle to 5-8%.

Chapter 5

Synthetic modeling

5.1 The Reflectivity Method

Synthetic seismogram modeling is a very useful tool for the interpretation of field seismograms recorded over a fractured and azimuthally anisotropic earth. This method can model almost all kinds of waves propagating in elastic or anelastic media with high numerical stability and accuracy but relatively less computation cost. Reflectivity modeling can also simulate wave propagation in fine layered earth models. The reflectivity method for one-dimensional models has proven to be an efficient and powerful method for interpretation of the amplitude and waveform of seismic record sections, which characteristics can be very useful in interpretation of fine structures in velocity models.

The method represents wave propagation in the frequency-wavenumber domain, and it mainly deals with coefficient (or propagator) matrix computation in the frequency-wavenumber domain [*Kennett*, 1975; *Kennett*, 1983; *Müller*, 1985]. Modeling in the frequency-wavenumber domain makes it easy to handle absorptions in anelastic media [*Temme and Müller*, 1982]. Finally, by use of Fourier transforms, the seismic modeling results can be transformed back into the time-space domain. The theories of reflectivity modeling are fully presented in *Kennett* [1983]. A description of the method in terms of

equations, e.g., the calculation of reflection and transmission coefficients at an interface, is described in detail in the tutorial by *Müller* [1985]. The synthetic seismograms sections are calculated using the reflectivity method [*Fuchs and Müller*, 1971]. The approach consists of performing a numericalal computation of the integral solution of the wave equation. It was later extended by *Kennett* [1983] to include the theory of a generalized reflection and transmission from layered system. These generalized responses include all possible multiples, mode conversions, and transmission losses. This is a sophisticated technique for the creation of the complete elastic, body-wave response from a horizontally layered system. It is especially useful when trying to obtain approximate solutions in certain areas, such as in an anisotropic media. Velocity gradient zones were approximated by a series of homogeneous layers introduced in the entire crust and upper mantle. However, reflectivity modeling has limitations. Major ones are complexity of the associated numerical computation of the integral equation, lack of established procedures for the selection of the proper values of the required parameters, and lengthier computation times. A weakness of the method also is that it is a 1D modeling method. Thus, when we try to model more complicated earth models, such as heterogeneous media, we have to turn to other modeling methods.

5.2 Computation of the synthetic seismogram

The main goal of this approach was to calculate a model that would fit the observed data. The comparison of the synthetic model with the observed record section then gives a more solid evaluation of how well the proposed model is able to explain the seismogram. This method also provides more detailed constraints on velocity anomalies in the crust and upper mantle. As both profiles p01 and p02 lie parallel to the trench axis, their velocity models are expected to be uniformly affected by faulting and fracturing of the subducting slab. Indeed, tomographic inversion results reveal anomalous behaviour in the crust and upper mantle uniformly along both profiles. In order to get a better insight into the velocity gradients here, we calculated the synthetic seismogram for the OBS14 station from the profile p01. The physical parameters are partly taken from other modeling techniques (P-wave and S-wave velocity) and partly

tested (Q). The one-dimensional P-wave and S-wave velocity-depth distributions for the starting model were derived from the results of the tomographic inversions. Q_S depth distribution was estimated using a relation from *Müller* [1985]. White noise is added to the synthetic seismogram for a better comparison with the recorded refraction seismogram. Figure 5.1 displays the resulting synthetic seismogram and the observed data.

Depth [km]	Vp	Qp	Vs	Qs	ρ [kg/m^3]	No. of layers
0.000	1.48	1000.0	0.0001	0.0	1.0	0
0.020	1.48	1000.0	0.0001	0.0	1.0	1
4.80	1.48	1000.0	0.0001	0.0	1.0	1
4.91	1.48	1000.0	0.0001	0.0	1.0	1
4.91	1.65	60.0	0.25	40.0	1.5	0
5.21	2.15	60.0	0.55	40.0	1.5	10
5.21	3.7	50.0	1.9	30.0	2.6	0
6.8	6.1	50.0	3.15	30.0	2.6	15
10.90	6.6	250.0	3.45	150.0	2.9	10
10.90	6.9	600.0	3.65	500.0	3.15	0
11.10	7.3	600.0	3.85	500.0	3.15	4
11.10	7.5	600.0	3.95	500.0	3.15	0
18.50	7.8	600.0	4.54	500.0	3.30	5
20.50	7.9	600.0	4.545	500.0	3.30	5

Table 5.1: Layer parameters for the reflectivity modeling.

The low velocities found in the entire crust and upper mantle have been atributed to intense cracking and hydrothermal alteration of the rocks due to the percolation of seawater. Upper crustal layer of significantly reduced velocities of 3.8-4.0 kms^{-1}, compared to the 'normal' 4.5 kms^{-1} for ∼25 My old oceanic lithosphere, indicate highly fractured and altered rocks. The PmP trace appearing in between ∼18-26 km range can be successfully modelled, when a velocity gradient within the lower crust is higher than expected for unaltered gabbroic layer, followed by a ∼200 m of transitional Moho layer to the upper mantle. Furthermore, very low upper mantle velocities of 7.3-7.4 kms^{-1} just below the Moho are most likely caused by extensive fracturing or/and

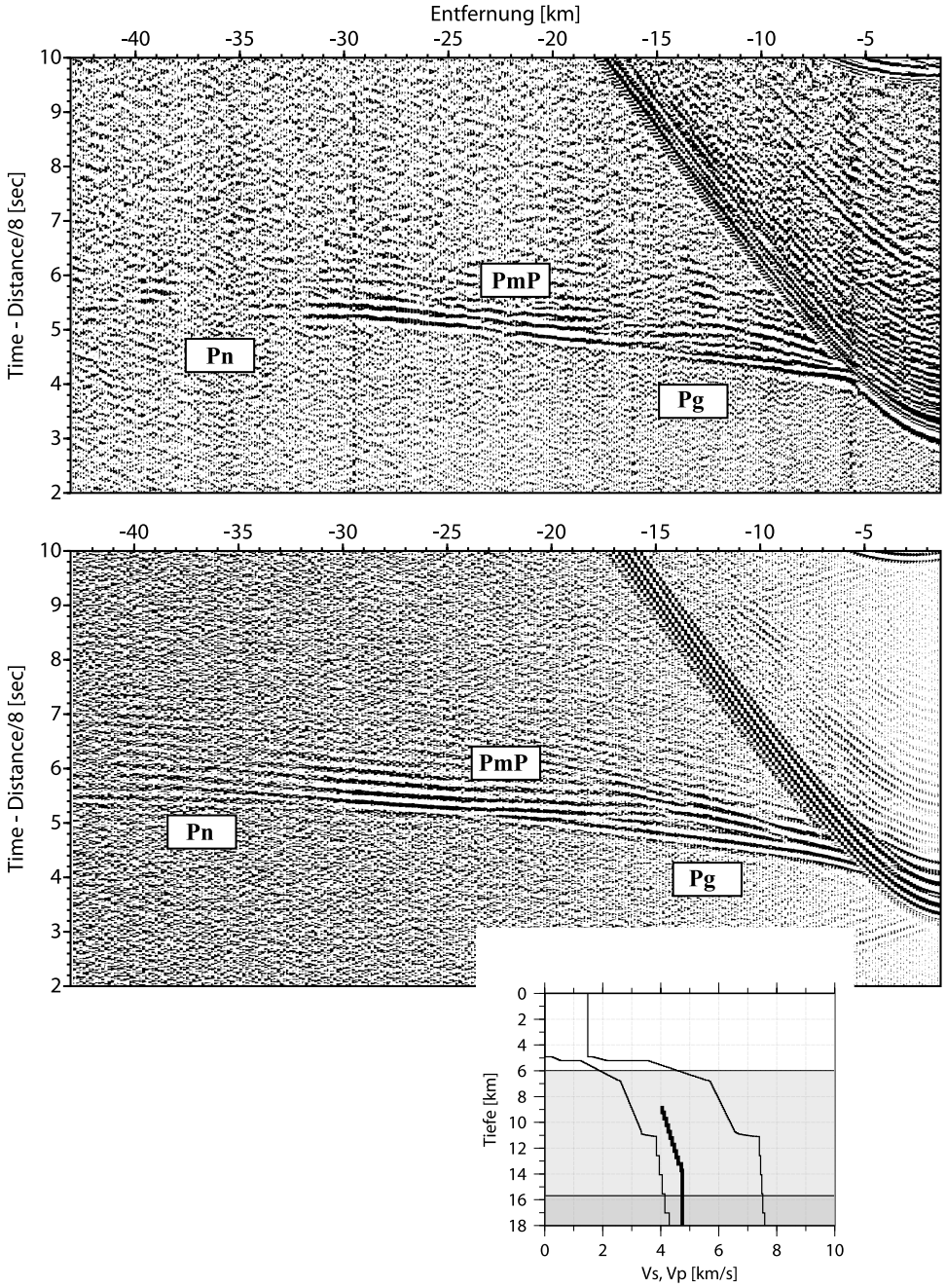

Figure 5.1: Synthetic seismogram of *OBS14*.

hydrothermal alteration of the upper mantle rocks. To obtain a good fitting with the observed Pn phases we had to increase a velocity gradient within the upper mantle. Higher velocity gradients within the crust and upper mantle are most likely a reflection of the depth distribution of hydrated minerals and cracks, in which alterations are most prominent at the top of the layers and decrease with the depth. Attenuation of both P-waves and S-waves is found to be significantly higher compared to values expected for normal unaltered mature oceanic lithosphere. Thus, these observations are consistent with the scenario in which fracturing and mineral alteration strongly affect the velocity structure of the subducting Cocos lithosphere.

Chapter 6

Disscusion and Conclusions

Subduction zones play a fundamental role in global volatile cycle. In this work we have focused on the outer rise processes prior the plate enters the trench in order to evaluate the impact of the incoming plate on the subduction process. The main aim was to quantify the amount of water carried with the subducting plate into the subduction factory. Water carried into subduction zones with the down-going plate and subsequently released by dehydration reactions at depth affects the composition of the mantle wedge, triggers partial melting and affects subduction zone seismicity. Serpentinized mantle seems to be the most stable agent to deliver chemically bound water through the sub-arc dewatering region to greater mantle depths, and, thus, it may play a significant role in fluid and element transfer through subduction zones. Depending on the thermal structure of the subducting slab up to 40% of the water stored in serpentinized mantle may be transfered into the deeper mantle. Thermal models constructed across the Nicaragua-Costa Rica subduction zone have shown that hydrated oceanic mantle subducted beneath Nicaragua and Costa Rica may still contain substantial amounts of H_2O at depths greater than 240 km (>8 GPa) [*Peacock et al.*, 2005]. Offshore of Nicaragua the system of bending related faulting seen in the bathymetry data is believed to facilitate inflow of seawater into the deep crust and upper mantle.

To test this hypothesis a number of wide angle reflection and refraction seismic profiles were conducted across the trench-outer rise area offshore of Nicaragua. First profile p50 from the cruise SO173-1 was placed nortwest of the Nicoya Peninsula,

where the MCS data reveal pervasively faulted subducting lithosphere. The profile is perpendicular to the trench-axis, covering the area which extends from the trench into the seaward of the outer-rise, where no faults were observed in the bathymetry map. The tomographic inversion method has revealed an anomalous behaviour of the seismic velocities in the crust and upper mantle in the part of the plate affected by the bending stresses, whereas the 'non-affected' part is of typical velocities for a mature non-altered oceanic lithosphere. The anomalous behaviour increases towards the trench, indicating changes in physical and chemical properties of the subducting lithosphere as it approaches the trench and supporting the idea that pervasive bending related normal faulting creates pathways for seawater to reach and react with cold mantle rocks producing serpentine. It is most likely caused by both mechanisms, extensive fracturing and serpentinization process. The crack-model for the lower crust and upper mantle, based on the Schoenberg & Douma's model for parallel fractures and aligned cracks has shown that water-filled cracks may have a significant impact on the seismic properties of the deep subducting lithosphere. In the S-wave velocity model of the profile p50 we find that crustal velocities are more profoundly reduced than in the P-wave model. This observation supports the crack-model, indicating that fracture porosity may play an important role in reducing the seismic velocities. The other two profiles acquired during M66 cruise lie parallel to the trench. This geometry has helped to get an insight into the lateral changes along the trench. Both profiles have revealed that anomalous seismic behaviour in the crust and upper mantle is typical for the entire subducting lithosphere offshore of Nicaragua. Based on the model of *Carlson and Miller* [2003] that relates the degree of serpentinization and water content of partially serpentinized peridotites to their seismic P-wave velocities, we estimate that water stored in the upper mantle in this region may range from 1.55 to 2.17 wt %, corresponding to a 12-17 % increase in serpentine content. These values are found just below the Moho and they decrease with depth, so that 4 km deeper velocities seem to return to those typical for anhydrous rocks. Considering the effects of fracture porosity, we assume that this number is an upper bound on the water content of the hydrated mantle and that the real value might be considerably lower. Thus, it seems to be reasonable to assume that at least 50% of the velocity anomaly is caused solely by water-filled cracks and fractures. This is in agreement with the thermo-dynamical model of *Ruepke et al.* [2004]. They find that *Hallam's* [1992] estimation of a maximum

sea level drop of 500m over the past 600Ma is consistent with less than 5% sub-Moho mantle serpentinization. Higher degrees of serpentinization seem to lead to too strong water recycling into the mantle to be consistent with global sea level changes since the Cambrian.

As the downgoing plate experiences higher pressures and temperatures, water trapped in the crust and upper mantle is gradually forced out and into the mantle of the overlying plate. Fluid output in the fore-arc region occurs at the deformation front and through mud diapirs and mud volcanoes. Fluid output at the volcanic arc occurs through magmatic devolatilization. Central American arc volcanism shows strong regional trends in lava chemistry, which reflects different slab contributions to arc melting. The Nicaraguan volcanic arc shows globally among the highest concentrations of geochemical tracers for oceanic crustal fluid. B/La, Ba/La, and 10Be/9Be signatures from Nicaraguan volcanics are among the highest ever measured in arc systems. It has been proposed that the stronger slab signal in Nicaraguan, compared to Costa Rican arc lavas, reflects greater amounts of fluid released from the dehydration of more extensively serpentinized slab mantle [*Rupke et al.*, 2002]. This is also consistent with the model of *Tonarini et al.* [2007], in which tectonic erosion, i.e. dragging down of slivers of serpentinized upper plate mantle, is responsible for the occurrence of serpentinite reservoir, 11B-enriched in the forearc by shallow fluids.

One of the goals of the SFB 574 project is to obtain information on the amount of water that is released from the subducted slab and returned to the surface. To constrain this water cycle, both the water input into a subduction zone and the amount of sub-arc water release have to be known. Thus, we compared our estimates with the results of the other two subprojects of SFB 574, which deal with forearc volatile turnover and slab-arc-atmosphere transfer. Estimated water flux at the Nicaraguan forearc [*C. Hensen*, pers. communication] is $0.06 \cdot 10^{13}$ kg/km·My and at the volcanic arc [*S. Kutterolf*, pers. communication] $2.3 \cdot 10^{13}$ kg/km·My. If we compare these values with the estimations of subduction flux of water released from sediments ($0.13 \cdot 10^{13}$ kg/km·My) and crust ($1.67 \cdot 10^{13}$kg/km·My) [*Jarrard et al.*, 2003] and the result of our model (Chapter 2) for water storage within the upper mantle of $1.7 \cdot 10^{13}$ kg/km·My, about 67% of water is returned to the surface (Fig. 6.1). It should be noted that this estimation represents an endmember model, in which we assume that velocity reduction in the subducting crust and upper mantle is caused solely by hydration. As

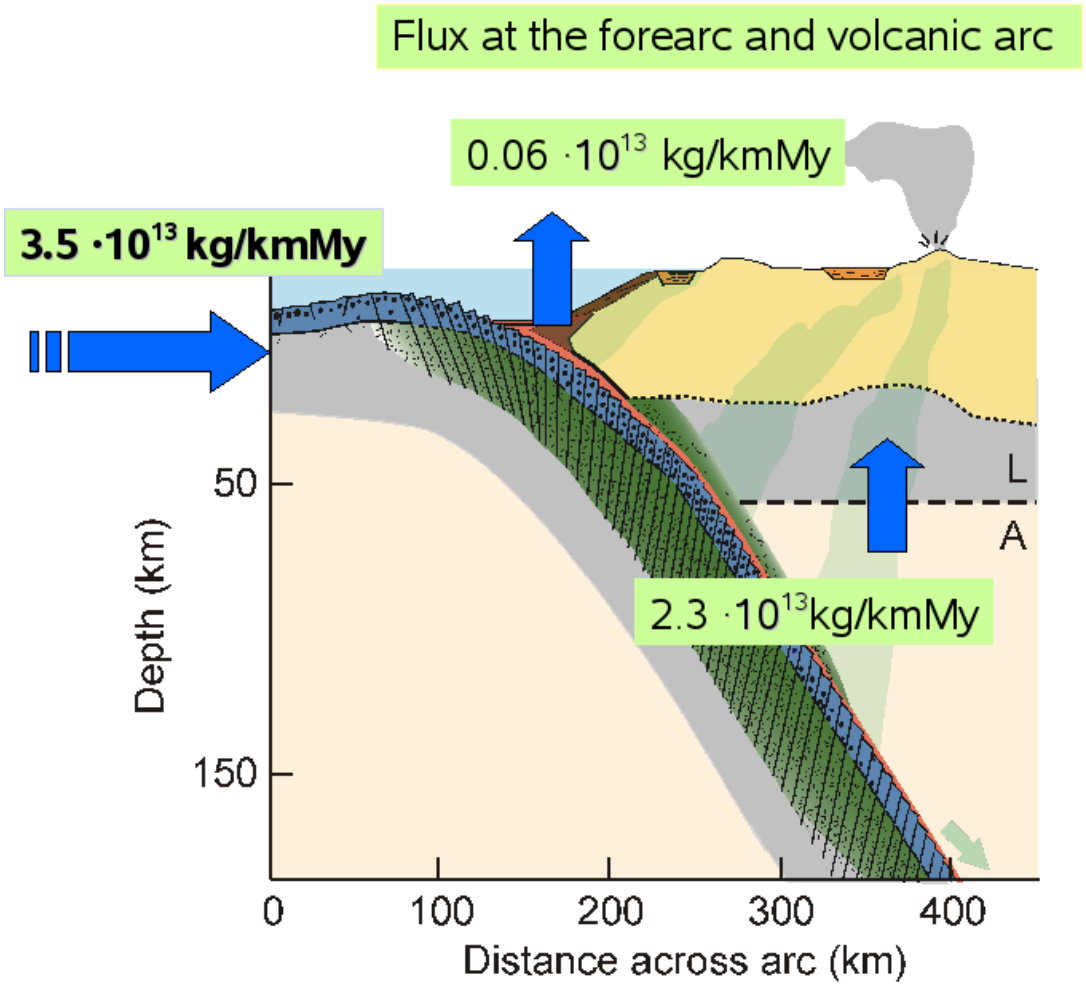

Figure 6.1: Subduction zone water cycle; water input into the subduction zone and the amount of sub-arc water release.

the anomalous behaviour in the velocity structure of the subducting lithosphere reflects both physical and chemical alterations, and as it is difficult to separate their effects on seismic properties, measurements of shear wave splitting and estimates of Poisson ratio would help to provide much more information than P-waves solely about the processes. In particular, we would know more about the internal geometry and distributions of the fluid-filled voids, and, thus, about their impact on the seismic properties of the subducting lithosphere. Together with a better insight into the nature of the low-temperature alteration reactions within the subducting oceanic crust, it would lead to an improved assessment model of the amount of water subducted within the Cocos lithosphere into the deep subduction zone.

Bibliography

Babuska, V., 1981. Anisotropy of Vp and Vs in rock-forming minerals. *J. Geophys.*, 50: 1-6.

Berhorst, A., 2006. Die Struktur des aktiven Kontinentalrands vor Nicaragua und Costa Rica - marin-seismische Steil- und Weitwinkelmessungen, *Dissertation Christian Albrechts University, Kiel*, pp 159.

Bialas, J. and Flueh, E. R., 1999. Ocean Bottom Seismometers. *Sea Technology*, 40, 4, 41-46.

Burbach, G. V., Frolhich, C., Pennington, W.D., Matumoto, T., 1984. Seismicity and Tectonics of the Subducted Cocos Plate, *J. Geophys. Res.,* 89, 7719-7735.

Budiansky, B. and O'Connell, R. J., 1980. Bulk dissipation in heterogeneous media: Solid earth geophys. and geotech., 42, 1-10.

Carr, M. J., Feigenson, M. D., and Bennet, E. A., 1990. Incompatible element and isotopic evidence for tectonic control of source mixing and melt extraction along the Central America arc. *Contrib. Mineral. Petrol.,* 105, 369-380.

Carlson, R.L., 1998. Seismic velocities in the uppermost oceanic crust: Age dependence and the fate of layer 2A. *J. Geophys. Res.*, 103, 7069-7077.

Carlson, R. L., 2003. Bound water content of the lower oceanic crust estimated from modal analyses and seismic velocities of oceanic diabase and gabbro. *Geophys. Res. Lett.,* 30.(22). doi:10.1029/2003GL018213.

Carlson, R. L., and Miller, D. J., 2003. Mantle wedge water contents estimated from seismic velocities in partially serpentinized peridotites. *Geophys. Res. Lett.*, 30. doi: 10.1029/2002GL016600.

Carlson, R. L., and Miller, D.J., 2004. Influence of pressure and mineralogy on seismic velocities in oceanic gabbros: Implications for the composition and state of the lower oceanic crust. *J. Geophys. Res.*, 109, B09205. doi:10.1029/2003JB002699.

Chapple, W. M., Forsyth, D. W., 1979. Earthquakes and bending of plates at trenches. *J. Geophys. Res.*, 84, 6729-6749.

Christensen, N.I., 1966. Shear wave velocities in metamorphic rocks at pressures to 10 kilobars. *J. Geophys. Res.*, 71, 3549-3556.

Christensen, D. H. and Ruff, L. J., 1983. Outer rise earthquakes and seismic cou-

pling. *Geophys. Res. Lett.,* 10(8), 697-700.

Christensen, D. H., Ruff, L. J., 1988. Seismic Coupling and Outer Rise Earthquakes, *J. Geophys. Res.*, 93, 13421-13444.

Christensen, N. I. and Szymanski, D. L., 1988. Origin of reflections from the Brevard fault zone. *J. Geophys. Res.*, 93, 1087-1102.

Collins, J.A., Purdy, G.M., Brocher, T.M., 1989. Seismic velocity structure at Deep Sea Drilling Project hole 504B, Panama Basin: evidence for thin crust. *J. Geophys. Res.*, 94, 9283-9302.

Contreras-Reyes, E., Grevemeyer, I., Flueh, E. R., Scherwath, M., Heesemann, M., 2007. Alteration of the subducting oceanic lithosphere at the southerncentral Chile trench–outer rise. *Geochem. Geophys. Geosyst.*, 8, Q07003, doi:10.1029/2007GC001632.

Contreras-Reyes, E., Grevemeyer, I., Flueh, E. R., Scherwath, M., Bialas, J., 2008. Effect of trench-outer rise bending-related faulting on seismic Poisson's ratio and mantle anisotropy: a case study offshore of Southern Central Chile, *Geophysical Journal International*, 173(1), 142-156, doi:10.1111/j.1365-246X.2008.03716.x.

Costin, L. S., 1987. "Time-Dependent Deformation and Failure," B.K. Atkinson (Editor), *Fracture Mechanics of Rock*, Academic Press, London, 534 pp.

Crampin, S., 1984. Effective elastic constants for wave propagation through cracked solids. Geophys. J. Roy. Astron. Soc., 76: 135-145.

Crampin, S., 1985. Evaluation of anisotropy by shear-wave splitting. *Geophysics*, 50, 142-152.

Crampin, S. and Booth, D. C., 1985. Shear-wave polarizations near the North Anatolian Fault - II. Interpretation in terms of crack- induced anisotropy. *Geophys. J. R. Astron. Soc.*, 83, 75-92.

DeMets, C., Gordon , R. G., Argus, D. F., Stein, S., 1990. Current plate motions, *Geophys. J. Int.,* 101, 425-478.

Dmowska, R., Zheng, G., Rice, J. R., 1996. Seismicity and deformation at convergent margins due to heterogeneous coupling. *J. Geophys. Res.*, 101, 3015-3029.

Dunn, R.A., D. R. Toomey, and S. C. Solomon, 2000. Three-dimensional seismic structure and physical properties of the crust and shallow mantle beneath the East Pacific Rise at 9 degrees 30'N, *J. Geophys. Res.*, 105, 23537–23555.

Escartin, J., Hirth, G. and Evans, B., 2001. Strength of slightly serpentinized peridotites: implications for the tectonics of oceanic lithosphere. *Geology*, 29, 1023-

1026.

Fisher, A. T., Stein, C. A., Harris, R. N, Wang, K., Silver, E. A., Pfender, M., Hutnak, M., Cherkaoui, A., Bodzin, R., Villinger, H., 2003a. Abrupt thermal transition reveals hydrothermal boundary and role of seamounts within the Cocos Plate, *Geophys. Res. Lett.*, 30 (11), 1550, doi:10.1029/2002GL016766.

Fisher, A. T., E. E. Davis, Hutnak, M., Spiess, V., Zühlsdorff, L., Cherkaoui, A., Christiansen, L., Edwards, K.M., Macdonald, R., Villinger, H., Mottl, M., Wheat, C. G., and Becker, K. 2003b. Hydrothermal recharge and discharge across 50 km guided by seamounts on a young ridge flank.*Nature*, 421, 618–621.

Flueh, E. R., and Bialas, J., 1996. A digital, high data capacity ocean bottom recorder for seismic investigations. *Int. Underwater Systems Design*, V.18, No. 3, 18-20.

Gaherty, J.B., Lizarralde, D., Collins, J.A., Hirth, G., Kim, S., 2004. Mantle deformation during slow seafloor spreading constrained by observations of seismic anisotropy in the western Atlantic, *Earth Planet. Sci. Lett.*, 228, 255–265.

Grevemeyer, I., Weigel, W., Whitmarsh, R.B., Avedik, F., Dehghani, G.A., 1997. The Aegir Rift: Crustal structure of an extinct spreading axis. *Mar. Geophys. Res.,* 19, 1-23.

Grevemeyer, I., Ranero, C. R., Flueh, E. R., Kläschen, D., Bialas, J., 2007. Passive and active seismological study of bending-related faulting and mantle serpentinization at the Middle America trench. *Earth Planet. Sci. Lett.*, 258, 528-542.

Grevemeyer, I., Kaul, N., Villinger, H., Weigel, W., 1999. Hydrothermal activity and the evolution of the seismic properties of upper oceanic crust. *J. Geophys. Res.*, 104,5069-5079.

Grevemeyer, I., Bartetzko, A., 2004. Hydrothermal ageing of oceanic crust: inferences from seismic refraction and bore hole studies. In: Davis, E.E., Elderfield, H. (Eds.), *Hydrogeology of Oceanic Lithosphere.* Cambridge University Press, pp. 128-150.

Grevemeyer, I., N. Kaul, J.L. Diaz-Naveas, H. Villinger, C.R. Ranero, C. Reichert, 2005. Heat flow and bending-related faulting at subduction trenches: case studies offshore of Nicaragua and Central Chile. *Earth Planet. Sci. Lett.*, 236, 238-248.

Grevemeyer, I., Weigel W., Jennrich, C., 1998. Structure and ageing of oceanic crust at 14 $^\circ$ S on the East Pacific Rise. *Geophys. J. Int.*, 135, 573-584.

Hallam, A., 1992. Phanerozoic Sea-Level Changes. *Columbia University Press*,

New York, 260 p.

Harris, R. N., Fisher, A.T., Chapman, D., 2004. Seamounts induce large fluid fluxes, *Geology,* 32 (8), 725-728, doi:10.1130/G20387.1.

Hasegawa, A., Horiuchi, S., Umino, N., 1994. Seismic structure of the northeastern Japan convergent margin: A synthesis. *J. Geophys. Res.*, 99(B11), 22295-22312.

Hess, H. H.,1964. Seismic anisotropy of the uppermost mantle under oceans. *Nature*, 203, 629-631.

Horen, H., Zamora, M., Dubuisson, G., 1996. Seismic waves velocities and anisotropy in serpentinized peridotites from Xigaze ophiolite: abundance of serpentine in slow spreading ridge. *Geophys. Res. Lett.*, 23, 9–12.

Hudson, J.A. 1980. Overall properties of a cracked solid. *Math. Proc. Camb. Phil. Soc.* 88, 133-150.

Hudson, J. A. 1981. Wave speeds and attenuation of elastic waves in materials containing cracks. *Geophys. J. Roy. Astr. Soc.*, 64, 133-150.

Hudson, J. A. 1988. Seismic wave propagation through material containing partially saturated cracks *Geophys. J. Internat.*, 92(1), 33–37.

Hudson, J. A., Liu, E., and Crampin, S., 1996. The mechanical proper- ties of materials with interconnected cracks and pores. *Geophys. J. Internat.*, 124, 105–112.

Iturrino, G. J., Christensen, N. I., Kirby, S., and Salisbury, M. H., 1991. Seismic velocities and elastic properties of gabbroic rocks from Hole 735B. In Von Herzen, R.P., Robinson, P.T., et al., *Proc. ODP, Sci. Results*, 118: College Station, TX (Ocean Drilling Program), 227-244.

Iturrino, G. J., Miller, D. J., Christensen, N. I., 1996. Velocity behavior of lower crustal and upper mantle rocks from a fast-spreading ridge at Hess Deep. Proc. ODP Sci. Results Leg 147, 417– 442. (College Station, TX).

Ivandic, M., Grevemeyer, I., Berhorst, A., Flueh, E. R., McIntosh, K., 2008. Impact of bending related faulting on the seismic properties of the incoming oceanic plate offshore of Nicaragua. *J. Geophys. Res.* (in press)

Jarrad, R.D., 2003. Subduction fluxes of water, carbon dioxid, chlorine, and potassium. *Geochemistry, Geophysics, Geosystems*, 4: doi: 10.1029/2002GC000392.

Kanamori, H., 1971. Seismological evidence for lithospheric normal faulting - the Sanriku earthquake of 1933. *Phys. Earth Planet. Inter.*, 4, 289-300.

Keen, C., Tramonti, C., 1970. A seismic refraction survey on mid-Atlantic ridge,

Geophys. J. R. Astron. Soc., 20, 473–491.

Kelly, R.K., and Driscoll, N.W., 1998. Structural controls on ^{10}Be occurrences in arc lavas. *Eos,* 79:45.

Kennett, B. L. N., 1975. The effect of attenuation on seismograms. *Bull. Seis. Soc. Am.*, 65, 1643–1651.

Kennett, B. L. N., 1983. Seismic wave propagation in stratified media. *Cambridge University Press*, p. 342.

Kern, H. and Tubia, J. M., 1993. Pressure and temperature dependence of P- and S-wave velocities, seismic anisotropy and density of sheared rocks from the Sierra Alpujata massif (Ronda peridotites, Southern Spain). *Earth Planet. Sci. Lett.*, 119, 191–205.

Kirby, S. H., 1995. Intraslab earthquakes and phase changes in subducting lithosphere. *Rev. Geophys.,* 33, 287-297.

Kobayashi, K., Nakanishi, M., Tamaki, K., Ogawa, Y., 1998. Outer slope faulting associated with western Kuril and Japan trenches. *Geophys. J. Int.*, 134, 356-372.

Korenaga, J., Holbrook, W. S., Kent, G. M., Kelemen, P. B., Detrick, R. S., Larsen, H.-S., Hooper, J. R., Dahl-Jensen, T., 2000. Crustal structure of the southeast Greenland margin from joint refraction and reflection seismic tomography. *J. Geophys. Res.*, 105, 21591-21614.

Koyi, H. and Skelton, A. D. L., 2001. Initiation of detachment faults: insights from centrifuge modelling. *Journal of Structural Geology*, 23, 1179-1185.

Kuster, G. T., Toksöz, M. N., 1974. Velocity and attenuation of seismic waves in two-phase media, Part I - Theoretical formulations. *Geophysics*, 39, 587-606.

Langseth, M. G., and Silver, E. A., 1996. The Nicoya convergent margin: a region of exceptionally low heat flow. *Geophys. Res. Lett.*, 23, 891-894.

Leeman, W.P., Carr. M.J., and Morris, J.D., 1994, Boron geochemistry of the Central American volcanic arc-Constraints on the genesis of subduction-related magmas: *Geochimica et Cosmochimica Acta*, v. 58, p. 149–168.

Lefeldt, M. and Grevemeyer, I., 2008. Centroid depth and mechanism of trench-outer rise. *Geophys. J. Int.*, 172, 240-251.

Lewis B.T.R., and J. McClain., 1977. Converted shear waves as seen by ocean bottom seismometers and surface buoys, *Bulletin of the Seismological Society of America*, 67, 1291-1302.

Li, Y.-G., Leary, P.C., and Henyey, T.L., 1988. Stress Orientation Inferred from Shear Wave Splitting in Basement Rock at Cajon Pass. *Geophysical Research Letter*, 15, 997-1000.

MacDonald, A. H. and Fyfe, W. S., 1985. Rate of serpentinization in seafloor enviroments, *Tectonophysics*, 116, 123-135.

Martin, B. and Fyfe, W. S., 1970. Some experimental and theoretical observations on the kinetics of hydration reactions with particular reference to serpentinization. *Chemical Geology*, 6, 185-202.

Masson, D. G., 1991. Fault patterns at outer trench walls. *Mar. Geophys. Res.*, 13, 209-225.

Meade, C., Jeanloz, R., 1991. Deep-focus earthquakes and recycling of water into the Earth's mantle. *Science*, 252, 68-72.

Menke, W., 1989. Geophysical Data Analysis: Discrete Inverse Theory, 2nd edn. Academic Press, London, 289 pp.

Morris, G. B., Raitt, R. W., Shor, G. G., 1969. Velocity anisotropy and delay time maps of the mantle near Hawaii. *J. Geophys. Res.*, 74, 4300–4316.

Morris, J., Leeman, W. P., Tera, F., 1990. The subducted component in island arc lavas: constraints from Be isotopes and B–Be systematics. *Nature*, 344, 31–36.

Moser, T. J., 1991. Shortest path calculation of seismic rays. *Geophysics*, 56, 59-67.

Moser, T. J., Nolet, G. and Snieder, R., 1992. Ray bending revisited. *Bull. Seismol.Soc. Am.*, 82, 259-288.

Muller G., 1985. The reflectivity method: A tutorial. *J. Geophys.*, 58, 153–174.

Nolet, G., 1987. *Seismic wave propagation and seismic tomography*, in Seismic Tomography, D Reidel, Norwell, Mass.

Nur, A., and G. Simmons, 1969. Stress-induced velocity anisotropy in rock: An experimental study. *J. Geophys. Res.*, 74, 6667-6674.

Nur, A. N. and J. Walder, 1990. Time-dependent hydraulics in the earth's crust. In: *The role of fluids in crustal processes*, Studies in Geophysics, Geophysics Study Committed, Commission on Geosciences, Environment and Ressources, National Academic Press, Washington, DC, p. 113-127.

Osler, J. C., Louden, K. E., 1995. The extinct spreading centre in Labrador Sea: I-crustal structure from a 2-D seismic refraction velocity model. *J. Geophys. Res.*, 100, 2261-2278.

Paige, C., Saunders, M., 1982. "LSQR: An Algorithm for Sparse Linear Equations and Sparse Least Squares." *ACM Trans. Math. Soft.*, 8, 43-71.

Patino, L. C., Carr, M. J., Feigenson, M. D., 2000. Local and regional variations in Central American arc lavas controlled by variations in subducted sediment input. *Contributions to Mineralogy and Petrology*, 138, 265-283.

Peacock, S. M., 2001. Are the lower planes of double seismic zones caused by serpentine dehydration in subducting oceanic mantle? *Geology,* 29, 299-302.

Peacock, S. M., 2004. Insight into the hydrogeology and alteration of oceanic lithosphere based on subduction zones and arc volcanisms. In: Davis E.E, Elderfield, H. (Eds.), *Hydrogeology of Oceanic Lithosphere.* Cambridge University Press, pp. 659-676.

Peacock, S. M., van Keken, P. E., Holloway, S. D., Hacker, B. R., Abers, G. A. and Fergason, R. L., 2005. Thermal structure of the Costa Rica – Nicaragua subduction zone. *Physics of Earth and Planetary Interiors*, v. 149, 187-200.

Phipps Morgan, J., 2001. The role of serpentinization and deserpentinization in bending and unbending the subducting slab (abstract). *Eos Trans. Am. Geophys. Un.*, 82, Fall Metting supplement: F1154

Popp, T. and Kern, H., 1994. The influence of dry and water saturated cracks on seismic velocities of crustal rocks - A comparison of experimental data with theoretical models. *Surv. Geophys.*, 15 (5), pp. 443-465.

Protti, M., Güendel, F., and McNally, K., 1994. The geometry of the Wadati-Benioff zone under southern Central America and its tectonic significance: results from a high-resolution local seismographic network. *Phys. of the Earth and Planet. Inter.*, 84, 271-287.

Protti, M., Güendel, F., and McNally, K., 1995. Correlation between the age of the subducted Cocos plate and the geometry of the Wadati-Benioff zone under Nicaragua and Costa Rica. In Mann, P. (Ed.), Geologic and Tectonic Development of the Caribbean Plate Boundary in Southern Central America. *Geol. Soc. Am. Special Paper*, 295, 309-326.

Pyrak-Nolte, L. J., Myer, L. R., and Cook, N. G. W., 1990a. Transmission of seismic waves across single natural fractures.*J. Geophys. Res.*, Vol. 95(B6), pp. 8617-8638.

Pyrak-Nolte, L. J., Myer, L. R., and Cook, N. G. W. 1990b, Anisotropy in seismic velocities and amplitudes from multiple parallel fractures.*J. Geophys. Res.*, Vol.

95(B7), pp. 11345-11358.

Raleigh, C. B., Paterson, M. S., 1965. Experimental deformation of serpentinite and its tectonic implications. *J. Geophys. Res.*, 70, 3965-3985.

Ranero, C. R., Phipps Morgan, J., McIntosh, K., Reichert, C., 2003. Bending, faulting, and mantle serpentinization at the Middle America Trench. *Nature*, 425, 367-373.

Ranero, C.R., Sallarès, V., 2004. Geophysical evidence for alteration of the crust and mantle of the Nazca Plate during bending at the north Chile trench. *Geology*, 32, 549-552.

Ranero, C. R., Villaseñor, A., Phipps Morgan, J., Weinrebe, W., 2005. Relationship between bend-faulting at trenches and intermediate-depth seismicity. *Geochemistry, Geophysics, Geosystems*, 6. doi: 10.1029/2005GC000997.

Roberts, G. and Crampin, S., 1986. Shear-wave polarizations in a Hot-Dry-Rock geothermal reservoir: anisotropic effects of fractures. *Int. J. rock mech. min. Sci.*, 23, 291-302..

Roggensack, K., Hervig, R. L., McKnight, S.B., Williams, S.N., 1997. Explosive basaltic volcanism from Cerro Negro volcano: Influence of volatiles on eruptive style. *Science*, 277, 1639-1642.

Ruepke, L. H., Phipps Morgan, J., Hort, M., Connoly, J.A.D., 2002. Are the regional variations in Central American arc lavas due to differing basaltic peridotitic slab sources of fluids? *Geology*, 30, 1035-1038.

Rupke L. H., Phipps Morgan J., Hort M., Connolly J., 2004. Serpentine and the subduction zone water cycle. *Earth and Planetary Science Letters*, 223, 17-34.

Scales, J. A., and Snieder, R., 1997. To Bayes or not to Bayes. *Geophysics*, 62, 1045–1046.

Schmitt, D. R., Han, Z., Kravchinsky, V., Escartin, J., 2007. Seismic and magnetic anisotropy of serpentinized ophiolite:Implications for oceanic spreading rate dependent anisotropy, *Earth and Planetary Science Letters*, 261 (3-4), 590-601.

Schoenberg, M. 1980. Elastic wave behaviour across linear slip interfaces. *J. Acoust. Soc. Am.*, Vol.68 (5), pp. 1516-1521.

Schoenberg, M., 1983. Reflection of elastic waves from periodically stratified media with interfacial slip,*Geophysical Prospecting*, 31, 265-292.

Schoenberg, M., and Douma, J., 1988. Elastic-wave propagation in media with

parallel fractures and aligned cracks. *Geophys. Prosp.*, 36, 571-590.

Schoenberg, M., and Muir, F., 1989, A calculus for finely layered anisotropic media, *Geophysics*, 54(5), 581-589.

Shaw, P. and Orcutt, J., 1985. Waveform inversion of seismic refraction data and applications to young Pacific crust. *Geophys. J. R. Astr. Soc.*, 82, 375-414.

Silver, E., Kastner, M., Fisher, A., Morris, J., McIntosh, K., and Saffer, D., 2000. Fluid flow paths in the Middle America Trench and Costa Rica margin. *Geology,* 28(8): 679-682.

Skelton, A. D. L., Whitmarsh, R., Arghe, F., Crill, P. and Koyi, H., 2005. Constraining the rate and extent of mantle serpentinization from seismic and petrological data: implications for hemosynthesis and tectonic processes. *Geofluids*, 5, 153-164.

Spencer, J. W. Jr. and Nur, A. M., 1976. The effects of pressure, temperature and pore water on velocities in Westerly granite. *J. Geophys. Res.*, 81, 899-904.

Staudigel, H., Plank, T., White, W. M. and Schmincke, H., 1996. Geochemical fluxes during seafloor alteration of the upper oceanic crust: DSDP Sites 417 and 418, Bebout and Kirby, eds., SUBCON: Subduction From Top to Bottom. *AGU Geophysical Monograph*, 96, 19-38.

Stein, C. and Stein, S., 1994. Constraints on hydrothermal flux through the oceanic lithosphere from global heat flow, *J. Geophys. Res*, 99,3081-3095.

Tarantola, A., 1987. *Inverse problem theory: methods for data fitting and model parameter estimation*, Elsevier Science Publisher, New York, 613 pp.

Temme, P., and Müller, G., 1982. Numerical simulation of vertical seismic profiling. *J. Geophys.*, 50, 177– 188.

Thomsen, L. 1995. Elastic anisotropy due to aligned cracks in porous rocks. *Geophys. Prospecting*, 43(6), 805-829.

Toomey, D. R., Foulger, G.R., 1989. Tomographic inversion of local earthquake data from the Hengill-Grensdalur central volcano complex, Iceland. *J. Geophys. Res.*, 94, 17497-17510.

Tonarini, S., Agostini, S., Doglioni, C., Innocenti, F., and Manetti, P., 2007. Evidence for serpentinite fluid in convergent margin systems: The example of El Salvador (Central America) arc lavas, *Geochem. Geophys. Geosyst.*, 8, Q09014, doi:10.1029/2006GC001508.

Turner, S., McDermott, F., Hawkesworth, C., and Kepezhinskas, P., 1998. A U-

series study of lavas from Kamchatka and the Aleutians: constraints on source composition and melt processes. *Contrib. Mineral. Petrol.*, 133, 217–234.

Yoshida, Y., Satake, K., Abe, K., 1992. The large normal-faulting Mariana earthquake of April 5, 1990 in uncoupled subduction zone. *Geophys. Res. Lett.*, 19, 297-300.

von Huene, R., Ranero, C.R., Weinrebe, W., and Hinz, K., 2000. Quaternary convergent margin tectonics of Costa Rica, segmentation of the Cocos plate, and Central American volcanism. *Tectonics*, 19, 314-334.

Walder, J. and Nur, A., 1984. Porosity reduction and crustal pore pressure development. *J. Geophys. Res.*, 89, 11539-11548.

Walter, C. H. E., Flueh, E.R., Ranero, C.R., von Heune, R., and Strauch, W., 2000. Crustal structure across the Pacific margin of Nicaragua: evidence for ophiolitic basement and a shallow mantle sliver. *Geophys. J., Int.*, 141, 759-777.

White, J. E., 1983. Underground sound: Application of seismic waves, Elsevier Sciences Publishing, Inc., New York, 253 p.

White, R. S., McKenzie, D., O'Nions, R.K., 1992. Oceanic crustal thickness from seismic measurements and rare earth element inversions. *J. Geophys. Res.*, 97, 19683-19715.

Whitmarsh, R. B., Manatschal, G. and Minshull, T. A., 2001. Evolution of magma-poor continental margins from rifting to seafloor spreading. *Nature*, 413, 150-154.

Wilkens, R. H., Fryer, G. J., Karsten, J., 1991. Evolution of porosity and seismic structure of upper oceanic crust: Importance of aspect ratios. *J. Geophys. Res.*, 96, 17981-17995.

Wilson, D. S., Teagle, D. A. H., Acton, G. D., et al., 2003. Proc. ODP, Init. Repts., 206: College Station, TX (Ocean Drilling Program). doi:10.2973/odp.proc.ir.206.2003

Zhao, D. and Mizuno, T., 1999. Crack density and saturation rate in the 1995 Kobe earthquake. *Geophys. Res. Lett.*, 26 (21), 3213-3216.

Acknowledgements

I am very grateful to my supervisor PD. Dr. Ingo Grevemeyer for his excellent guidance and support during the last few years.

Many thanks to the participants of RV 'Sonne' Cruise SO173-1 & RV 'Meteor' Cruise M66-4, scientists and crew, for the acquisition and pre-processing of the data.

I thank Prof. Dr. Wolfgang Rabbel for acting as my coreferee.

I am most grateful to my family for their great support and encouragement. I have to thank all my friends here in Kiel who made me feel at home, and my friends in Slavonski Brod who made me feel like I never really left home.

Special thanks to all members of the SFB 574 for many interesting and very helpful discussions.

Erklärung

Hiermit erkläre ich, dass die vorliegende Abhandlung, abgesehen der Beratung durch meine akademischen Lehrer, nach Inhalt und Form meine eigene Arbeit darstellt. Ferner habe ich weder diese noch eine ähnliche Arbeit an einer anderen Abteilung oder Hochschule im Rahmen eines Prüfungsverfahrens vorgelegt.

Curriculum Vitae

Personal data

Name:	Monika Ivandić
Date and Place of birth:	11 October 1978, Slavonski Brod, Croatia
Nationality:	Croatian

Education

1993-1997	Secondary School of Natural Sciences and Mathematics, Slavonski Brod, Croatia
1997-1999	University of Zagreb, Faculty of Science, Department of Physics, Zagreb, Croatia
1999-2004	University of Zagreb, Faculty of Science, Department of Geophysics, Zagreb, Croatia
Since 2005	PhD Student, SFB 574 Volatile und Fluide in Subduktionszonen, IFM-GEOMAR

Appendix

Tomographic inversion

The solution of the inverse problem involves a search over the model space for the most plausible model m that is able to explain the recorded data *d*. Therefore we choose a starting model that is likely to be close to the real subsurface. We trace rays in this model and obtain a first set of synthetic travel times. The comparison of these computed travel times with the actually measured data results in the travel time misfit or travel time residual Δd.

The traveltime along a ray path P is

$$t_{obs} = \int_P u(r)dr \tag{6.1}$$

where r is the position vector, dr is the infinitesimal ray path length and *u(r)* is the slowness at point r. If *u(r)* changes, the ray path changes, thus the ray path depends on the solution of this nonlinear problem. The perturbational model *u(r)* is related to an initial model $u_0(r)$ by

$$\delta u(r) = u(r) - u_0(r) \tag{6.2}$$

According to Fermat's variational principle the traveltime along the ray path P with the minimum traveltime is stationary for an infinitesimal perturbation δu, resulting in a small change in traveltime:

$$\delta t = t(u + \delta u) - t(u) \approx \int_P \delta u dr \tag{6.3}$$

In linearizing the problem it is assumed that small changes in traveltime are solely related to velocity heterogeneities. Therefore, the deviation of the ray path is ignored. Under the assumption that small changes of the model Δm result in only small changes of the travel times Δd we can establish a linear relationship:

$$d = G\delta m \tag{6.4}$$

with G being a Fréchet derivative matrix [e.g. *Menke*, 1989; *Toomey et al.*, 1994], and δm is the uknown model perturbation vector. We apply now small changes to the model in order to reduce the misfit. The new model remains in the region of linearity that surrounds the previous model. This procedure is repeated consecutively until the misfit between the observed and predicted traveltimes is minimized, i.e. until a satisfactory reduction of the travel time residual is achieved.

If one assumes that the error in the relationship $d_{obs} \approx d_{pred} = G\,\delta m_{est}$ is Gaussian, then a least-squares measure of this difference is suitable [e.g. *Menke*, 1989]:

$$min\|d_{obs} - G\delta m_{est}\|^2 \tag{6.5}$$

Uncertainties based on the assigned picking errors σ_i, $i = 1,...,n$ are used to weight the data according to their quality by writing the objective function $\Psi(m)$ that has to be minimized as:

$$\Psi\delta m_{est} = (d_{obs} - G\delta m_{est})^T C_d^{-1}(d_{obs} - G\delta m_{est}), \tag{6.6}$$

where C_d is the data covariance matrix with diagonal elements σ_i^2 [e.g. *Menke*, 1989]. If equation is under-determined, the unconstrained parameters can take any value without affecting a least-squares solution, and hence many m will fit the data. To address this non-uniqueness, model regularization adds additional constraints to the inverse problem. In practice, one often uses a priori information to regularize the a posteriori solution [*Scales and Snieder*, 1997]. Within the FAST algorithm, a user-specified combination of smallest, flattest and smoothest perturbation constraints, each being allowed to vary with depth, is used to tune the iterative inversion in such a way

that the retrieved model has agreeable features. The inversion strategy used is an iterative "jumping" [*Shaw and Orcutt*, 1985] which selects the smoothest model that provides a satisfactory fit to the data.

To reduce the misfit between the observed data d_{obs} and the modeled data d_m we formulate an optimization function F:

$$F = (d_{obs} - G\delta m_{est})^T C_d^{-1}(d_{obs} - G\delta m_{est}) + (m_{est} - m_0)^T C_m^{-1}(m_{est} - m_0), \tag{6.7}$$

where $\mathrm{m}_{est_n} = \mathrm{m}_n + \delta\mathrm{m}_{est_n}$, m_n is the slowness model after n iterations, m_0 is the slowness of the starting model, and C_m is an a priori model covariance matrix. C_d contains the travel time uncertainties while C_m contains the model uncertainties, which are divided into velocity and interface depth uncertainties.

Inversion is achieved as a series of linear steps, in which successively improved models are generated. At each step, the inversion algorithm requires a set of synthetic traveltimes - computed by tracing rays between each source–receiver pair in the current model - and their Fréchet derivatives, the partial derivatives of the traveltimes with respect to each model parameter. Since all regularization terms in equation are allowed to vary with depth, the rows of the regularization matrices are finally scaled with additional depth-weighting factors. The resulting system of linear equations is solved, using the sparse matrix solver LSQR [*Nolet*, 1987]. After each nonlinear iteration, the updated perturbational model is regridded on the finite-difference grid and ray paths and traveltime residuals are computed again until finally the predicted data fit the observed data within the limits of preassigned uncertainty. A good estimate of the quality of fit can be obtained by calculating the normalized X^2 parameter:

$$X^2 = \frac{1}{N_{res}} \sum_{j=1}^{N_{res}} \frac{\delta t_j}{\sigma j}^2 \tag{6.8}$$

where δt_j is the element of d corresponding to the *jth* traveltime datum, σj is the pickuncertainty in that datum, and N_{res} is the absolute number of traveltime residuals. If the uncertainties are well-estimated, uncorrelated and follow a Gaussian distribution, then a satisfactory fit is obtained on average across the model if $X^2 = 1$.